Politecnico di Torino

Master of Science in Energy and Nuclear Engineering

Master Thesis

"Experimental Setup and Tests to Extract the Parameters of an Equivalent Circuit for Two High Efficiencies Photovoltaic Modules"

Supervisors:

Prof. Filippo Spertino

Prof. Munoz Diez Jose Vicente

Ing. Gabriele Malgaroli

Candidate:

Muhammad Aoun Ejaz Qureshi

October 2021

Academic Year 2020/2021

Acknowledgement

On this page, I want to thank everyone who supported me during my university experience. A cordial thanks go to ***Professor Filippo Spertino****, my supervisor at the* ***Politecnico of Turin****, who proposed this thesis work and guided me in its realization. A special thanks is a must for* ***Ing. Gabriele Malgaroli****, who followed me and helped me with outstanding commitment every time and in all possible ways, he can.*

Secondly, I want to thank my external ***Professor José Vicente Muñoz Díez*** *for his support during the development of this master's thesis at the Higher Polytechnic School of the University from Jaén. His utmost commitment and support during and after the mobility period resulted in this thesis production.*

A special thanks go to my parents, who have supported me in these years of university. Thanks to them, who braced me morally and economically, I was able to complete my university career. I am sure I will give them great satisfaction by graduating. Other thanks go to my friend ***Hafsa Siddiqi*** *who have been close to me over the years, and to me, she helped not only in university times but in the entire period of thesis work.*

Finally, I want to thank Spain and its citizens for warmly welcoming me to this new country, especially the UJA community.

Aoun Qureshi

Contents

List of Figures

List of Tables

Glossary of Acronyms

Acronyms	Meanings
CIEMAT	“Centro de Investigaciones Energéticas, Medioambientales y Tecnológicas” in Madrid
AM	Air Mass
ADC	Analog-to-Digital Converter
FF	Fill Factor
GUI	Graphical User Interface
IDEA	Grupo de Investigación y Desarrollo en Energía Solar y Automática
LM	Levenberg-Marquardt algorithm
MPP	Maximum Power Point
MPPT	Maximum Power Point Tracker
NOCT	Nominal Operating Cell Temperature (G_{NOCT} = 800 Wm^{-2}, $T_{c,NOCT}$ = 20 °C, WS_{NOCT} = 1 ms^{-1})
NRMSE	Normalized Root Mean Square Error
OC	Open Circuit
PV	PhotoVoltaic

Acronyms	Meaning
SC	Short Circuit
RTD	Resistance Temperature Detector
5P	Single diode 5 parameters model
STC	Standard Test Condition (G_{STC} = 1000 Wm^{-2}, $T_{c,STC}$ = 25 $°C$, AM 1,5)
TRC	Temperature Coefficient of Resistance
Pt100	Temperature sensor ("Pt" platinum, "100" resistance in Ω at 0 °C)
UJA	Universidad de Jaén
I-V	Voltage and current characteristics of photovoltaic generator
P-V	Voltage and power characteristics of photovoltaic generator
PoliTO	Politecnico Di Torino

Glossary of Symbols

Symbols	Meaning	Units
χ	A-dimensional empirical coefficient of the diode saturation current	-
T_a	Ambient Air Temperature	°C
APE	Average Photon Energy	eV
C	Capacitor Capacitance	F
t_c	Capacitor charging time	s
I	Current	A
I_{model}	Current (estimated from model)	A
I_{exp}	Current (experiment value)	A
I_j	Current in the diode (5P model)	A
I_{sh}	Current in the parallel resistance (5P model)	A
I_{MPP}	Current point in MPP	A
$I_{0,STC}$	Diode saturation current at STC	A
G	Irradiance	$W \cdot m^{-2}$

Symbols	Meaning	Units
E_{model}	Energy (estimated from model)	J
E_{exp}	Energy (experimental value)	J
E_g	Energy gap	J
$E_{g,STC}$	Energy gap at STC	J
E_{ph}	Energy of the photon	J
X_{cor}	Estimation from correlation parameter X value	-
X_{exp}	Experimental parameter X value	-
ν	Frequency	Hz
b	Ideality factor correlation effect in irradiance	$W^{-1} \cdot m^2$
c	Ideality factor correlation effect in temperature	C^{-1}
a	Ideality factor correlation intercept	-
n	Ideality factor of the diode (5P model)	-
$P_{Osterwald}$	Power at MPP by the Osterwald method	$W \cdot m^{-2}$

Table of Constants

Symbols	Significance	Value	Units
$T_{a,NOCT}$	Air temperature in NOCT	25	°C
k_b	Boltzmann constant	$1{,}38.10^{-23}$	$J \cdot K^{-1}$
q_e	Electron charge	$1{,}602.10^{-19}$	C
G_{NOCT}	Module (or cell) irradiance in NOCT	800	Wm^{-2}
G_{STC}	Module (or cell) irradiance in STC	1000	Wm^{-2}
$T_{C,STC}$	Module (or cell) temperature in STC	25	°C
h	Plank constant	$6{,}626\ .10^{-34}$	$J \cdot s$
α_{Pt100}	Pt100 temperature coefficient	0.00385	$\Omega \cdot \Omega^{-1} \cdot K^{-1}$
c	Speed of light in vacuum	$2{,}998\ .10^{8}$	$m \cdot s^{-1}$

Introduction

The photovoltaic generator's operating principle can be described using an equivalent circuit with variable parameters, which can be assumed to be constant. Moreover, the knowledge of their dependence concerning irradiance and cell temperature permits the prediction of the generated power of photovoltaic arrays in any environmental condition. This specific information allows us to trace the current-voltage (I-V) characteristics curve of the photovoltaic generators. This knowledge may be used in future works to evaluate the state of health of photovoltaic arrays by investigating the shape of the I-V curve and the values of circuit parameters predicted in any environmental condition.

This thesis focuses on the experimental validation of an innovative technique to predict the parameters of the equivalent circuit in any weather condition. This work is a part of a joint activity between Politecnico di Torino and the Universidad de Jaén (Spain): my main task of this thesis has been developed in Universidad de Jaén.

In the first part of the thesis, an ad hoc Graphical User interface (GUI) of MATLAB was used to analyse the PV module; the GUI tools allows to perform four operations: the pre-processing of the dataset; the extraction of the circuit parameters; the identification of equations, aiming at describing the dependence of each parameter concerning irradiance and cell temperature; and the comparison between experimental energy and the predicted value with several methods. Experimental data may be affected by measurements errors, or the photovoltaic generators may work in mismatch conditions due to shadowing or other issues. However, the present analysis requires experimental measurements of photovoltaic generators correctly operating: thus, the pre-processing step removes complex measures integrating ad hoc filters. Firstly, empirical data with measurement errors are filtered by comparing the irradiance and the temperature detected by the sensors.

In case of high deviations among the measured quantities, the empirical data are excluded.

The parameters extraction step is the tool's core: in this step, the parameters are numerically determined starting from the filtered measurements. The third step of the analysis regards the identification of the dependence of circuit parameters for cell temperature and irradiance. In particular, the most common equations in literature are used, and nonlinear optimisation of specific coefficients is performed. Finally, the generated energy during the experimental campaign is compared to the predicted value by several methods. The GUI allows estimating expected power using theoretical models and the optimised equations. Using the knowledge of the parameters, the I-V curve is traced at each time step, and the corresponding maximum power is identified.

In the later step in this thesis, the GUI is applied to two monocrystalline silicon photovoltaic modules with high efficiencies, such as the Sharp NU series with a rated power of 245W and Luxor with a rated capacity of 100W. The experimental campaign under analysis lasted six months. During this experimental campaign, two different measuring systems were used to analyse the modules: one was Automated Tracker System, while another one was a manual system using a PVPM (I-V) electronic tracer device. Both modules were measured during clear sunny days at the University of Jaén (Spain), from low to high global irradiance, to record the behaviour of the modules at different cell temperatures. Later, using GUI measured data processed through 4 steps to reach the final stage.

Moreover, the single diode model, the most common circuit model in literature, is used. Furthermore, regarding the numerical algorithm, the Levenberg Marquardt was adopted. Finally, the energy prediction results are compared between experimental data, the optimised equations and the Osterwald model (the most common theoretical model in literature to estimate photovoltaic power).

Chapter 1

1 Photovoltaic Generation System

1.1 Introduction to Solar Energy

Sunlight is a form of electromagnetic radiation consisting of a range of energy bands, also called a solar spectrum. In this sense, the solar spectrum can be divided into different wavelengths that are characterized by different energies. The essential components of the spectrum consist of ultraviolet radiation (UV), visible radiation and infrared radiation (IR). Most of the UV radiation is filtered out by the atmosphere. Therefore, it never reaches the surface like the Earth's surface energy is mainly made of visible radiation (400 to 700 nm).

The electromagnetic spectrum describes light as a wave with a particular wavelength. However, for some specific applications, such as photovoltaic technologies, the light behaviour can be defined according to the Plank definition. As if it was made of 'particles' of energy with no mass that travel at the speed of light. These particles are called photons. Each photon is characterized by either a wavelength or a power, which are inversely proportional with each other.

1.2 Monocrystalline Silicon Technology

The monocrystalline silicon made cells are pure and has a single continuous crystal lattice structure. The main advantage is their high efficiency, which is around 15% while disadvantage is complex manufacturing process which result in higher cost than other technologies. The cells are square shaped with round corner and their typical colours are dark blue and black, as in the figure below.

Figure 1-1: Monocrystalline Module

1.3 Polycrystalline Silicon Technology

The polycrystalline silicon is manufactured from cast square ingots, produced by cooling and solidifying molten silicon. The solidification of material results in cells containing many crystals, making the surface less perfect; due to this, the polycrystalline cell absorbs less solar energy, producing less electricity and thus less efficiency than monocrystalline. In addition, due to lower efficiency, cells are a bit larger, resulting in a large PV module. However, since they are more manageable, so they are cheaper to produce.

Figure 1-2: Polycrystalline Module.

1.4 Solar Cell – Operating Principles

Solar cell, also called photovoltaic cell, any device that directly converts the energy of light into electrical energy through the photovoltaic effect. This is the fundamental unit of photovoltaic module, which are made up of semiconductor material: Photovoltaic (PV) conversion takes place inside them. The Figure below shown the NREL chart showing the highest confirmed conversion efficiencies for research cells for a range of photovoltaic technologies, from 1976 to 2021.

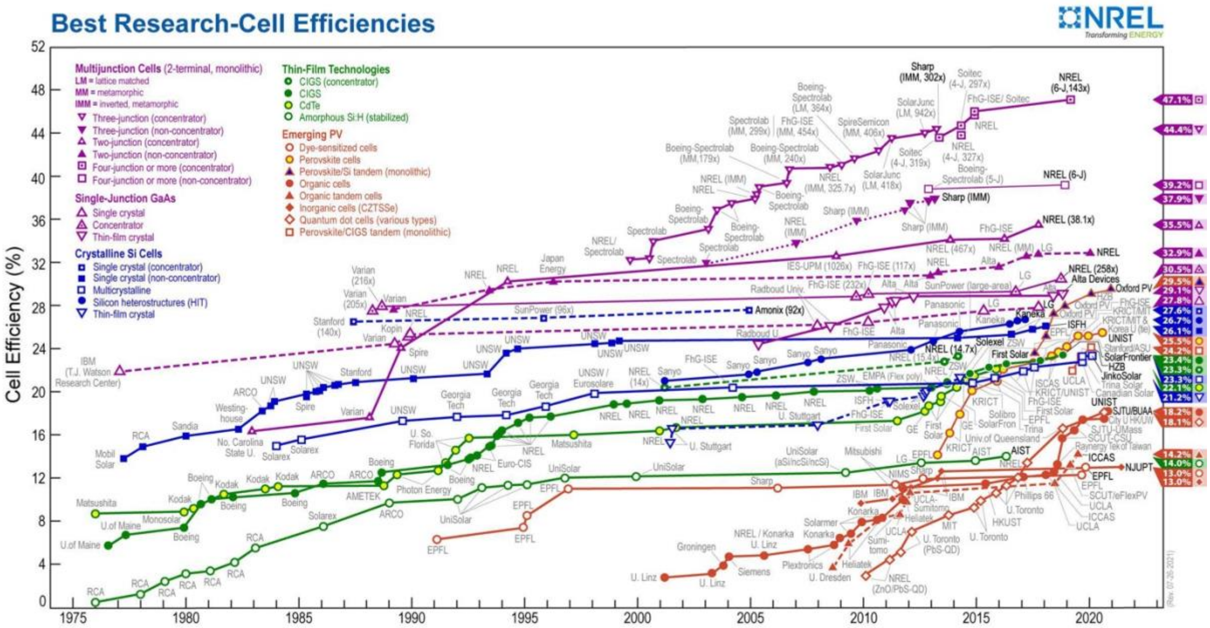

Figure 1-3: Best Research Efficiencies.

A solar cell has an open circuit voltage of 0,6 V and a short circuit current which depends on the cell surface. So, a single cell has a small, rated output power around 3 or 4 Watts. The figure shown below explains the electrical behaviour of a solar cell with the aid of I-V curve.

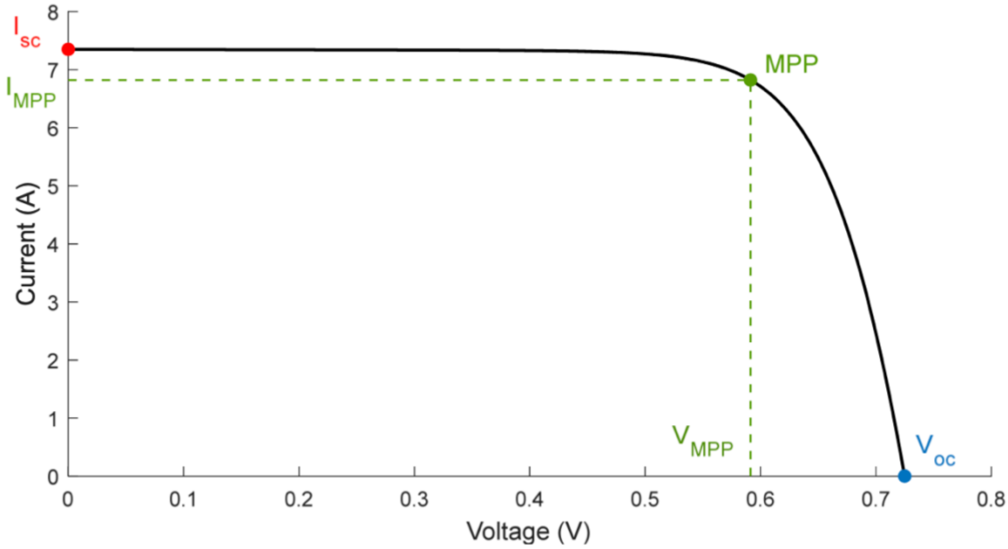

Figure 1-4: Solar Cell I-V Curve

These characteristic points can be identified:

- I_{sc} is the short circuit current, the maximum current at zero voltage (A)
- V_{oc} is the open circuit voltage (V)
- P_{mpp} is the point of maximum power produced by the cell (W). This is the ideal operating power, while the corresponding values of current and voltage are called maximum power current I_{mpp} and maximum power voltage V_{mpp}, respectively.

The basic one of the properties of *I-V* curves connected with V_{oc} and I_{sc} is tension which increases logarithmically with irradiation: V_{oc} decreases as the temperature increase, so these dependencies are translated into the following simplified formula, though dependence on irradiance does not appear.

$$V_{oc}(Tc) = V_{oc,STC} \cdot (1 + \beta_{Voc} \cdot (T_c - T_{c,STC}))$$

Where:

- $V_{oc,STC}$ is the open circuit voltage in STC conditions (V)
- β_{Voc} is the open circuit voltage temperature coefficient (°C^{-1})
- T_c is the cell temperature (°C)
- $T_{c,STC}$ is the cell temperature in STC (°C)

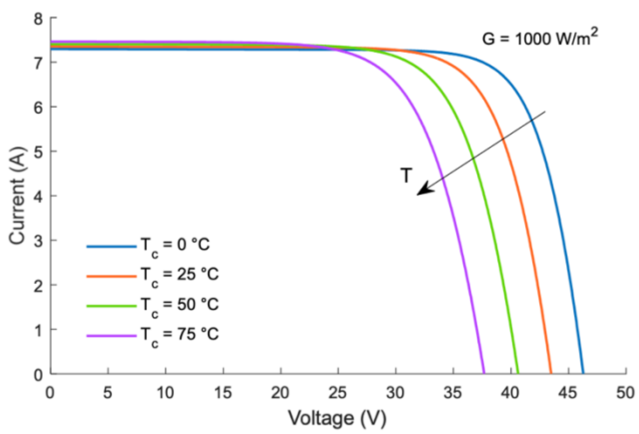

Figure 1-5: Dependence of the I-V curve on Temperature

Moreover, the current is directly proportional to the radiation and I_{sc} increases somewhat as the temperature rises.

$$I_{sc}(G,T_c) = I_{sc,STC} \cdot \frac{G}{G_{STC}} \cdot \left(1 + \alpha_{I_{sc}} \cdot \left(T_c - T_{c,STC}\right)\right)$$

Where:

- $I_{sc,STC}$ is the short circuit current in STC conditions (A)
- G is the incident irradiance (W · m $^{-2}$)
- G_{STC} is the incident irradiance in STC (W · m $^{-2}$)
- α_{Isc} is the short circuit current temperature coefficient (°C^{-1})

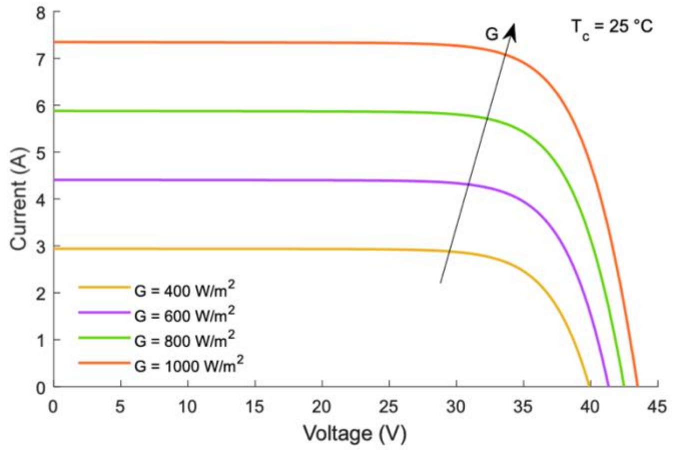

Figure 1-6: Dependence of the I-V curve on irradiance

1.5 Photovoltaic Effect and Energy Gap

Photovoltaic (PV) effect is a process by which PV cell converts the absorbed sunlight energy into electricity. PV system operates with zero carbon-dioxide emissions which has benefits for environmental safety. The photon energy absorbed by nanomaterials is transferred to the electrons in the atoms.

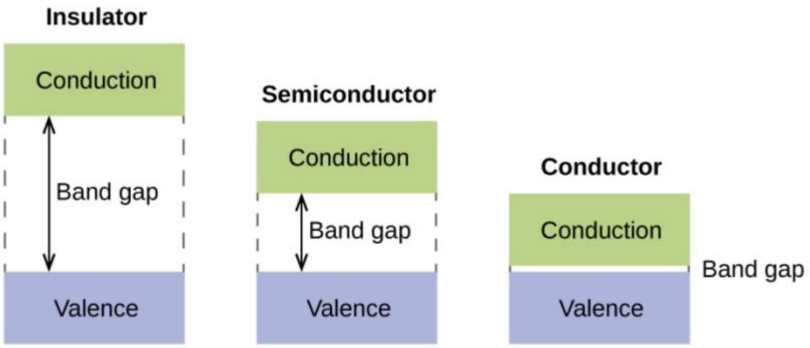

Figure 1-7: Energy Gap Phenomena

The energy band gap principle explains the phenomena of a solar cell. It represents the energy jump required by the electron to move from the valence band to the conduction band. All materials are catalogued according to their energy gap, as reported in Table below. In the case of conductors, this energy gap is low and very high for insulators. On the other hand, the in-between situation referrers to semiconductors. Therefore, when an electron receives sufficient energy, it can switch from the valence band to the conduction band.

Table 1-1: Energy gap of the major material used for PV cells

Material	**Energy gap (*eV*) @ 300 K**
Crystalline silicon (c-Si)	1.12
Amorphous silicon (a-Si)	1.75
Germanium (Ge)	0.67
Gallium Arenside (GaAs)	1.42

Iridium Phosphide (InP)	1.34
Copper Indium Diselenide ($CuInSe_2$)	1.05
Cadmium Telluride (CdTe)	1,45
Cadmium Sulfide (CdS)	2,40

The movement of electron from valence band to the conduction band because of the energy absorption of a photon of light and this could only happen if photon has energy greater than or equal to the energy gap E_g. The equation that characterizes the energy of the photon can be expressed this relationship in analytical terms:

$$E_{ph} = h * \nu = h * \frac{c}{\lambda}$$

Where:

- E_{ph} is the light photon energy (J) or (eV)
- h is the Plank's constant i.e. 6.626e-34 (j*s)
- ν is the light frequency (Hz)
- c is the speed of light in the vacuum 2.9979e (m/s)
- λ is the wavelength of the light (m)
- E_g is the energy gap

$E_{ph} \geq E_g$

Conventionally the solar cell work like the electric field is obtained by union of two regions of a semiconductor crystal. So, in case of silicon one of the regions is dosed with phosphorous which makes this region more concentration of electrons than holes hence it is called n-type region. Further, other region is dosed with boron, which makes the region with more concentration holes, and it is called as p-type region. Combination of these two regions are knows as p-n junction. As much is the difference in concentration of electron and holes, it creates an electric filed orientated with p-type region.

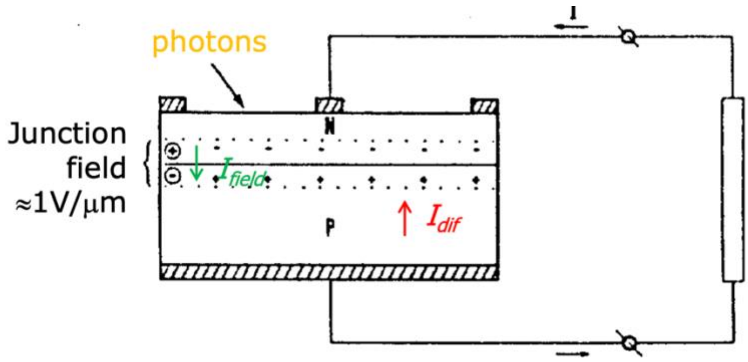

Figure 1-8: Schematic representation of p-n junction connected with load.

This field separates the electrons and the holes when the cell receives the light. Therefore, the photovoltaic current is generated, and it is mainly proportional to the irradiance.

1.6 Standard Test Conditions (STC)

The standard test conditions (STC) are defined in the IEC/EN60904 to ensure that the modules are tested under the same conditions. The legislation requires that, during tests for the characterization of electrical paraments and performance of the module, the STC conditions are met. The STC conditions are following:

- Irradiance of 1000 W ·m-2
- Cell Temperature of 25 ºC
- Air Mass AM 1,5

1.7 Nominal Operating Cell Temperature (NOCT)

The Nominal Operating Cell Temperature (NOCT) is the equilibrium temperature of solar cells inside a module exposed to the sun, in standardized conditions (CEI EN 60904-3):

- Irradiance of 800 W/m2 (AM = 1.5)
- Ambident Temperature of 20ºC
- Wind speed of 1 m/s

$$T_c = T_a + \frac{NOCT - T_{a,NOCT}}{G_{NOCT}} \cdot G$$

Where:

- T_c is the cell temperature (*ºC*)
- T_a is the air temperature (*ºC*)
- $T_{a,NOCT}$ is the air temperature at NOCT (*ºC*)
- G is the irradiance ($W \cdot m^{-2}$)
- G_{NOCT} is the irradiance at NOCT

1.8 Single Diode Model

The photovoltaic cells behavior can be understood with electrical circuit which consist of current generator, that represents radiation and of an antiparallel diode. The ideal current generator produces a current proportional to the irradiance received by cell. The diode (D) represents the straightening effect of the electric field generated by the p-n junction. In absentia of radiation, the equivalent circuit is simply a diode, in-addition, two resistances are inserted tot his basic circuit:

- R_s is the series resistance is sole responsible for the strength of the volume of the material, interconnections and the resistance between metal contacts and semiconductors.

- R_{sh} is the parallel resistance due to the non-ideality of the p-n junction and the impurities close to the junction.

The obtained circuit is the 5-parameters model, schematic in the figure below.

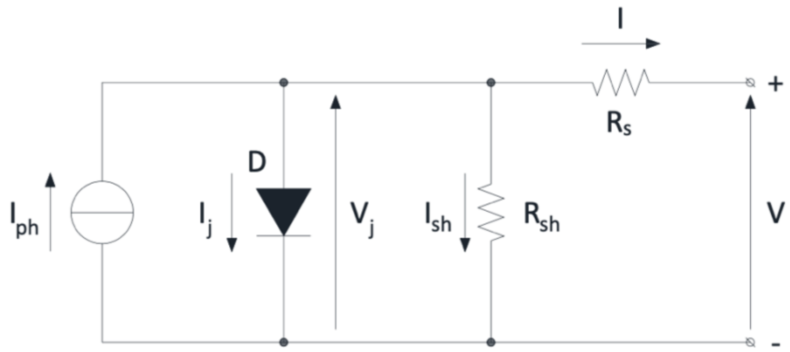

Figure 1-9: Equivalent Circuit with 5 Parameters.

Moving on there is a parameter associated with this needs to be introduced. The fill factor, FF, is a measure of the quality of the p-n junction and the cell resistances.

$$FF = \frac{V_{MPP} \cdot I_{MPP}}{V_{oc} \cdot I_{sc}}$$

Where:

- The numerator defines the point of maximum power (W)
- V_{MPP} is the maximum power point voltage (V)
- I_{MPP} is the MPP current (A)
- V_{oc} is the open circuit voltage (V)
- I_{sc} is the short circuit current (A)

The fill factor (FF) improves for high values of R_{sh} and for low values of R_s. Interestingly, the parallel resistance is related to the slope of the *I-V* curve around *Isc*. Moreover, the series resistance is related to the *Voc*. So, to get the better quality of the cell, the fill factor should be as higher as possible. The figure below shows the schematic the influence of R_{sh} and R_s on *I-V* curve.

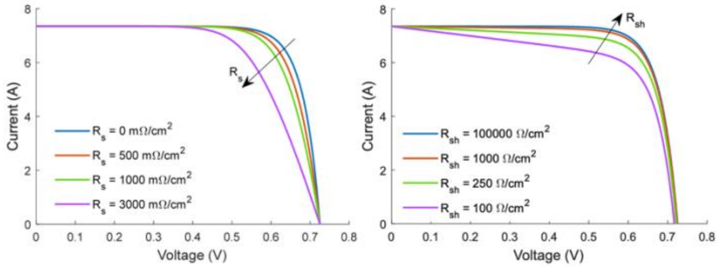

Figure 1-10: I-V curve dependence on series and parallel resistance.

The above shown 5-paramter circuit in the figure, can be solved with respect to current and with respect to voltage.

The current balance equation defines the relation:

$$I = I_{ph} - I_j - I_{sh}$$

Where:

- I is the cell output current (A)
- I_{ph} is the photogenerated current (A)
- I_j is the current in the diode (A)
- $I_{sh} = V_j/R_{sh}$ is the current in the parallel resistance (A)

Irradiance controlled current source is represented in equation:

$$I_{ph} = q_e \cdot N_{ph} \cdot S$$

Where:

- $q_e = 1.602 \cdot 10^{-19}\ C$ is the charge of the electron
- N_{ph} is the number of incident photons in ($m^{-2} \cdot s^{-1}$)
- S is the surface of the cell (m^2)

The equation is of junction current with single exponential:

$$I_j = I_o \cdot \left(e^{\frac{q_e \cdot V_j}{n \cdot k_B \cdot T_C}} - 1\right)$$

Where:

- I_0 is the reverse saturation current of the diode (A)
- Vj is the voltage on the diode (V)
- N is the ideality factor of the diode
- $k_B = 1.38 \cdot 10^{-23}$ J · K^{-1} is the Boltzmann constant
- Tc is the p-n junction temperature (K)

By combining all the previous equations, I can be expressed:

$$I = I_{ph} - I_o \cdot \left(e^{\frac{q_e \cdot V_j}{n \cdot k_B \cdot T}} - 1\right) - \frac{V_j}{R_{sh}}$$

Moving on tension (voltage) can be expressed with the following formulas.

The voltage balance represented here:

$$V = V_j - R_s \cdot I$$

Where:

- V is the cell output voltage (V)

By obtaining V_j from () and replacing in (), voltage becomes:

$$V_{oc} = \frac{n \cdot k_B \cdot T}{q_e} \cdot ln\left(\frac{I_{ph} - I_{sh} + I_o}{I_o}\right)$$

Voltage and current equations can be combined substituting () in (), hence get I

$$I = I_{ph} - I_o \cdot \left(e^{\frac{q_e \cdot (V + R_s \cdot I\,)}{n \cdot k_B \cdot T_c}} - 1 \right) - \frac{V + R_s \cdot I}{R_{sh}}$$

The short circuit current is obtained when $V = 0$

$$I_{sc} = I_{ph} - I_o \cdot \left(e^{\frac{q_e \cdot R_s \cdot I}{n \cdot k_B \cdot T_c}} - 1 \right) - \frac{R_s \cdot I}{R_{sh}}$$

Chapter 2

2 Optimization Algorithm

This chapter discusses the generic concept of optimization, which is an essential part of parameters extraction. The aim of the optimization is by using an approximation to find or reach the optimal value of a particular function.

- **Levenberg– Marquardt Algorithm**

LM developed the Levenberg-Marquardt algorithm in the early 1960s to solve the nonlinear least-square problems. Most minor squares problems arise in the context of fitting a parametrized mathematical model to a set of data points by minimizing an objective expressed as the sum of the squares of the errors between the model function and a bunch of data points. It has become a standard technique for nonlinear least-squares problems, widely adopted in a broad spectrum of disciplines. Thus, LM can be thought of as a combination of steepest descent and the Gauss-Newton method.

This method evolves as a correlation between The Gradient Descent Method and The Gauss-Newton method. The former generates a variation of the parameters in the opposite direction concerning the gradient to minimize the objective function. The latter derives, in turn, from Newton's method, which develops an algorithm to meet approximations of the roots of an objective function and, therefore, the minimum of a process. For nonlinear least square estimation problems, the Newton approach may modify to originate a simple iterative algorithm. Unlike Newton's method, the Gauss-Newton algorithm does not need the second derivatives. The principle is based on a first-order Taylor series approximation of the nonlinear regression function, replaced in the nonlinear model. Therefore, a linear approximation that minimizes a sum of squared function values is obtained.

When the current solution is far from the correct one, the algorithm behaves like a steepest descent method: slow but guaranteed to converge. When the current solution is close to the correct solution, it becomes a Gauss-Newton method. Therefore, the characteristic equation of the Levenberg Marquardt method is:

$$[J(p)^T J(p) + \lambda I]\delta = J(p)^T \cdot \left(y - \hat{y}(p)\right)$$

Where:

- J is the Jacobian matrix
- p is the vector of n parameters (variable to be optimized for the algorithm)
- λ damping parameter
- I is the identity matrix
- δ is the length of the calculated step
- y independent variable
- $\hat{y}(p)$ model curve

The λ factor is a control parameter as it determines the behavior of the algorithm. A low value of λ corresponds to a behavior close to the Gauss – Newton method, whereas a high value corresponds to moving the solution in a direction roughly opposite to the gradient, consequently, with a behavior more like the method of descending the gradient. The value of λ is adapted to each iteration, increasing it if the previous iteration produced a limited reduction in the objective function, or diminishing it in case of rapid decrease.

Chapter 3

3 Data Acquisition System

It is imperative to explain the adopted system to acquire the data on which experiment was done. So, in this chapter, this data acquisition system will be described in detail, which help us to study the I-V curves of the PV modules.

3.1 Principle of I-V curve measurement

To analyze the *I-V* curve of the photovoltaic generator is necessary to connect the PV module with the variable load, as shown in the figure below. This variable load is regulated as a variable resistor; it is adjusted according to different working points while assuming a PV module as a current generator. Moreover, another way to force the variation of the output impedance connected to the PV module is obtained as delighted to the transient charging property. Alongside this, a voltmeter and ammeter are required to record the voltage and current on the output terminal of the PV module.

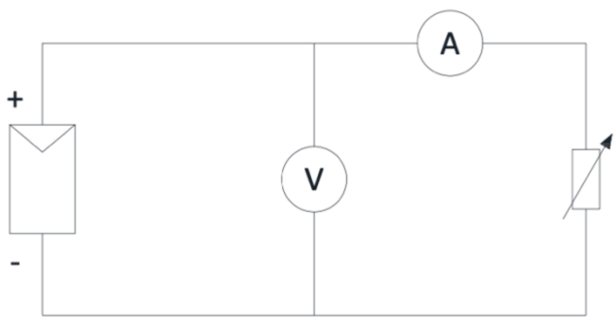

Figure 3-1: Main characteristics of I-V curve of measuring system.

To apply proper tracking of an appropriate *I-V* curve requires at least 100 points *I-V* in a process lasting a time ranged between 20 and 100 ms. Therefore, the effect of weather and environment is negligible after these certain points.

3.1.1 Capacitive Load

Instead of resistor, there is another option to use in above mention system and that is capacitor, to avoid the issue of the sinking the heat generator during the test. Moreover, the capacitor has a wide range of ability for voltage, current and power signals, because the signals last for short time: the transient charge lasts usually for less than 1s. The charging transient of a capacitor is the simplest method that can be used to trace the I-V curve. Compressively, the charging time of the capacitor can be defined by the following equation:

$$i(t) = C \cdot \frac{dv(t)}{dt}$$

Where:

- *i(t)* is the current (A) flowing in the capacitor
- *C* is the measured capacitance (F)
- *v(t)* is the voltage (V) across the capacitor

Let's assume, capacitor is totally discharged, the voltage and current evolve from short circuit condition into open circuit condition when the switch is closed. The charging time (t_c) could be defined as the tie for a voltage sweep from 0 uo to 99,33% of the V_{oc}, which represents the final charging voltage. Current and voltage at terminals of the capacitor are represented as function of time, as shown in the figure below.

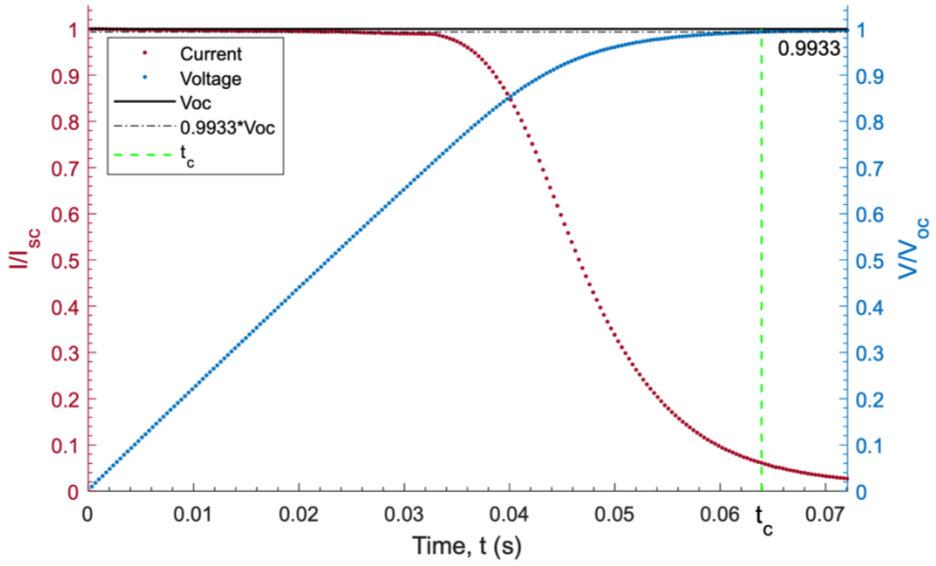

Figure 3-2: Charging transient of a capacitor connected with a PV module.

Capacitor's charging time mainly depends on two quantities of the PV module, i.e., irradiance and temperature. Following expression represents that the charging time can be evaluated looking at the short circuit current and open circuit voltage:

$$t_c = \frac{C}{A} \cdot \frac{V_{oc} \cdot N_s}{I_{sc} \cdot N_p}$$

Where:

- t_c is the charging time of the capacitor (s)
- A = 0,55 is the proportionality factor (-)
- V_{oc} is the open circuit voltage (V)
- I_{sc} is the short circuit current (A)
- N_s is the number of cells in series (-)
- N_p is the number of cells in parallel (-)

The charging time is the most difficult and essential parameter to estimate because it determines the correct synchronization of the multimeters and it allows to properly set the reading rate. Therefore, the charging time must be estimated before acquiring the I- V curve. This estimation may be performed from the measure of the module irradiance and temperature. These two weather conditions influence the short circuit current and the open circuit voltage, respectively.

3.1.2 Maximum Power Point Tracker

It is also known as Power point tracker, a technology used with variable power to extract energy maximum in every condition. The efficiency of the system is optimized when the characteristic load varies to maintain the transfer power at highest efficiency. This characteristic load is maximum power point: MPPT is the process to find this point and keep the load characteristic there. In example, solar inverters convert the DC to AC and includes MPPT: these inverters sample the I-V curve from the solar modules and apply the load as to obtain maximum power. This maximum power (P_{mpp}) is the product of the MPP voltage (V_{mpp}) and MPP current (I_{mpp}).

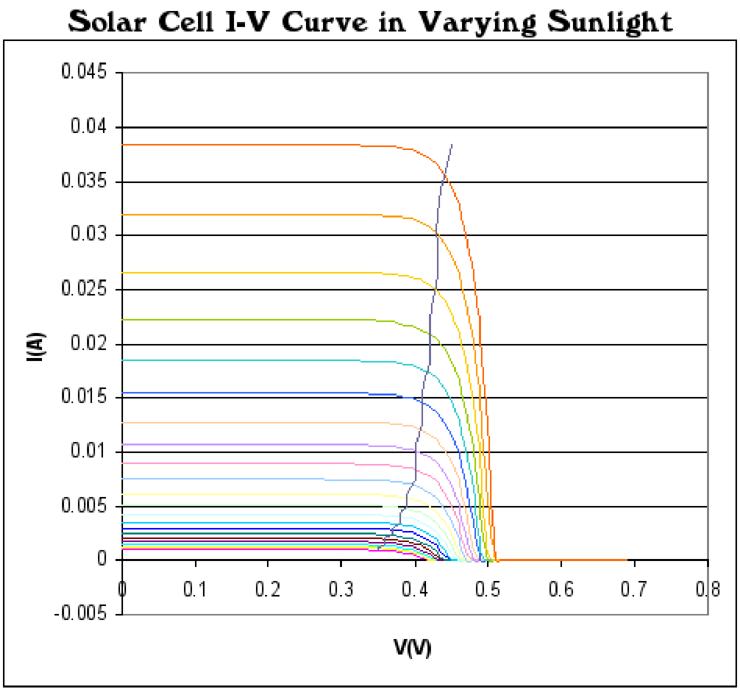

Figure 3-3: Influence of irradiance on maximum power point.

With decreasing irradiance, the short-circuit current proportionally decreases and the open-circuit voltage is almost constant. In Figure 3-3, the influence of irradiance and the maximum power points locus (that is almost a vertical line) are shown. Photovoltaic solar cell I-V curves where a line intersects the knee of the curves where the maximum power transfer point is located.

3.1.3 Variable Resistance

As schematized in the figure below, It is the simplest way to measure the I-V curve of a PV module. So, the value of resistance varies between 0 and infinity in order to obtain points between short circuit current I_{sc} and open circuit, by measuring the voltage and current at each step. The common application to this method is low-power modules.

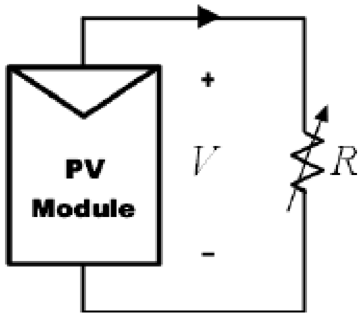

Figure 3-4: Scheme of variable resistance connected with PV module.

3.1.4 Electronic Load

This method uses a transistor as a load and in this case, transistor usually is MOSFET (Metal oxide semiconductor field effect transistor). The resistance between drain and source is modulated through the gate-source voltage, and consequently the flow of current supplied by the module. Using this method in order to obtain the I-V curve, MOSFET must operate in certain conditions; cut-off, active and ohmic region. It allows the fast variation of the equivalent load resistance of the MOSFET.

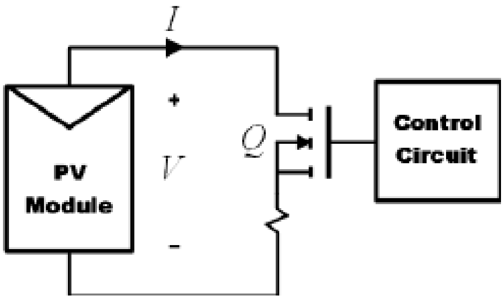

Figure 3-5: Electronic load Scheme.

3.2 Measuring Setup at UJA

The measurement system used in this experiment to obtain the data for the thesis is located on the roof terrace of the laboratory of solar energy in the "*Escuela Politécnica Superior – Universidad de Jaén*". This laboratory is equipped with an automatic tracker system and a semi-automatic fixed support system. We will deal with both the fixed support system and tracker for our thesis, also our Graphical User Interface (GUI) is developed to work with both systems. The only difference between these two systems is the placement of the PV module. In the case of the tracker system, the modules are placed on the tracker, and then the tracker using its automated programming follows the sun and record the measurements. While the fixed support system works differently as PV modules are placed on them, and their orientation is fixed at optimal angle and direction, and it measures the reading accordingly.

Figure 3-6: University of Jaen

3.2.1 Automatic Tracker System

The laboratory of IDEA Solar Energy Research Group at University of Jaen has implemented an automatic measurement system able to sequentially record the I-V curve of up to 4 PV modules together with the weather conditions. In figure below, the schematic of measurement system is shown. The common characteristics are represented in the light blue while the peculiar characteristics are marked in violet for the tracker system and in orange for the fixed system, respectively.

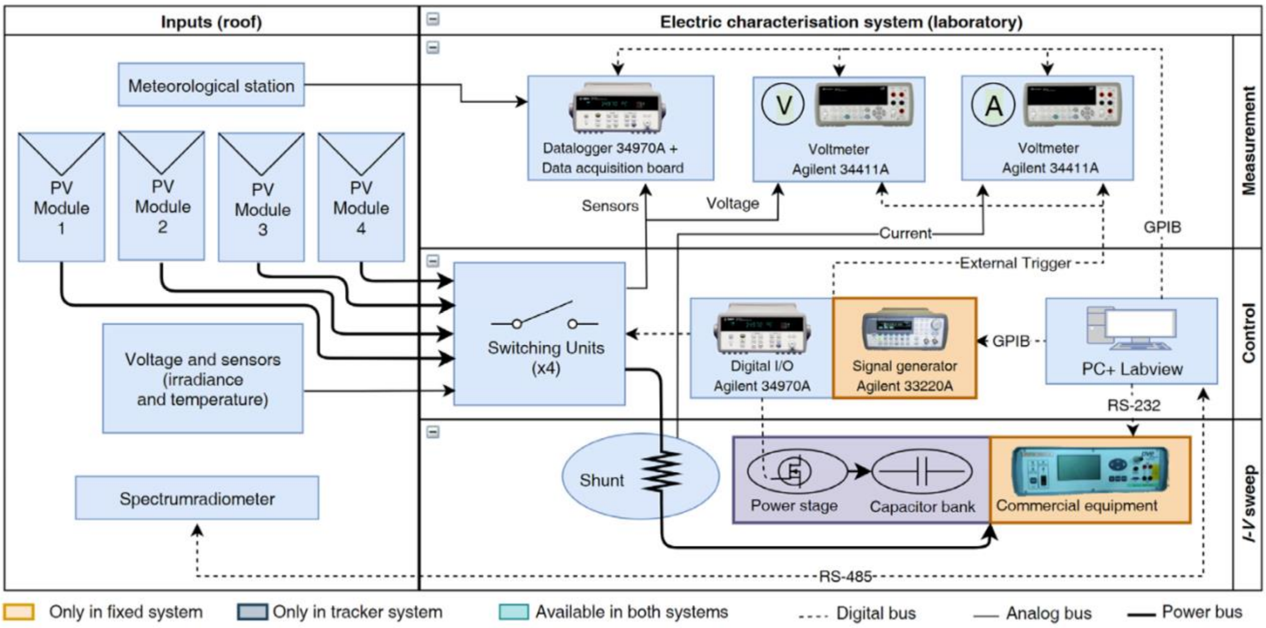

Figure 3-7: Schematic of UJA measurement system.

The "tracker system" shown in figure below, uses a BSQ D150/6 Solar 2-axes tracker. The system is designed with a 2-axis solution to hold the PV module perpendicularly always to the direct sun light. The tracker is designed to carry out activity on concentration solar with a maximum misalignment of ±0,5° so, this way possible angular reflection losses are avoided. This system is integrated with all instruments such as temperature probe, pyranometer, and air temperature. In addition, the two multimeters are synchronized by the Agilent 34970A datalogger that provides a trigger signal through the Agilent 34907A Digital Multifunction Module.

Figure 3-8: Picture of tracker system (on the left the external part, on the right the internal equipment)

As regards the implemented load to plot the I-V-curve, the system includes a capacitive load as shown in Figure below This load mainly consists of three elements: the first one is the electrolytic capacitor with a capacitance of 47 mF and a maximum voltage of 100 V; the second one is the discharge resistance which is used to discharge the capacitor; finally, the last one is a voltage generator used to negative pre-charge the capacitor and to get the short circuit current.

Figure 3-9: View of the inside of the capacitive load.

The working principle of the load is described as follows. The Agilent 34970A datalogger controls the charge and discharge of the capacitive load using relays. Firstly, the datalogger closes only SW7, shown in Figure below, to negative pre-charge the capacitor. This process is essential to get the short circuit current point. Besides, a diode is necessary to avoid problems linked to the internal diode of the solid-state relays.

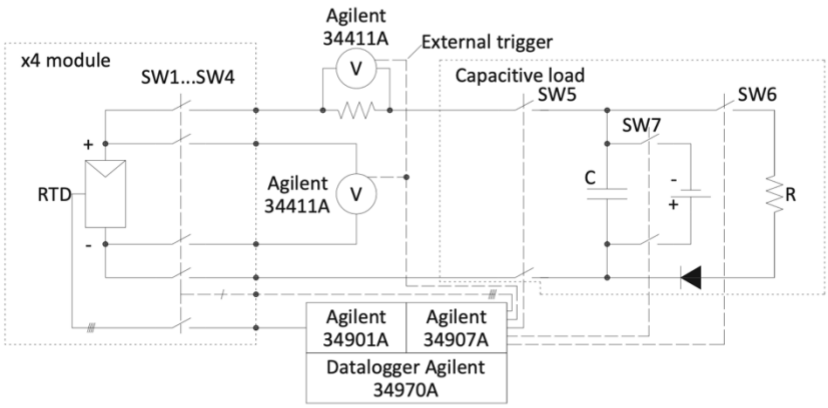

Figure 3-10: Electrical scheme of the tracker system

Secondly, always with reference to Figure 3-8, the datalogger opens SW7 and then it closes SW5. This sequence of commands connects the PV module to the capacitor load C. Then, the multimeters may acquire the voltage and current synchronously. The data acquisition is done in a specific time referred to the capacitive load properties. In fact, the estimation of the charging time (t_c) is essential to meet the timing requirement. The time between two samples is settled properly for acquiring the entire curve with enough points. Finally, the datalogger reopens SW5 at the end of the transient and it closes SW6 to discharge the capacitor on a resistor for the next acquisition.

3.2.2 PVPM – Automated I-V Tracer

The PV modules are placed manually on the fixed support system, as shown in the figure below, oriented with 0° zenith and 35° tilt angles. This system integrates the module temperature probe and same oriented pyranometer. As shown in the figure, it is designed to acquire *the I-V* curve of a specific PV module placed on the fixed support. A capacitive load is used to trace the *I-V* curve. Also, the external trigger is used to synchronize the multimeter, and it comes from HP datalogger Agilent 34970A. In this case, a commercial device PVE PVPM 2540C controlled by the LabVIEW program is used to trace the I-V curve. The LabVIEW software communicates directly with the *I-V* curve tracker through an RS232 link.

Figure 3-11: (Left) Fixed system connected with (Right) PVPM and data logger controlled by LabVIEW program.

3.2.3 Lab VIEW Program

The entire system is managed with an ad-hoc LabVIEW software on a dedicated PC. The devices are attached to the PC through GPIB connections, except for the spectroradiometer that needs a RS485-RS232 serial connection.

Figure 3-12: LabVIEW graphical user interface of tracker system.

The LabVIEW software operation is represented in the flowchart Figure below. Moreover, the software is designed to provide the user with extra facilities to configure the measurement process. In addition, the graphical interface shows in real-time the acquired data such as the I-V curves, the value of irradiance and temperature or the shape of the solar spectrum. A snapshot of the software's user interface is shown in the figure above. The program saves the data from different sensors and instruments in one "CSV" file for each acquisition. The output CSV file is structured with one column for each measured quantity. All columns contain 1500 values, forming a matrix. All 1500 values are equal in the case of a physical amount with a single point (i.e., temperature, irradiance, etc.).

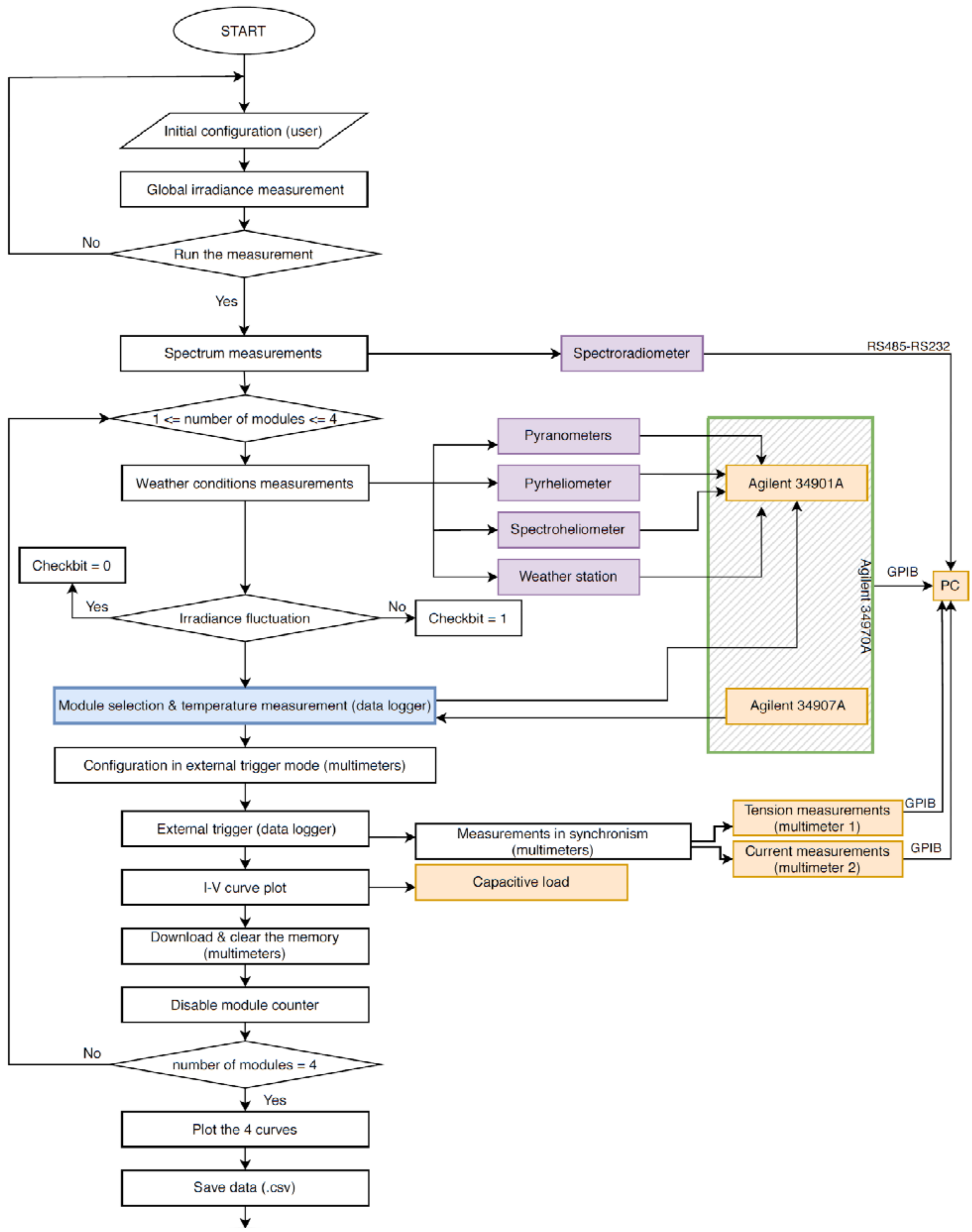

Figure 3-13: LabVIEW measurement control software flowchart.

3.2.4 Measurement Sensors

The instruments used to measure the environmental condition will be described here. All the sensors are connected with Agilent 34901A 20-Channel general purpose multiplexer boards included in the HP data logger Agilent 34970A. The LabVIEW software acquire sensors data from datalogger and using PVE PVPM device to trace the `I-V curve and store all the data in the same .csv file.

3.2.4.1 Measurement of Module Temperature (T_c)

The module temperature (T_c) is measure using a resistance temperature detector (RTDs) of Pt100 type with 4-wire connection is adopted. This sensor consists of a probe made of platinum (Pt) with 100 Ω resistance at 0°C. The temperature coefficient "α_{Pt100}" of this sensor is 0,00385 $\Omega \cdot \Omega^{-1} \cdot K^{-1}$. This coefficient describes the linear approximated characteristic of the probe resistance variation with temperature:

$$\alpha_{Pt100} = \frac{R_{100} - R_0}{100 \cdot R_0}$$

Where:

- α_{Pt100} is 0,00385 $\Omega \cdot \Omega^{-1} \cdot K^{-1}$ is the temperature coefficient
- R_{100} is the sensor resistance at 100°C measured (Ω)
- R_0 is the sensor resistance at 0°C measure (Ω)

The temperature value is calculated by a measurement of the resistance of the Pt sensor in a 4-wire configuration. Thanks to 4-wire measurement as it is precise and unaffected by the length of the laboratory wires. So, the datalogger is adjusted according to make conversion and this probe has a capability to measure in the range of -50°C to +150°C.

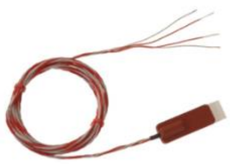

Figure 3-14: Pt-100 probe used to measure module temperature.

3.2.4.2 Measurement of Global Irradiance (G)

The global in-plane irradiance (G) represents the global solar power per unit of the area received by a surface with an azimuth and zenith angle. As in the figure below, the irradiance (G) is measured by a Kipp and Zonnen CMP11 pyranometer. The instrument is placed co-planar with the modules under study, and the pyranometer provides an output voltage signal proportional to the incidental irradiance. Moreover, The ADC can convert this voltage signal in irradiance units with the calibration constant. This calibration constant came from the manufacturer calibration or external calibration in an accredited laboratory (i.e. CIEMAT in Madrid). Finally, the output signal from the pyranometer is measured with the datalogger.

Figure 3-15: Picture of Kipp and Zonnen CMP11 pyranometer.

3.3 Evaluation of Measurement Uncertainty

Every experimental data has some range of fluctuation, and it is not possible to consider any measuring device or measured data 100% accurate. In order to make it more precise, its percentage uncertainty is evaluated, which help us to compare the experimental data with theoretical results. The uncertainty interval should be compared with the theoretical model to quantify the accuracy of the results. The calculated tolerances for the worst scenario are reported in this section. The worst scenario indicates the case in which the relative tolerance (***$U_{x,worst}$***) is the highest.

Table 3-1: Worst case Uncertainties.

Measurands	***$U_{x,worst}$***
Voltage (*V*)	±0.02
Current intensity (*A*)	±1.0
Irradiance '*G*'(*W/m^2*)	±2.0
Module Temperature (T_c)	±1.16
Maximum Power (*W*)	±1.3

Chapter 4

4 Graphical User Interface

The data pre-processing is a step to read the .csv files from the measurement systems and automatically remove the unphysical information by applying them. After, this some filters are used to brush up the raw measured data further. Further, I will explain the graphical interface and the operation of the software in this chapter.

4.1 Step 1: Data Pre-Processing

The most intuitive and user-friendly interface containing all the settings needed, as shown in the figure below

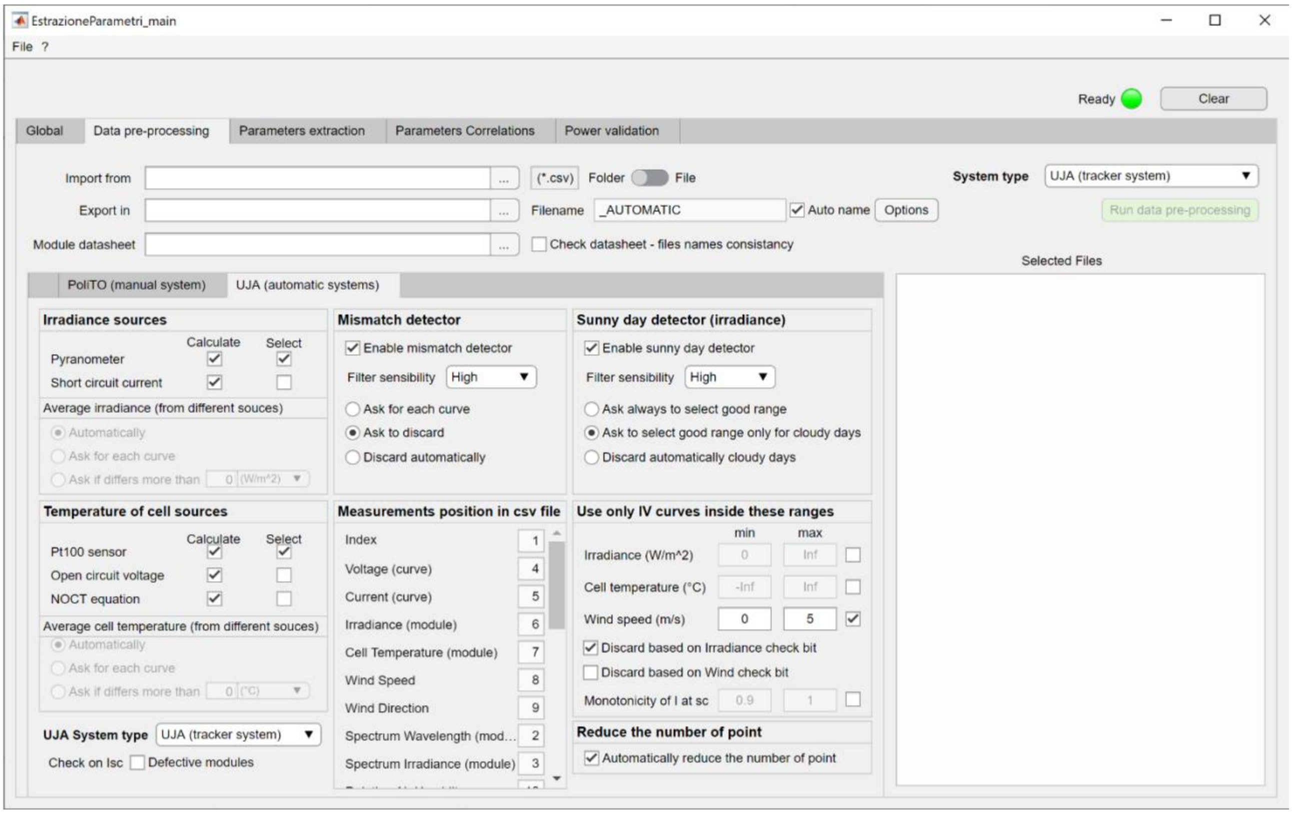

Figure 4-1: Picture of the graphical user interface tab for the pre-processing task.

As it can been seen from the figure above, in the tab of data pre-processing, there are two sections: one deals with import, export and insertion of module datasheet while section below contains settings and filter. Also, in this section there are two tabs, one is about UJA (automatic system) which will be explained later while other one is PoliTO (manual system) which will not be explained as that wasn't used for this thesis.

4.1.1 Import and Export Settings

The import and export settings are situated in the upper part of the interface. Three edit fields and a list box may be seen. They are described in the following lines.

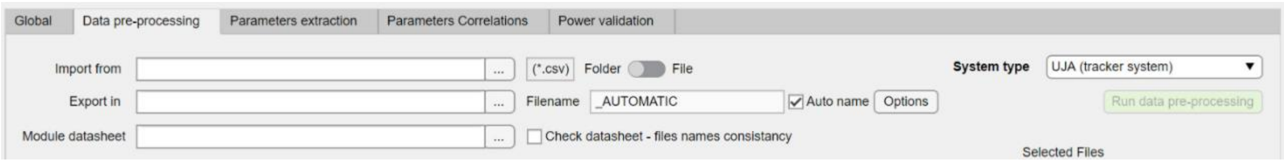

Figure 4-2: Picture of the graphical user interface for the pre-processing task-import and export settings.

The first edit field allows the user to select the file path: in this section there are 2 types of input selection, i.e. the choice of a group of files or of an entire folder. Only the CSV files are picked up in case of in the case of a UJA system.

On the other hand, the second element allows the user to choose the data export folder in the desired format. The format selection can be made by clicking the "Options" button present in the same line as the second edit field. The options button opens a new window, shown in the Figure below and described in the following lines.

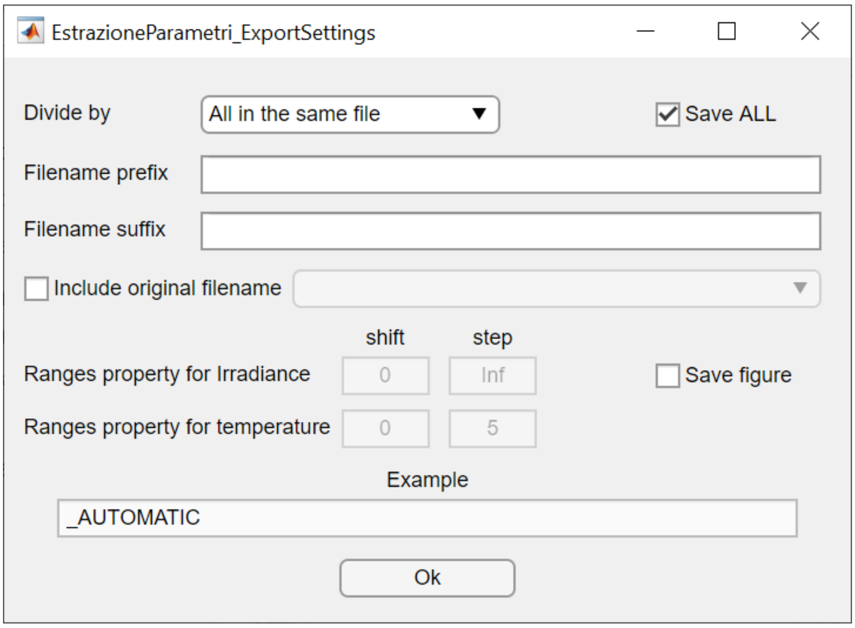

Figure 4-3: Picture of the window for selecting the saving properties

The saving settings in the list box permits to divide the data in various ways. There are different types of data division: “All in the same file”, “Divide by days”, “Divide by months”, “Divide by years”, ‘’Divide by irradiance”, “Divide by temperature (module)”, “Divide by irradiance and temperature (module)”. The selection of saving data by irradiance and/or temperature involves a further specification called “the ranges property”. Here, the user has to insert two values for quantity: an initial shift value from zero and a step value. The ranges division is created only between the minimum and maximum rounded values of the quantity. An example for the irradiance case with shift = 25 and step = 50 means the division of the irradiance in the ranges (0-25], (25,75], (75,125], ..., (975,1025].

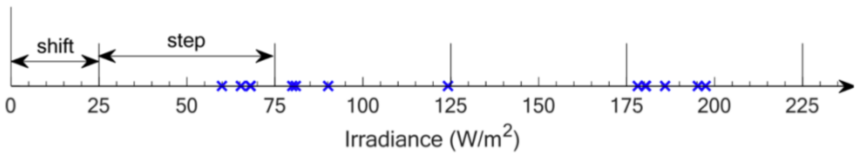

Figure 4-4: Example of ranges division.

The same logic is adopted for the module temperature classification. In the options window, there are two optional edit fields that allow the user to insert a prefix and a suffix to the name of the output data. Moreover, in the final file name, the user can also decide to include the original filename of the CSV file. Finally, two checkboxes can be seen. On the one hand, the “Save ALL” checkbox keeps a copy of all loaded information before applying the filters. On the other hand, the “Save figure” checkbox saves the figures of the day irradiance and the I-V and P-V curves of each acquisition.

The third edit field of the import and export settings is the selection of the Excel datasheet files.

	Value	Unit of measurement	Notes
module name	Sharp	-	Must finish with '_'
$P_{max,STC}$	243,4	W	Power MPPT in STC conditions
$I_{sc,STC}$	8,74	A	Short circuit current in STC conditions
$V_{oc,STC}$	37,44	V	Open circuit voltage in STC conditions
α (I_{sc})	0,053	%/K	Coefficiente di temperatura Isc
β (V_{oc})	-0,347	%/K	Coefficiente di temperatura Voc
γ (P_{max})	-0,485	%/K	Coefficiente di temperatura Pmax
NOCT	47,5	°C	NOCT temperature
Ns	60	-	Number of cell in series
Nc	1	-	Number of cell in parallel
Cell dimension	157	mm	
G_{STC}	1000	W/m^2	Irradiance in STC conditions
Tc_{STC}	25	°C	Cell temperature in STC conditions
G_{NOCT}	800	W/m^2	Irradiance in NOCT conditions
Ta_{NOCT}	20	°C	Air temperature in NOCT conditions

Figure 4-5: Example of module datasheet in Excel.

This Excel file shall be created with a proper model as in Figure above

Lastly, there is the list box, “System type” where user declares the measurement system e.g. PoliTO or UJA ones.

4.1.2 Implementation of Data Pre-Processing for UJA

Once this tab is selected, it can be seen in the figure below that the settings are grouped into several panels: some are related with data acquisition while other use for data filtration.

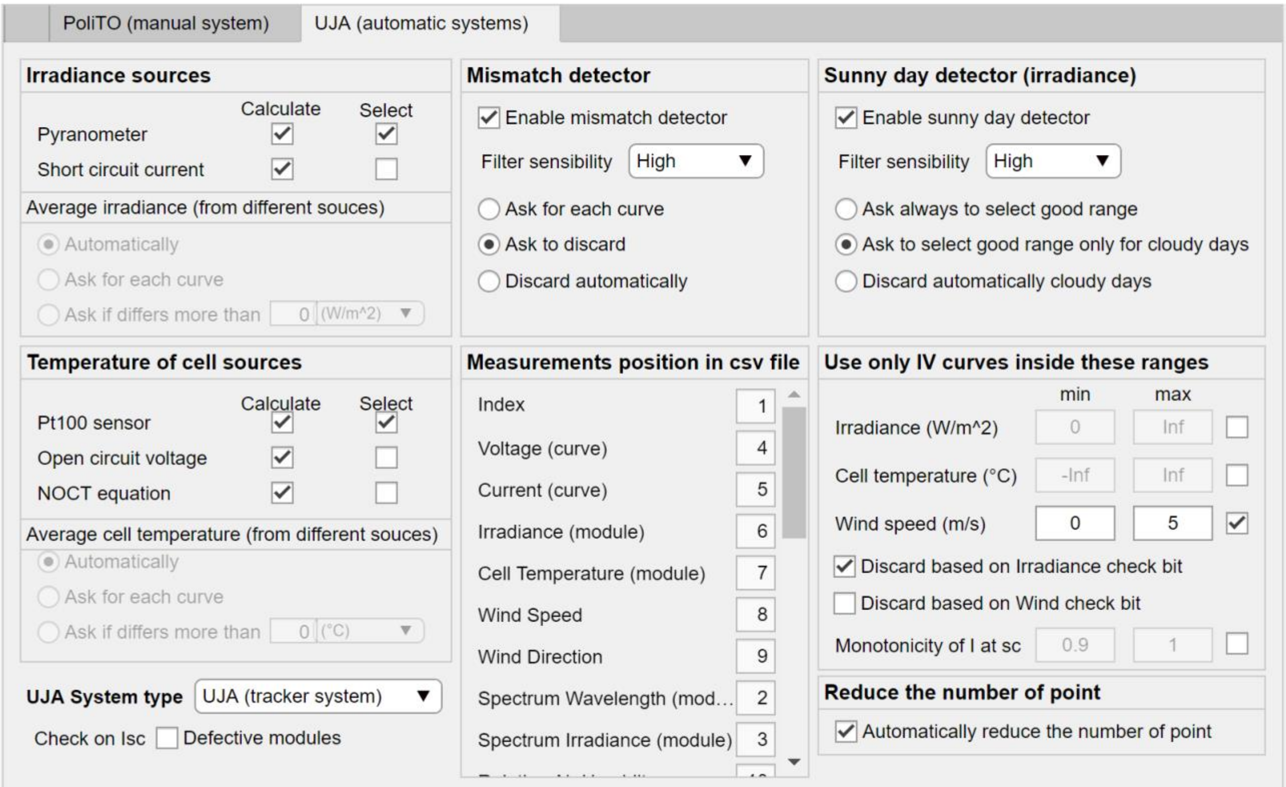

Figure 4-6: Picture of the graphical user interface for the pre-processing task- UJA (automatic system)

The data acquisition involves following panels.

- The “Irradiance sources” panel allows the user to choose the irradiance sources to be used in the next steps. The sources are the pyranometer, the short-circuit current or they may be both. In the last case, the user may decide the method of calculating the average value of the two sources. The selected method between “automatically”, “Ask for each curve” or “manually” defines the level of user intervention.

- The “Temperature sources” panel allows the user to choose the temperature sources to be used in the next steps. The sources of module temperature are the Pt100 probe, the open circuit voltage and the NOCT equation. The temperature considered is the average value if more than one source is selected. Moreover, a window, in Figure below, shows up in case of user intervention.

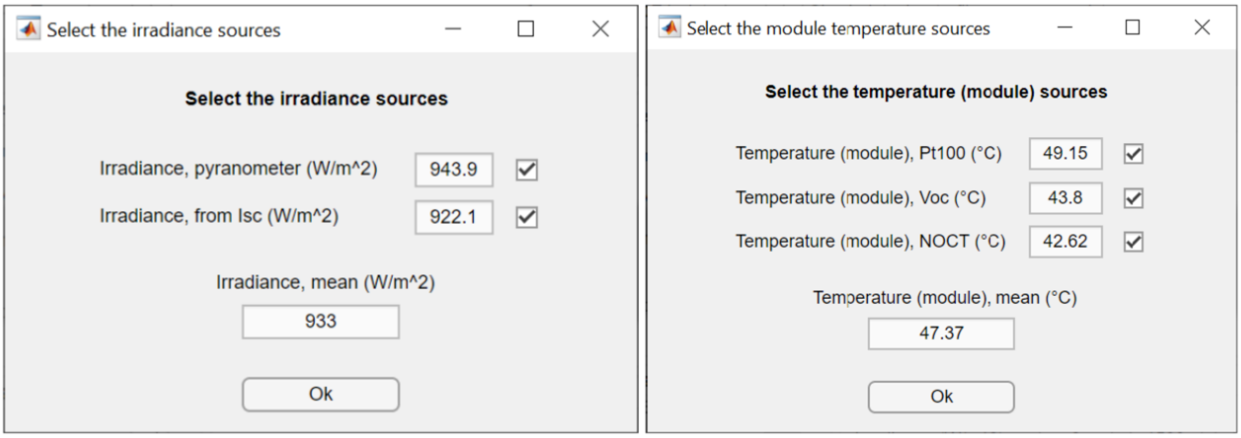

Figure 4-7: Picture of the irradiance and temperature manual selection

- The "Measurement position in .csv file" panel indicates the column position for each measured quantity in the .csv file. The position of each quantity is provided in preloaded profile for the fixed system. These profiles are selectable from the "UJA System type" list box. In addition, in this list box there is a fourth option called "Custom profile". Only in this case the edit fields of the quantities are editable. If a quantity is absent in the .csv file, a value of "-1" should be written down. Furthermore, it is important to indicate that a .csv file contains the values of the measurements for an I-V curve acquisition.

The panels those deals with filtering process are explained here.

- The "Mismatch detector" and the "Sunny day detector (irradiance)" panels are made up of three elements. They have a similar interface presented below. Firstly, the check box enables the mismatch/sunny day detector. Secondly, the list box allows the user to specify three level of filter's sensibility (high, medium, low). Finally, the button group defines the user's level of interaction (automatically, semi-automatically or manually).

- The "Use only I-V curve inside these ranges" panel is composed of editable fields for four quantities. These quantities are irradiance, cell temperature, wind, and current monotonicity at short circuit ranges. Besides, this panel includes two check boxes for filtering the data with the irradiance and/or wind check-bits.
- The "Reduce the number of points" panel contains the check box that enables a reduction in the *I-V* curve points. This reduction is necessary to solve the accumulation of points near the open circuit point.

4.2 Step 2: Parameters Extraction

The parameter extraction process consists of a numeric optimization used to solve the equations linked to the PV cells equivalent circuit. The Graphical User Interface consists of two different PV models and three different extraction algorithms. The two models are 5 parameters systems and 7 parameters system: only 5 parameter model is used in this thesis. The three algorithms are the following: Levenberg-Marquardt (LM), the combination of Simulated Annealing and Nelder-Mead (SA-NM), and lastly, We can add the third algorithm for future analysis. The five parameters model and the LM algorithms are used for the elaboration. The graphical interface is designed to contain all needed settings most simply. The below Figure shows the interface used for parameter extraction.

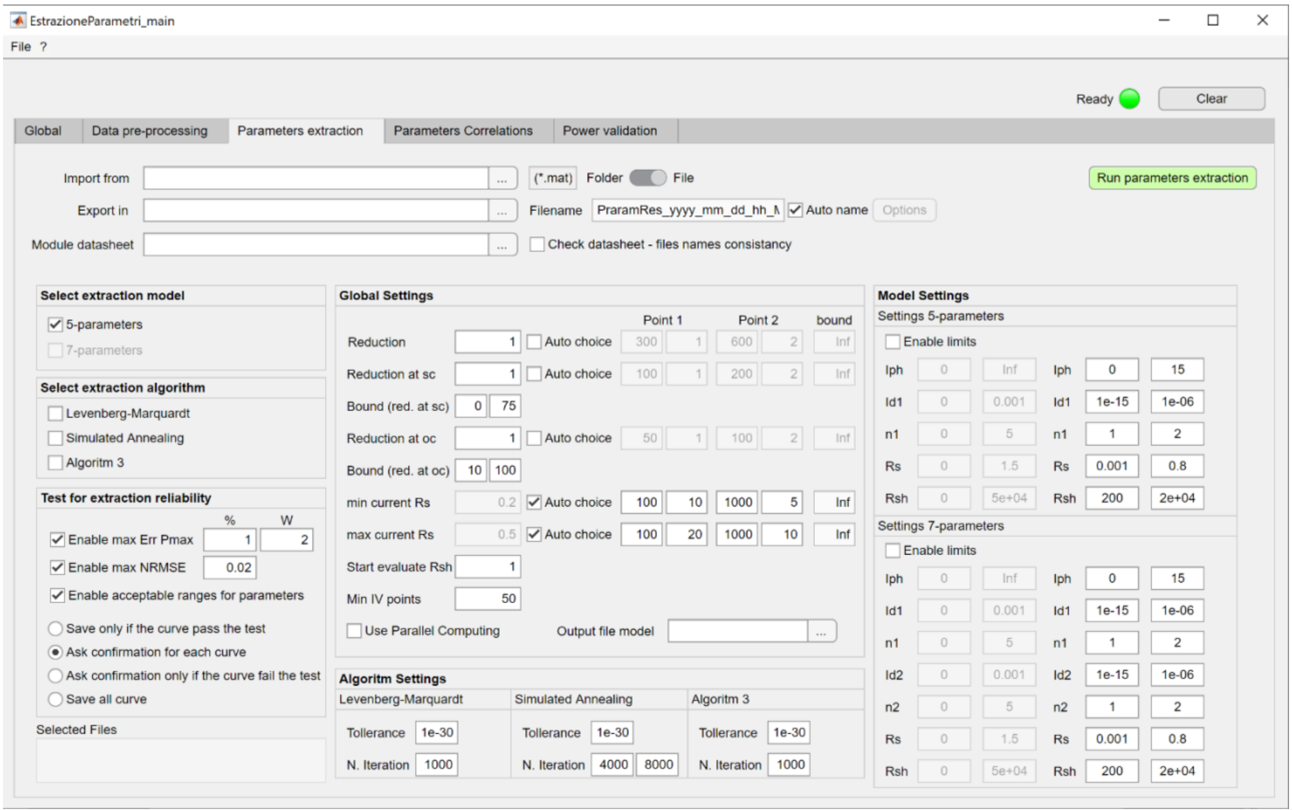

Figure 4-8: Picture of the graphical user interface tab for the parameter's extraction

There are six panels in the settings of parameters extraction: the first panel is "Select extraction model". It includes the option of two PV models, 5 parameters and 7 parameters, which works automatically after selection. The second panel is called "Select extraction algorithm". The calculations for the parameter's extraction are done using one of its algorithms. Finally, the third panel is "Test for the extraction reliability", related to setting filters to extracted parameters. The test consists of three validations: the maximum error on power, the maximum *NRMSE*, and the value of the parameters in a user-defined range.

Moreover, the filter can operate in four modes: first automatically (only saves the curve passes the test), second, semi-automatically (it asks confirmation for saving if the curve fails the test), third, manually (it asks confirmation for saving for each curve), and finally disabled (it saves all the curves).

In the “Global settings” panel, the user selects the main conditions of the extraction process; following are under follow:

- “Reduction”. It reduces the number of points in I-V curve to speed the optimization. The user can select a number between 1 and infinite, so the value of reduction can be computed automatically to maintain a constant number of points of the I-V curve.
- “Reduction at SC”. It is identical operation as Reduction but only in the current source section, between SC and MPP points.
- “Bound (red. at SC)”. It restrcits the section where the “Reduction at SC” operates.
- “Reduction at OC”. It is identical to Reduction only in the voltage source section, between MPP and OC points.
- “Bound (red. at OC)”. It restricts the section where “Reduction st OC” operates.
- “min current Rs” and “max current Rs”. It helps for algorithms in convergences, these are minimum and maximum values of current used to estimate the initial condition of the R_s.
- “Start evaluate Rsh”: starting point to estimate the first value of R_{sh}.
- “min I-V points”: minimum number of point that the I-V curve must have to be elaborated.

“Algorithm Settings”. This panel contains the settings of maximum number of iteration and the end tolerance for each algorithm.

“Model settings”. This panel contains the bounds for the optimization and the limits for the test on the output.

4.3 Step 3: Parameters Correlations

The “Parameters Correlations” also known as “Regression”, is a step to identify the trend of each parameter with irradiance and/or temperature. Every parameter is fitted with correlation in literature. The curve fitting function of MATLB is based on the algorithm, Levenberg Marquarlt. In results, as an output optimized coefficient of each parameter are obtained.

4.3.1 Equations related with Parameters Correlations

The correlations obtained are valid only for the five parameters model (i.e. I_{ph}, I_0, n, R_s, R_{sh}).

1. **Photogenerated Current Correlation**

The photogenerated current has a trend proportional to the irradiance and linear with the temperature. The following equation is optimized:

$$I_{ph} = I_{ph,STC} \cdot \left(1 + \left(\alpha \cdot \left(T_c - T_{c,STC}\right)\right)\right) \cdot \frac{G}{G_{STC}}$$

Where:

- Iph is the photogenerated current of the five paramter model (A)
- Iph,STC is the photogenerated current in STC (A)
- G is the module irradiance (W · m-^{2})
- G_{STC} is the module irradiance in STC (W · m^{-2})
- T_c is the cell temperature (K)
- *Tc,STC* is the cell temperature in STC (K)
- α is the short circuit temperature coefficient (K^{-1})

In such case, the optimization coefficient are $I_{ph,STC}$ and α, where α can be optimized or fixed to a specific value from the datasheet.

2. **Saturation Current Correlation**

From the diodes, the saturation current has a cubic trend proportional to the temperature, []. The following are the optimized equations:

$$I_0 = I_{0,STC} \cdot \left(\frac{T_c}{T_{c,STC}}\right)^3 \cdot \exp\left(\left(\frac{E_{g,STC}}{T_{STC}} - \frac{E_g(T_c)}{T_c}\right) \cdot \frac{1}{k_B}\right)$$

$$E_g(T_c) = E_{g,STC} \cdot \left(1 - 0{,}0002677 \cdot \left(T_c - T_{c,STC}\right)\right)$$

$$\text{(for m-Si @ 298 K)} \qquad E_{g,STC} = 1{,}121 \cdot q_e$$

Where:

- I_0 is the diode saturation current (A)
- $I_{0,STC}$ is the diode saturation current in STC (A)
- E_g (T_c) is the energy gap at T_c (J)
- $E_{g,STC}$ is the energy gap in STC (J)
- k_B is the Boltzmann constant (J · K^{-1})
- $q_e = 1{,}602 \cdot 10^{-19}$ C is the charge of the electron

It is important to mention here that above mentioned equations are studied in context of some specific technologies as their energy gas are well known. A new a-dimensional empirical coefficient χ is added to take in account the different behaviours of the energy gap. In this case following equations is optimized using coefficients are $I_{0,STC}$ and χ where χ can be optimized or fixed to specific value between 0 – 1.

3. **Ideality Factor Correlation**

It has a little trend with temperature and irradiance [], following are the optimized equation.

$$n = a + b \cdot G + c \cdot T_c$$

Where:

- n is the diode ideality factor (-)
- a is the intercept term (-)
- b expresses the linear effect in irradiance ($W^{-1} \cdot m^2$)
- c expresses the linear effect in module temperature (C^{-1})

a, b, c, are optimization coefficients.

4. **Series Resistance Correlation**

The series resistance has a trend proportional to the temperature and logarithmical to the irradiance. The following equation is optimized:

$$R_s = R_{s,STC} \cdot \frac{T_c}{T_{c,STC}} \cdot \left(1 - \lambda_{R_s} \cdot \log\left(\frac{G}{G_{STC}}\right)\right)$$

Where:

- R_s is the series resistance (Ω)
- $R_{s,STC}$ is the series resistance at STC (Ω)
- λ_{R_s} is an empirical coefficient that expresses proportionality to the logarithmic variation of the irradaince (-)

The optimization coefficients are $R_{s,STC}$, λ_{R_s}

5. **Shunt Resistance Correlation**

The trend of shunt resistance has a trend inversely proportional to the irradiance, [], following equation is optimized:

$$R_{sh} = R_{sh,STC} \cdot \frac{G_{STC}}{G}$$

Where:

- R_{sh} is the shunt resistance (Ω)

- $R_{sh,STC}$ is the shunt resistance in STC (Ω)

The optimization coefficient is $R_{sh,STC}$

4.3.2 Normalized Root Mean Square Error (*NRMSE*)

The Normalized Mean Square Error (NMSE) is a measure of the mean relative scatter and reflects the random errors. It is used to compute the errors between the experimental points and fitting surfaces. This operation is performed for the 5 parameters of the model using the same expression. The X symbols can be replaced by the symbol of the parameter analysed (i.e. I_{ph}, I_0, n, R_s, R_{sh}).

$$NRMSE_X = \frac{\sqrt{\frac{\sum_{i=1}^{N_{points}}(\chi_{cor} - \chi_{exp})^2}{N_{points}}}}{\frac{\sum_{i=1}^{N_{points}} \chi_{exp}}{N_{points}}} \cdot 100$$

Where:

- $NRMSE_X$ is the normalized root mean square error for parameter χ (%)
- χ_{exp} is the experimental paramter value
- χ_{cor} is the estimation from correlation parameter value
- N_{points} is the number of points in the experiemtal samples

4.4 Step 4: Power Validation

The last step of this research consists of maximum power point or power validation from weather conditions (module irradiance and temperature). In this procedure, input an experimental set of data, the module datasheet information, and the correlation coefficient of each model. The estimation of the power is calculated with the application of the correlation. The five parameters (i.e. $I_{ph}, I_0, n, R_s, R_{sh}$) are calculated from the coefficients (i.e. $I_{ph,STC}, \alpha, I_{0,STC}, \chi, a, b, c, R_{s,STC}$, $\lambda, R_{sh,STC}$

) for a given couple of irradiance and temperature (*G, T_c)*. By drawing the I-V curve and the maximum power point is found on the curve. Later, the power is calculated with the Osterwald method to compare the two approaches. In this case, the Osterwald equation is following:

$$P_{Osterwald} = P_{STC} \cdot \frac{G}{G_{STC}} \cdot \left(1 + \frac{\gamma}{100} \cdot \left(T_c - T_{c,STC}\right)\right)$$

Where:

- $P_{Osterwald}$ is the power calculated by the Osterwald method (W)
- P_{STC} is the power in STC from the datasheet (W)
- γ is the power thermal coefficients ($\% \cdot K^{-1}$)
- G is the module irradiance ($W \cdot m^{-2}$)
- T_c is the module temperature (K)
- G_{STC} is the irradiance in STC (i.e. 1000 $W \cdot m^{-2}$)
- $T_{c,STC}$ is the module temperature in STC (i.e. 298,15 K)

The goodness of the power estimation may be assessed with the Normalized Root Mean Square Error (*NRMSE)* between the experimental power and the estimated ones. This computation is performed for each model using the same expression.

$$NRMSE_{P_{MPP}} = \frac{\sqrt{\frac{\sum_{i=1}^{N_{points}} \left(P_{MPP,model} - P_{MPP,exp}\right)^2}{N_{points}}}}{\frac{\sum_{i=1}^{N_{points}} P_{MPP,exp}}{N_{points}}} \cdot 100$$

Where:

- $NRMSE_{P_{MPP}}$ is the normalized root mean square error on the power at MPP (%)
- $P_{MPP,exp}$ is the experiemental power at MPP (W)
- $P_{MPP,model}$ is the estimated power at MPP with the model under exam (W)

- N_{points} is the number of points in the dataset (-)

Chapter 5

5 Experimental Campaign

I will comment on the experimental data used in this thesis in this chapter. I developed this thesis during exceptional circumstances caused by COVID-19, thanks to the ease in the restriction, which let me complete the planned six-month activity physically.

I used the measuring system described in chapter 3 to carry out the experimental campaign. Moreover, the PV modules selected for this study belong to monocrystalline silicon technology. In particular, the Sharp module was measured using PVPM – Automated I-V tracer, while the Luxor was measured using Automated Tracker system. In addition, it is essential to state that before starting the experimental campaign, the PV modules under test were calibrated by an independent certified laboratory (CIEMAT laboratory). The calibration aimed to obtain the main electrical characteristics and check for the electrical response of the modules. This step was necessary to guarantee non-defective I-V curves and, therefore, to ensure the overall study's accuracy and significance.

In this chapter, a brief description of the module under-test and the corresponding experimental campaign will be carried out, emphasising the data set available and the filtering procedure applied for this study.

5.1 Profile of Sharp Module

The Monocrystalline Silicon Technology is composed of pure form of silicon in which cells are made from thin slices from the block of crystals. As already explained in the chapter 1.2, it is highly efficient technology compared to others on the other costly too.

In particular, the model of the module under test is a Sharp NU-E245J5 module. The main specifications from the manufacturer and calibration are summarized in the following tables:

Table 5-1: Main specification of Sharp module.

	P_{MPP} (W)	***V_{MPP} (V)***	***I_{MPP} (A)***	***V_{oc} (V)***	***I_{sc} (A)***	***FF (%)***
Manufacturer	245	30.5	8.04	37.5	8.73	74.9
CIEMAT Lab	243.4	30.2	8.07	37.44	8.74	74.4

Table 5-2: Temperature coefficients of the Sharp module.

	α (I_{sc}) (%/K)	***β (V_{oc}) (V/K)***	***`γ (P_{max}) (%/°C)***	***NOCT (°C)***
Manufacturer	0.053	-0.347	-0.485	47.5

I carried out the experimental measurement campaign of the monocrystalline silicon Sharp module between April and July 2021. Throughout these four months of measurement, the module was tested in different weather conditions. A series of charts is reported in the following pages to show the conditions in which the measures took place. The analysis in the Figure below is made to see the distribution of the most critical weather conditions using the histogram representations. The irradiation data were recorded at high GTI due to the sun tracking, especially in the ranges between 250 and 1100. Instead, the module temperature shows a more widespread tendency thanks to the campaign, mainly covering the fields between 35 and 65 °C. Furthermore, a high quantity of measurements is recorded under scattered air temperature and low wind speed values (below 5 m/s).

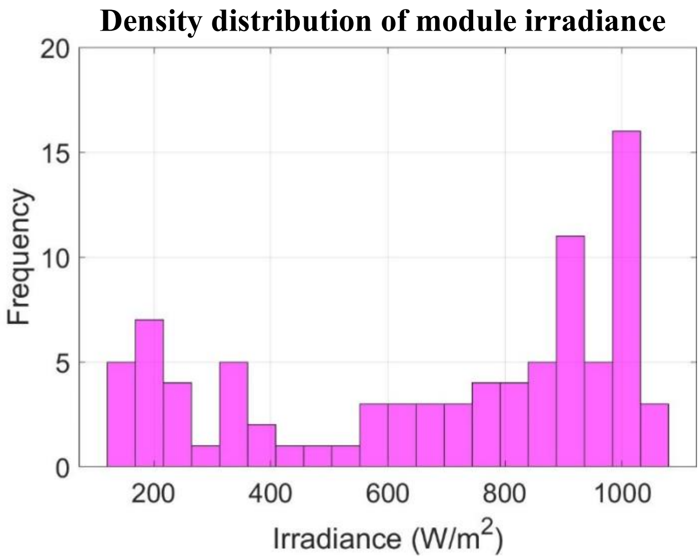

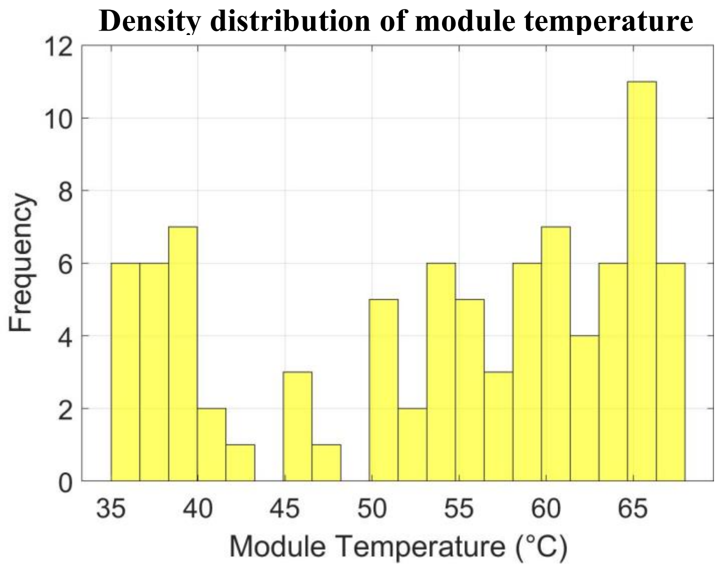

Figure 5-1: Density distribution of the irradiance and temperature conditions for Sharp module

The parameters extraction is made on a limited dataset which only involves the use of 198 I-V curves. This dataset is composed of all the reliable I-V curves for parameters extraction. Figure below shows the couples of irradiances and temperature of the I-V curves.

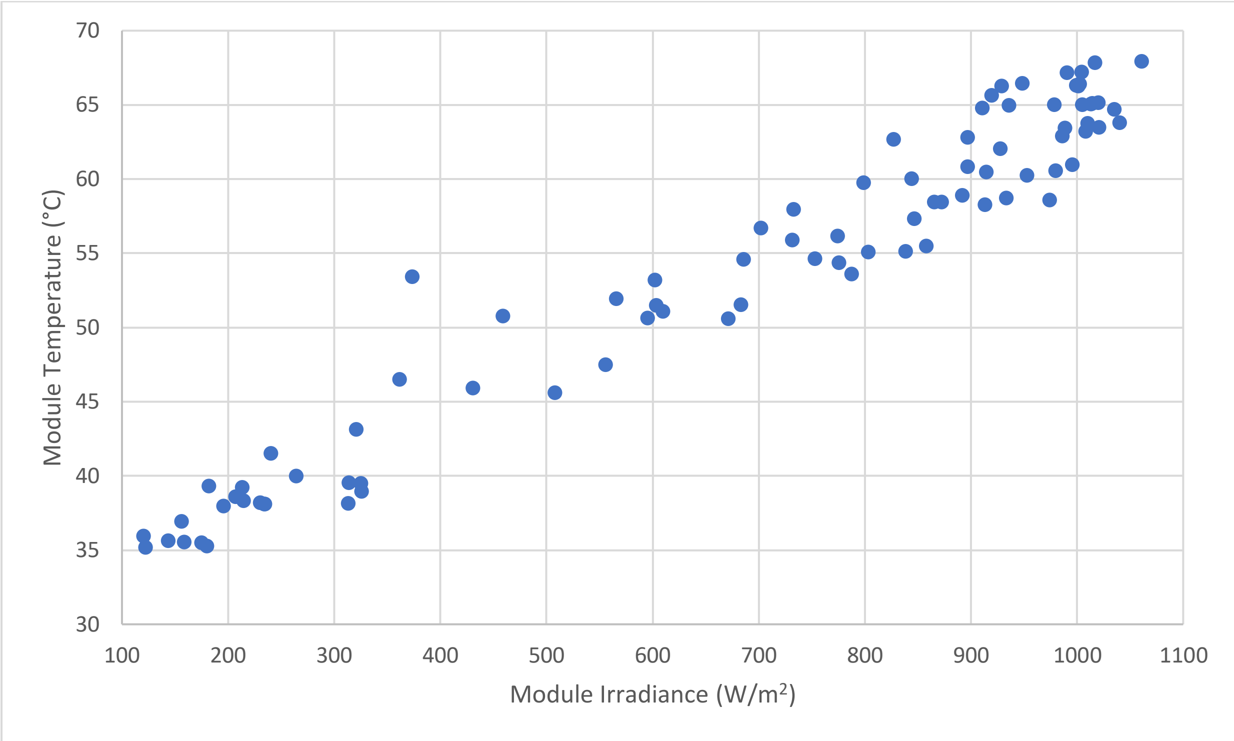

Figure 5-2: Irradiance and temperature of the I-V curves for parameters extraction.

In the end, of the 87 measures acquired, only 85 are reliable and have been used for energy estimation purposes. Moreover, for what concerns the parameter extraction, only 87 curves remained after the various filter

5.2 Profile of Luxor Module

The technology of this module same as that of the Sharp: monocrystalline silicon, As mentioned previously, it is composed of a pure form of silicon in which cells are made from thin slices from the block of crystals. As already explained in chapter 1.2, it is highly efficient technology compared to others costly.

In particular, the module model under test is a Luxor LX-100M, 125-36 module. The main specifications from the manufacturer and calibration are summarized in the following tables:

Table 5-3: Main specifications of Luxor module.

	P_{MPP} (W)	***V_{MPP} (V)***	***I_{MPP} (A)***	***V_{oc} (V)***	***I_{sc} (A)***	***FF (%)***
Manufacturer	100	18.70	5.39	21.60	5.87	79.5
CIEMAT Lab	99.178	18.218	5.444	22.892	5.750	75.3

Table 5-4: Temperature coefficient of the Luxor module.

	α (I_{sc}) (%/K)	***β (V_{oc}) (V/K)***	***`γ (P_{max}) (%/°C)***	***NOCT (°C)***
Manufacturer	0.05	-0.35	-0.49	45.9

I carried out the experimental measurement campaign of the monocrystalline silicon Luxor module between April and July 2021. Throughout these four months of measurement, the module was tested in different weather conditions. A series of charts is reported in the following pages to show the conditions in which the measures took place. The analysis in the Figure below is made to see the distribution of the most critical weather conditions using the histogram representations. The irradiation data were recorded at high GTI due to the sun tracking, especially in the ranges between 250 and 1100. Instead, the module temperature shows a more widespread tendency thanks to the campaign, mainly covering the fields between 35 and 65 °C. Furthermore, a high quantity of measurements is recorded under scattered air temperature and low wind speed values (below 5 m/s).

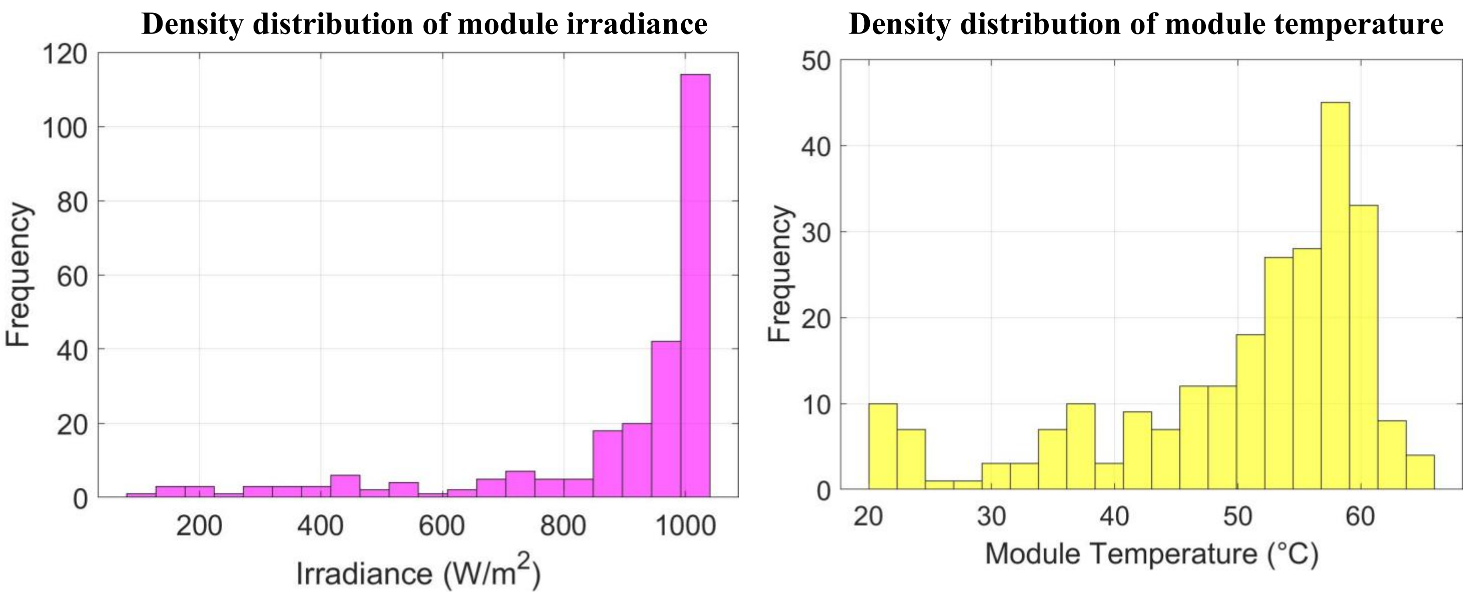

Figure 5-3: Density distribution of the irradiance and temperature conditions for Luxor module

The parameters extraction is made on a limited dataset which only involves the use of 198 I-V curves. This dataset is composed of all the reliable I-V curves for parameters extraction. The figure below shows the couples of irradiances and temperature of the I-V curves.

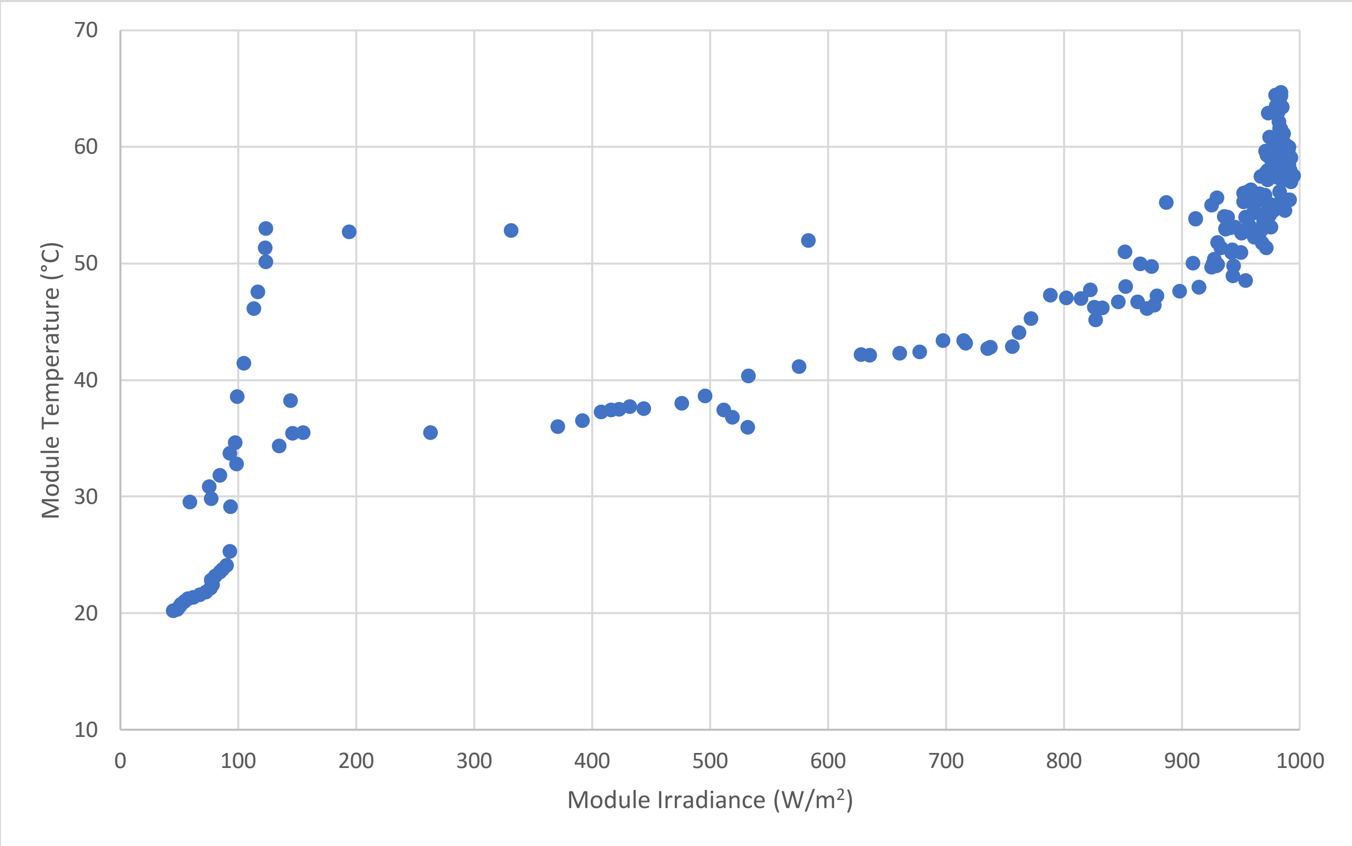

Figure 5-4: Irradiance and temperature of the I-V curves for parameters extraction.

Chapter 6

6 PV Module: Sharp Results

The analysis of the monocrystalline silicon module of sharp will going to be present in this chapter. This will include the results of parameter extraction, moreover, the founded correlations for each parameter. Lastly, the module power and energy results will be shown. The analysis is carried out with optimization method, the Levenberg – Marquardt (LM).

6.1 Parameters Extraction

The goal of the parameter's extraction procedure is to obtain a set of parameters that can approximate as best as possible the I-V curve in analysis using the explicit transcendental equation. This process has applied to all the 88 curves. Nonetheless, after the extraction, the set of parameters has been filtered to remove those affected by overfitting. The following filters have been applied:

- 5 parameters extraction model.
- Optimization algoritm: LM (tolereance 1×10^{-30}, No. of iteration is 1000).
- Error on Maximum Power below 2%.
- NRMSE below 0.02.
- Series Resistance below 0.8 Ω.
- Shunt Resistance below 20000 Ω.

In the end, the feasible parameters left were 85 for Levenberg – Marquardt.

6.2 Parameters Correlation

The extracted parameters have been used to estimate the correlations that describe their behaviours as a function of the atmospheric conditions. In particular, the procedure has been applied to the parameters extracted with the LM method: since all the parameters will be analysed separately to discuss the accuracy of the correlations and the physical meaning associated with each behaviour. Nonetheless, the coefficients of the correlations obtained from the non-linear regressions are summarised in the following tables.

Table 6-1: Coefficients of the correlations with LM method for Sharp module.

	$I_{ph}(A)$	$I_0(A)$	*n (-)*	R_s *(Ω)*	R_{sh} *(Ω)*
a	8.53	2.06×10^{-08}	1.07	0.30	526.32
b			$3.14 \cdot 10^{-05}$	0.0304	
c			$6.62 \cdot 10^{-04}$		

The correlations estimate how the five parameters vary with respect to the irradiance and cell temperature. The trend of each parameter is graphically presented for LM optimized method. The parameters are represented in the following order: photogenerated current, diode saturation current, diode ideality factor, series resistance and shunt resistance.

Firstly, the photogenerated current (I_{ph}) presents a main dependence on the irradiance. It can be observed that the dependence on cell temperature is negligible. In addition, the correlation equation comes from the equation. The $I_{ph,STC}$ coefficient is optimized by the correlation while the α is taken from the manufacturer datasheet. Figure below clearly show the irradiance tendence respectively for LM.

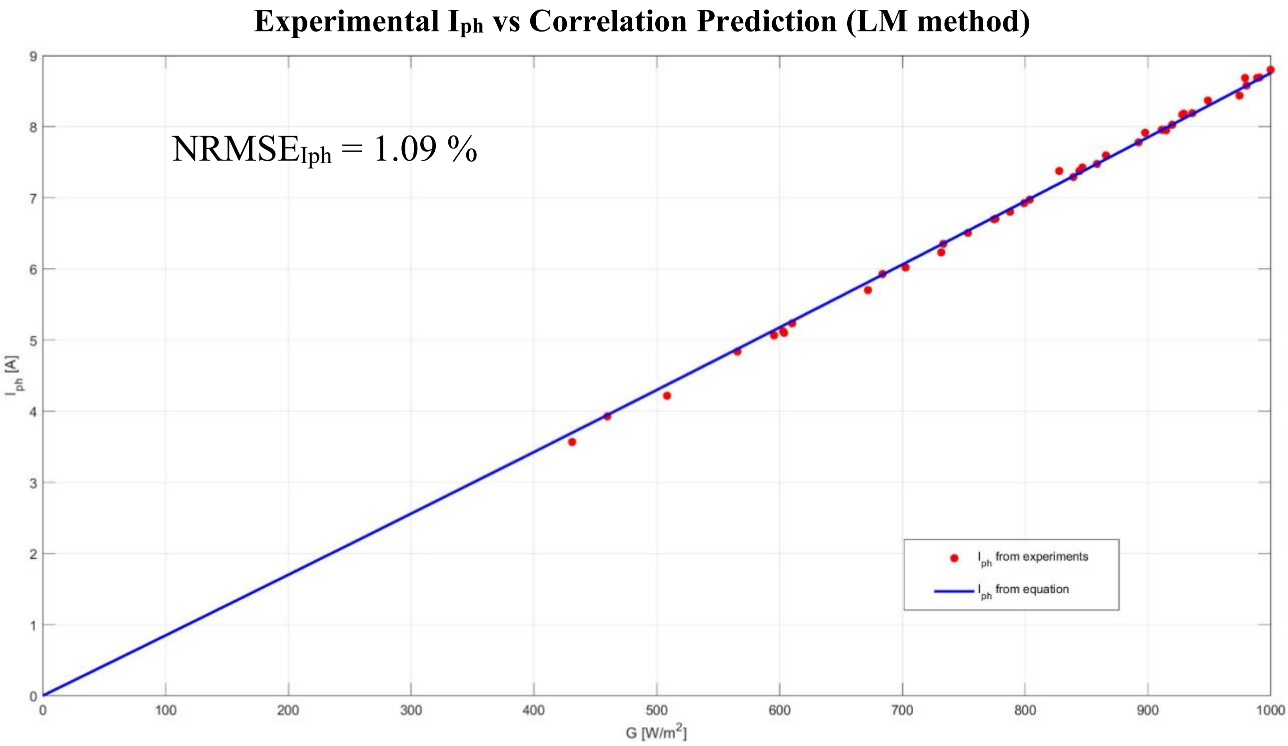

Figure 6-1: I_{ph} tendency with irradiance (LM algorithm).

$$I_{ph} = 8.53 \cdot \left(1 + \left(5.3 \cdot 10^{-4} \cdot \left(T_c - T_{c,STC}\right)\right)\right) \cdot \frac{G}{G_{STC}}$$

The red dots show the I_{ph} values from the LM optimization (i.e. experimental) while the blue line shows the trend of the correlation in the above equation. The goodness of the correlation is confirmed by the NRMSE value of 1.09%.

Secondly, the diode saturation current (I_0) presents only a dependence on the cell temperature. The correlation equation comes from the equation (xx). The $I_{0,STC}$ and χ coefficients are optimized by the correlation. Figure below show this tendence.

Experimental I_0 vs Correlation Prediction (LM method)

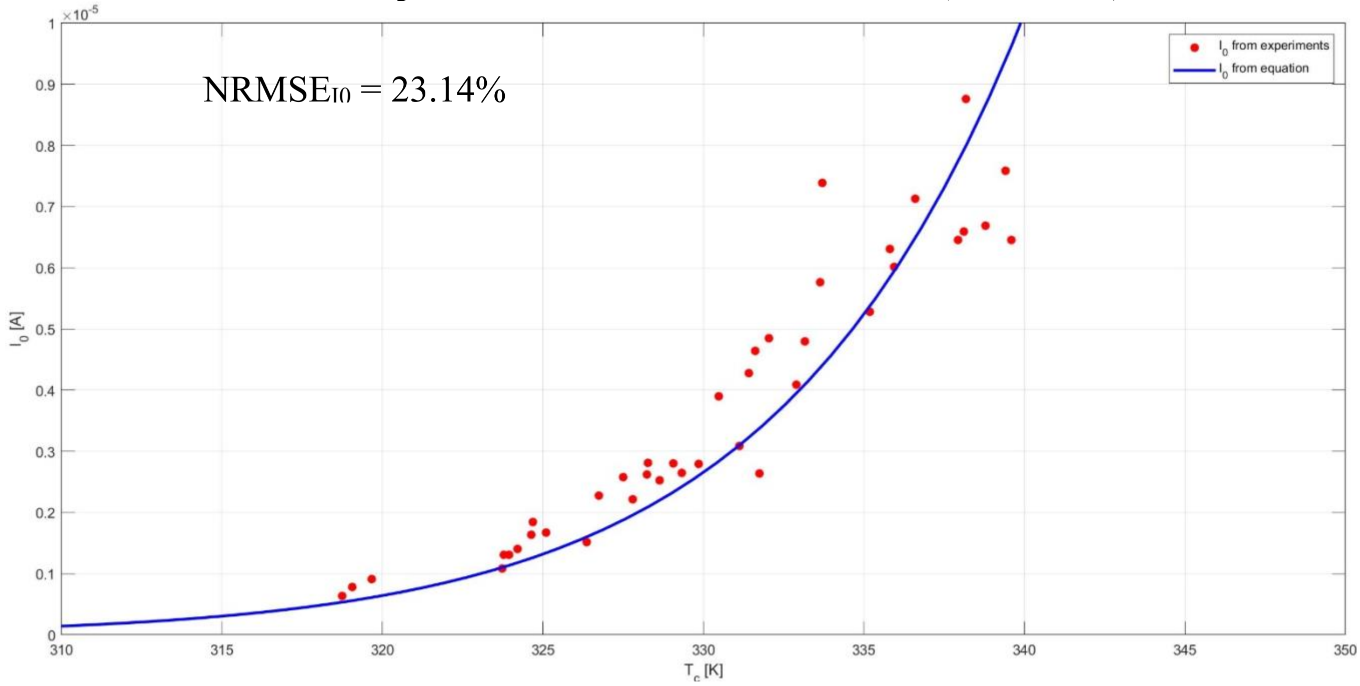

Figure 6-2: I_0 tendency with temperature.

$$I_0 = 2.06 \cdot 10^{-08} \cdot \left(\frac{T_c}{T_{c,STC}}\right)^3 \cdot \exp\left(\left(\frac{E_{g,STC}}{T_{STC}} - \frac{E_g(T_c)}{T_c}\right) \cdot \frac{1}{k_B}\right)$$

The red dots indicate the I_0 values from the LM optimization (i.e. experimental) while the blue line shows the trend of the correlation in the above equation. The goodness of the correlation is confirmed by the NRMSE value of 23.14%. Moreover, this value is typical for the diode saturation current correlation.

Thirdly, the diode ideality factor (n) presents low variation with irradiance and cell temperature. The correlation equation comes from the equation (xx). In addition, the a, b and c coefficients are optimized by the correlation. Figure below evidently show the irradiance and temperature tendencies respectively for LM methods.

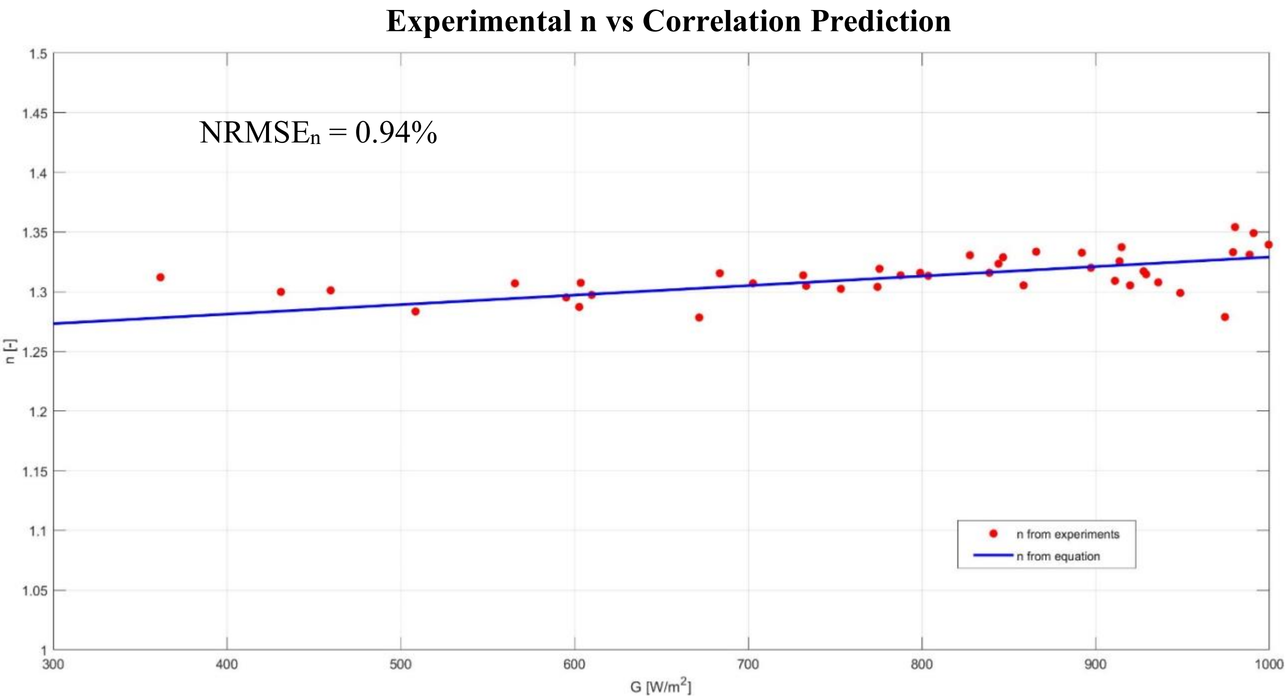

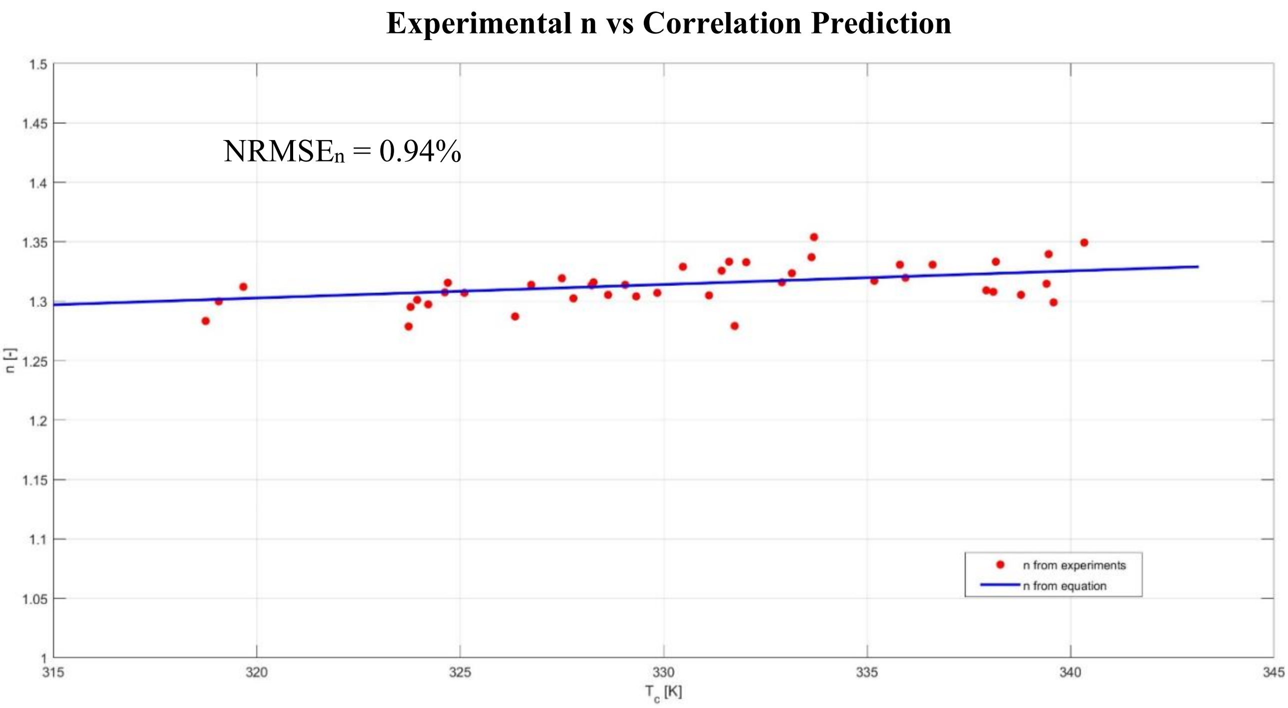

Figure 6-3: n tendency with irradiance and temperature.

$$n = 1.07 + 3.13 \cdot 10^{-05} \cdot G + 6.62 \cdot 10^{-04} \cdot T_c$$

The red dots highlight the n values from the LM optimization (i.e. experimental) while the blue line shows the trend of the correlation in the above equation. The goodness of the correlation is confirmed by the NRMSE value of 0.94%. Finally, this value is typical for the diode ideality factor correlation. The ideality factor shows an increased tendency with both irradiance and temperature.

Fourthly, the series resistance (R_s) shows variation with irradiance and cell temperature. The correlation equation comes from the equation. The $R_{s,STC}$ and λ_{Rs} coefficients are optimized by the correlation. Figure below evidently report the irradiance and temperature tendencies respectively for LM method.

Experimental R_s vs Correlation Prediction

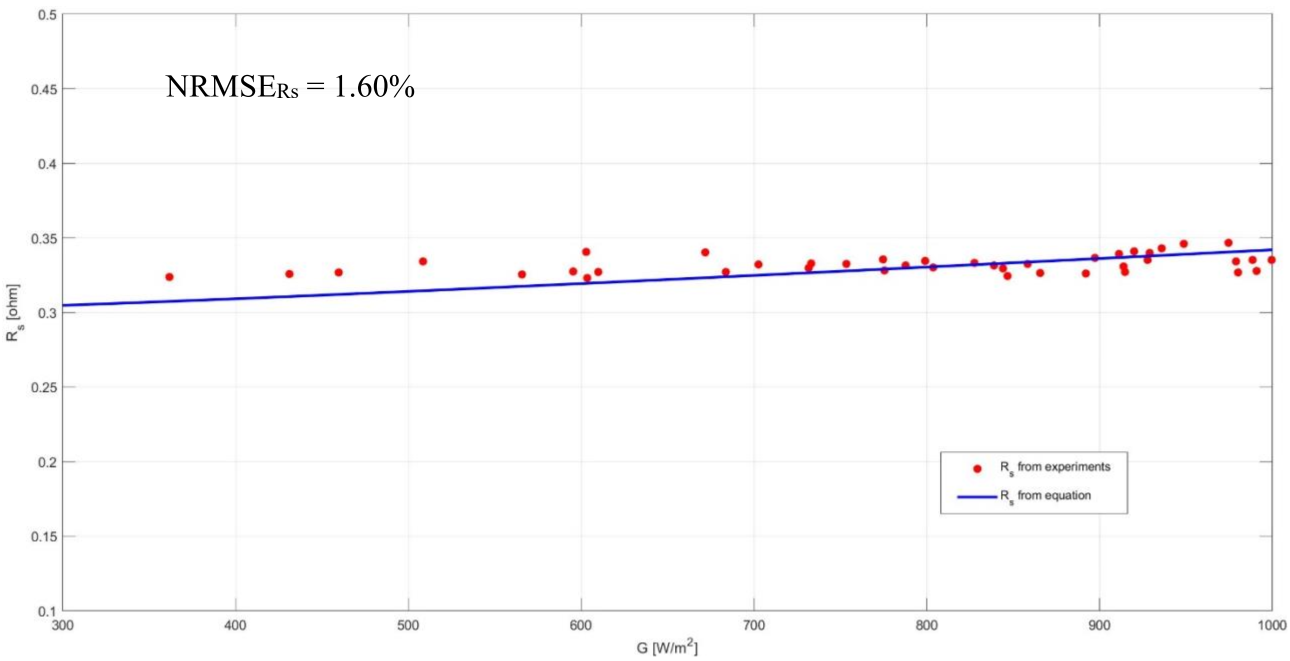

Experimental R_s vs Correlation Prediction

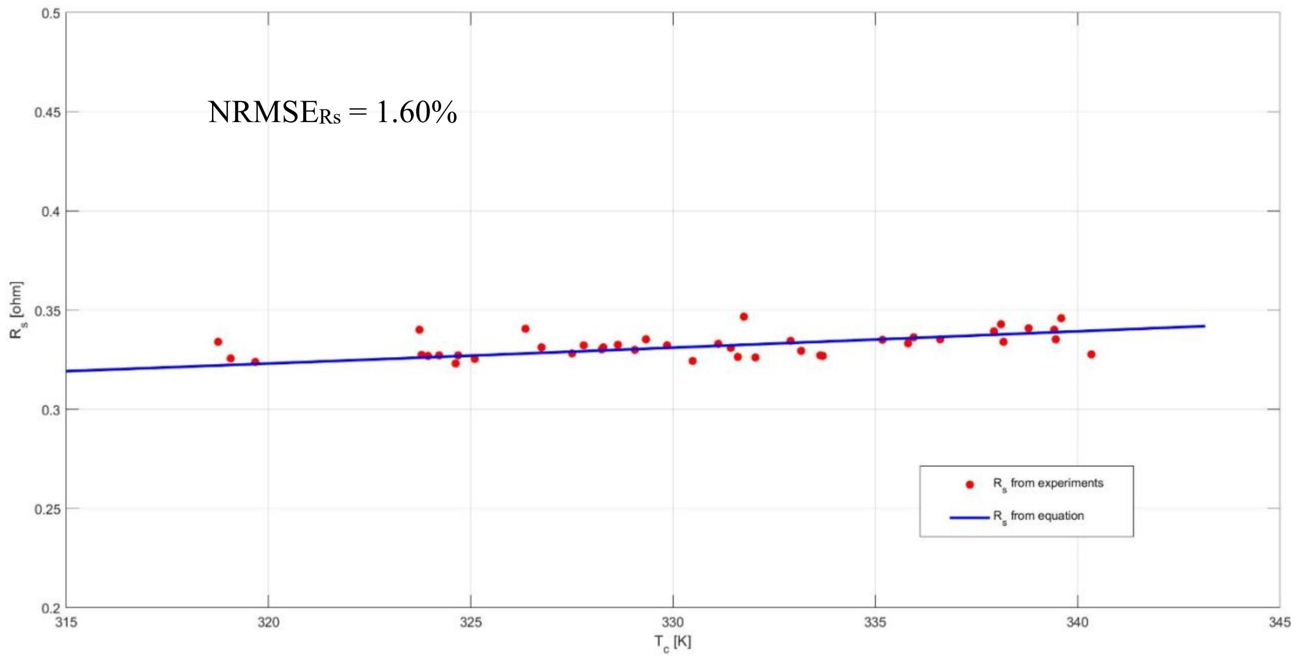

Figure 6-4: R_s tendency with irradiance and temperature.

$$R_s = 0.30 \cdot \frac{T_c}{T_{c,STC}} \cdot \left(1 - 0.0304 \cdot \log\left(\frac{G}{G_{STC}}\right)\right)$$

The red dots show the R_s values from the LM optimization (i.e. experimental) while the blue line shows the trend of the correlation in the above equation. The goodness of the correlation is confirmed by the NRMSE value of 1.60%. This value is typical for the series resistance correlation. The series resistance shows an increased tendency with both irradiance and temperature.

Finally, the shunt resistance (R_{sh}) shows variation with irradiance and cell temperature. The correlation equation comes from the equation. The $R_{sh,STC}$ coefficient is optimized by the correlation. Figure below illustrate the irradiance tendency respectively for LM method

Experimental R_{sh} vs Correlation Prediction

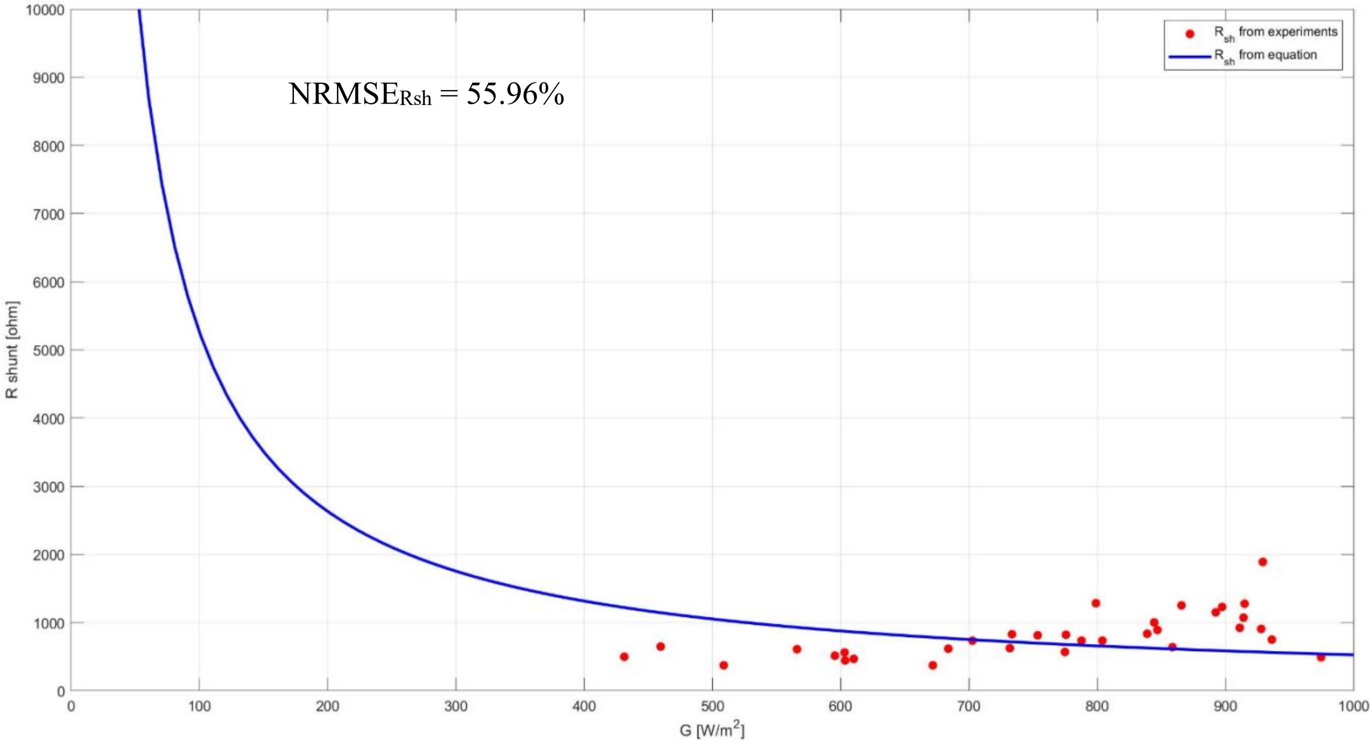

Figure 6-5: R_{sh} tendency with irradiance.

$$R_{sh} = 55.96 \cdot \frac{G_{STC}}{G}$$

The red dots indicate the R_{sh} values from the LM optimization (i.e. experimental) while the blue line highlights the trend of the correlation in the above equation. Besides, the plot shows a scattered tendency. This tendency is typical for the shunt resistance because this parameter has little influence in the optimization process if big enough. Therefore, the NRMSE value of 55.96% is acceptable.

The last analysis on the results of the correlation consists in redrawing the experimental I-V curve with the found correlations. Figure shown below the seven experimental I-V curves compared to the respective approximations found with the correlations.

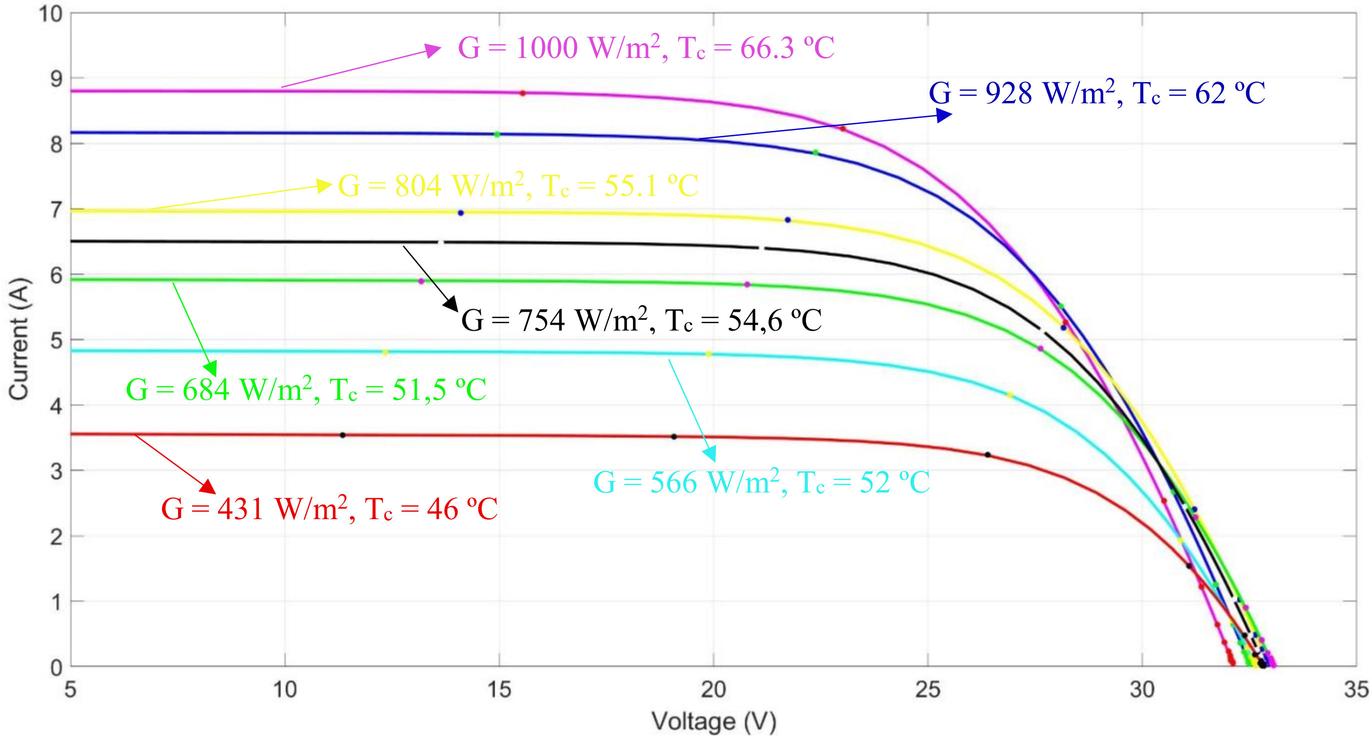

Figure 6-6*: I-V* curves experimentally measured (dots) and trend estimated with the correlation.

The model trends fit the experimental I-V curve with a good approximation for all the levels of irradiance.

6.3 Power Validation

The maximum power experimental data are compared to the maximum power estimated data from the two models (i.e. LM, and Osterwald). This comparison is performed in two ways. The first analysis is performed on a single day. Figure below shows the shape of the power during a day. They overestimate the experimental power especially during the central hour. In particular, the LM method presents a NRMSE 4.59% for that day. On the other hand, the Osterwald method overestimates even more the experimental data. In this case, the NRMSE value is 6.14%. In summary, the use of the proposed correlation method leads to a reduction of the NRMSE, compared to the Osterwald method.

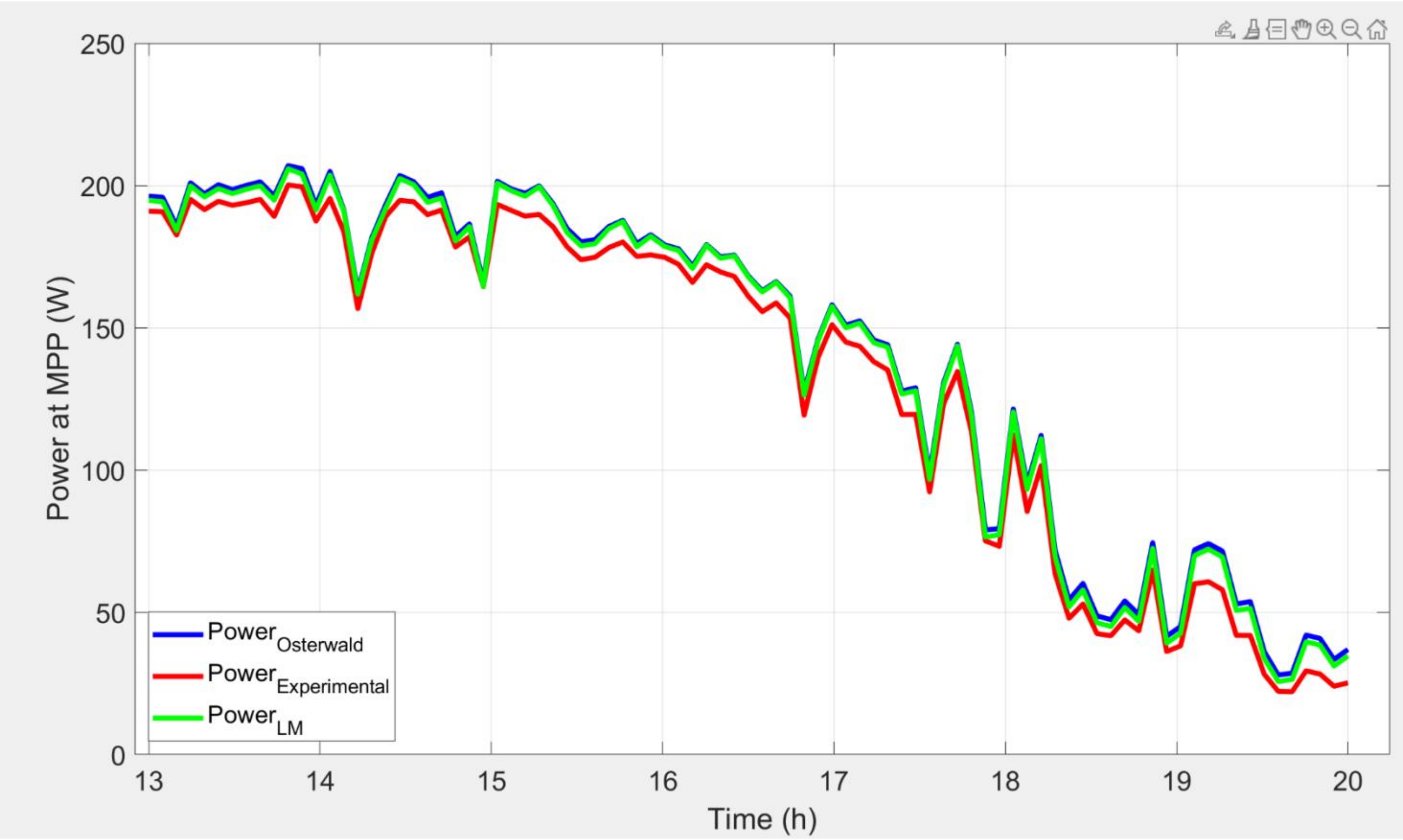

Figure 6-7: Comparison of power estimation for one day. LM and OM are overlapped.

In particular, a set of 85 curves is obtained with the LM algorithm. The most significant error on the energy with the LM dataset is respective in power profile. The curve estimated with LM is closer to experimental data than the Osterwald one.

Chapter 7

7 PV Module: Luxor Results

The analysis of the monocrystalline silicon module of Luxor will be going to be present in this chapter. This will include the results of parameter extraction, moreover, the founded correlations for each parameter. Lastly, the module power and energy results will be shown. The analysis is carried out with the optimization method, the Levenberg – Marquardt (LM).

7.1 Parameters Extraction

The goal of the parameter's extraction procedure is to obtain a set of parameters that can approximate as best as possible the I-V curve in analysis using the explicit transcendental equation. This process has been applied to all 198 curves. Nonetheless, after the extraction, the parameters were filtered to remove those affected by overfitting. The following filters have been applied:

- 5 parameters extraction model.
- Optimization algorithm: LM (tolerance, No. of iteration is 1000).
- Error on Maximum Power below 2%.
- NRMSE below 0.02.
- Series Resistance below 0.8 Ω.
- Shunt Resistance below 20000 Ω.

In the end, the feasible parameters left were 126 for Levenberg – Marquardt.

7.2 Parameters Correlation

The extracted parameters have been used to estimate the correlations that describe their behaviours as a function of the atmospheric conditions. In particular, the procedure has been applied to the parameters extracted with the LM method; since all the parameters will be analysed separately to discuss the accuracy of the correlations and the physical meaning associated with each behaviour. Nonetheless, the coefficients of the correlations obtained from the non-linear regressions are summarised in the following tables.

Table 7-1: Coefficients of the correlations with LM method for Sharp module.

	$\boldsymbol{I_{ph}(A)}$	$\boldsymbol{I_0(A)}$	***n (-)***	$\boldsymbol{R_s}$ ***(Ω)***	$\boldsymbol{R_{sh}}$ ***(Ω)***
a	5.74	1.52×10^{-09}	0..85	0.35	5112.13
b			$2.27 \cdot 10^{-04}$	0.115	
c			$2.63 \cdot 10^{-04}$		

The correlations estimate how the five parameters vary concerning the irradiance and cell temperature. The trend of each parameter is graphically presented for LM optimized method. The parameters are represented in the following order: photogenerated current, diode saturation current, diode ideality factor, series resistance and shunt resistance.

Firstly, the photogenerated current (I_{ph}) presents a primary dependence on irradiance. It can be observed that the reliance on cell temperature is negligible. In addition, the correlation equation comes from the equation. The correlation optimizes the coefficient while it is taken from the manufacturer datasheet. The figure below clearly shows the irradiance tendency respectively for LM.

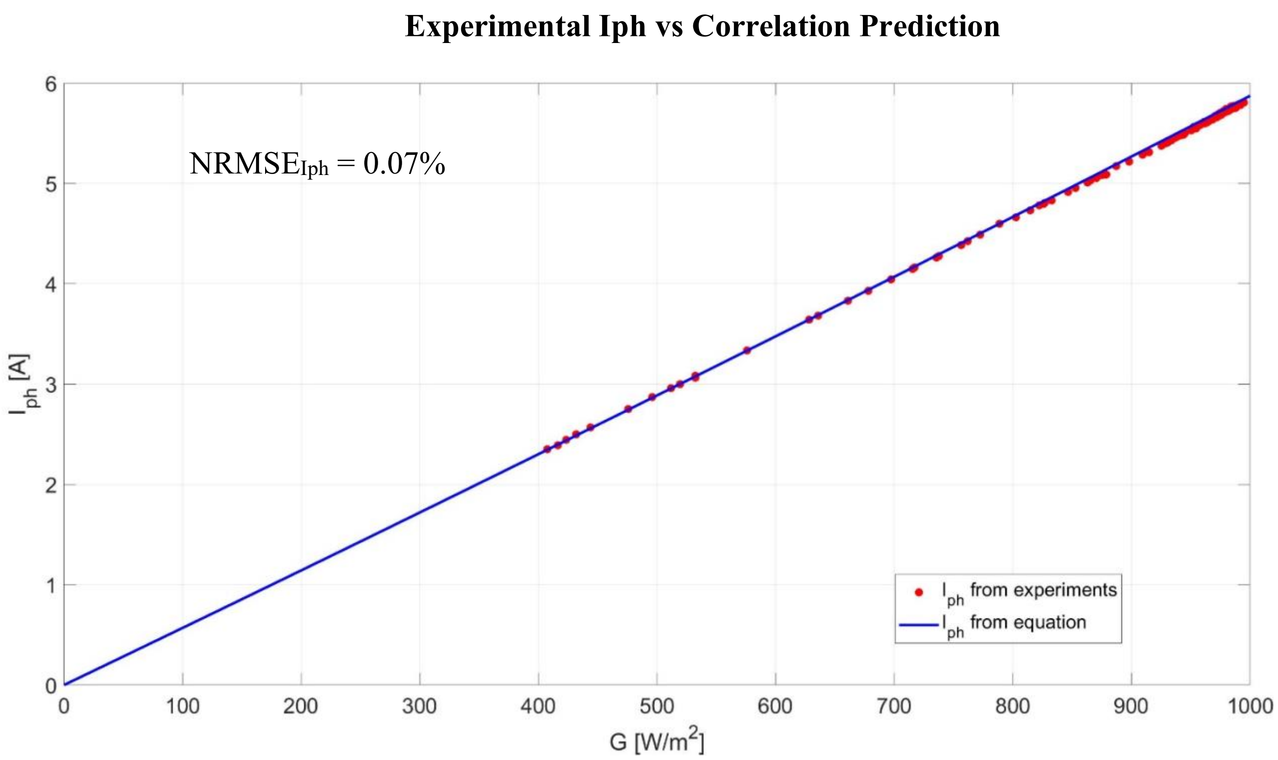

Figure 7-1: I_{ph} tendency with irradiance

$$I_{ph} = 5.74 \cdot \left(1 + \left(5.3 \cdot 10^{-4} \cdot (T_c - T_{c,STC})\right)\right) \cdot \frac{G}{G_{STC}}$$

The red dots show the I_{ph} values from the LM optimization (i.e., experimental) while the blue line shows the trend of the correlation. The goodness of the correlation is confirmed by the NRMSE value of 0.07%.

Secondly, the diode saturation current (I_0) presents only a dependence on the cell temperature. The correlation equation comes from the equation. The $I_{0,STC}$ and χ coefficients are optimized by the correlation. Figure below shows this tendence.

Experimental I_0 vs Correlation Prediction (LM method)

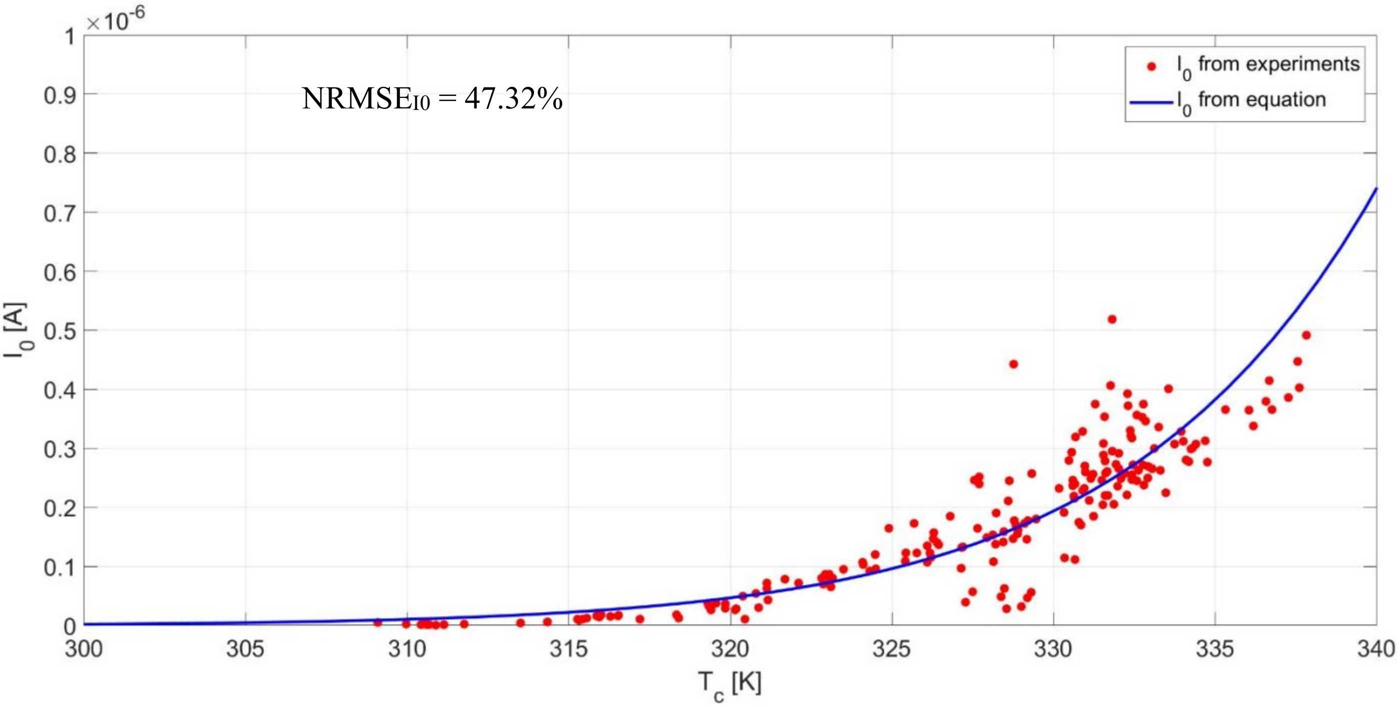

Figure 7-2: I_0 tendency with temperature.

$$I_0 = 1.52 \cdot 10^{-09} \cdot \left(\frac{T_c}{T_{c,STC}}\right)^3 \cdot \exp\left(\left(\frac{E_{g,STC}}{T_{STC}} - \frac{E_g(T_c)}{T_c}\right) \cdot \frac{1}{k_B}\right)$$

The red dots indicate the I_0 values from the LM optimization (i.e., experimental) while the blue line shows the trend of the correlation in the above equation. The goodness of the correlation is confirmed by the NRMSE value of 47.32%. Moreover, this value is typical for the diode saturation current correlation.

Thirdly, the diode ideality factor (n) presents low variation with irradiance and cell temperature. The correlation equation comes from the equation. In addition, the a, b and c coefficients are optimized by the correlation. Figure below evidently show the irradiance and temperature tendencies respectively for LM methods.

Experimental n vs Correlation Prediction

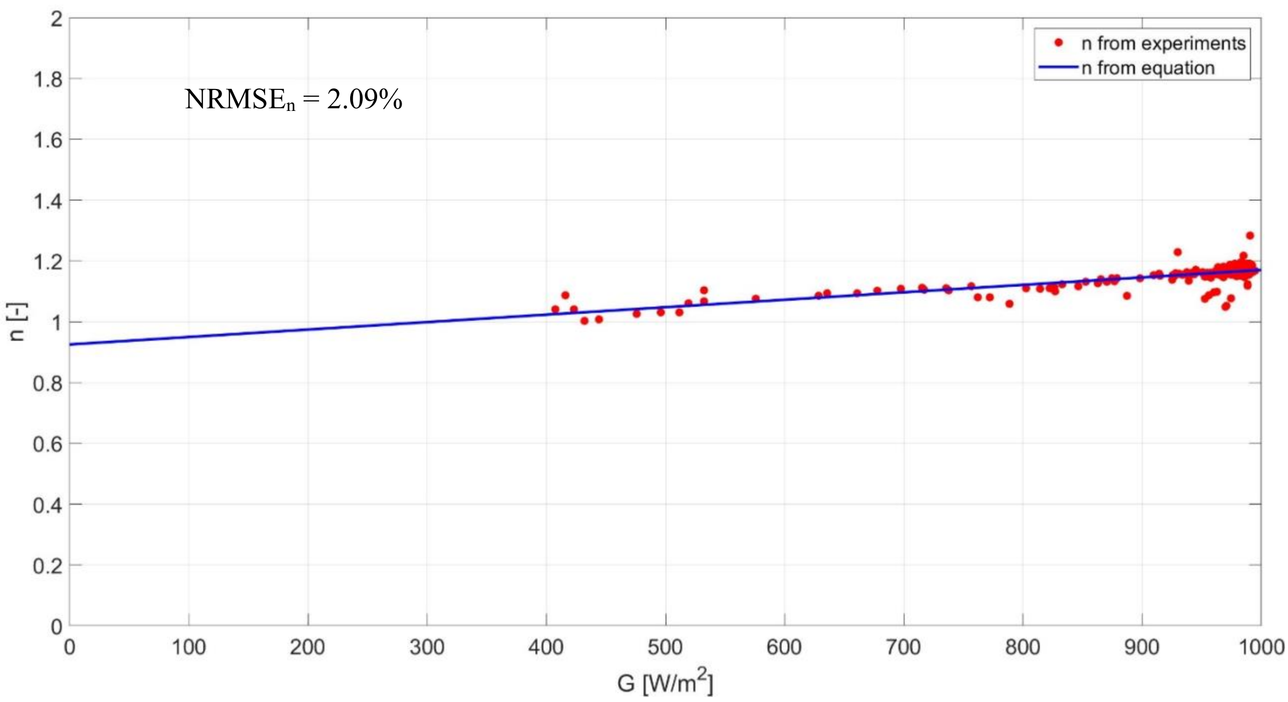

Experimental n vs Correlation Prediction

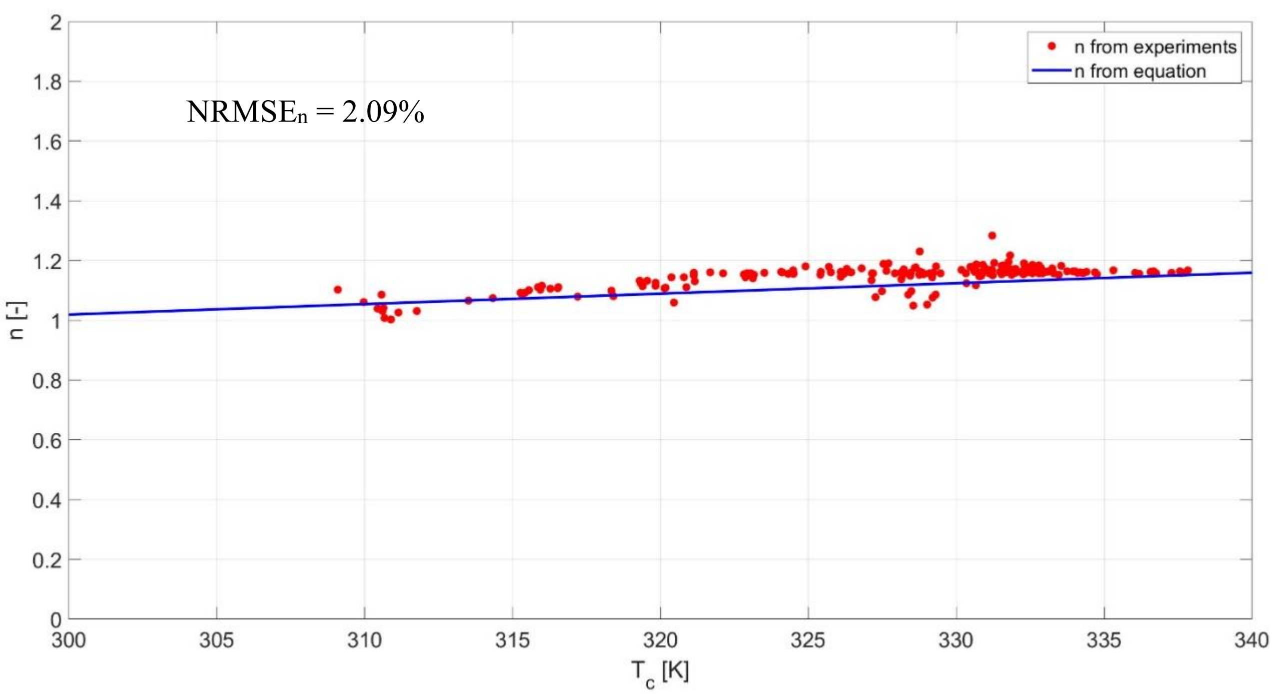

Figure 7-3: n tendency with irradiance and temperature.

$$n = 0.85 + 2.27 \cdot 10^{-04} \cdot G + 2.63 \cdot 10^{-04} \cdot T_c$$

The red dots highlight the n values from the LM optimization (i.e. experimental) while the blue line shows the trend of the correlation in the above equation. The goodness of the correlation is confirmed by the NRMSE value of 2.09%. Finally, this value is typical for the diode ideality factor correlation. The ideality factor shows an increased tendency with both irradiance and temperature.

Fourthly, the series resistance (R_s) shows variation with irradiance and cell temperature. The correlation equation comes from the equation. The $R_{s,STC}$ and λ_{Rs} coefficients are optimized by the correlation. Figure below evidently report the irradiance and temperature tendencies respectively for LM method.

Experimental R_s vs Correlation Prediction

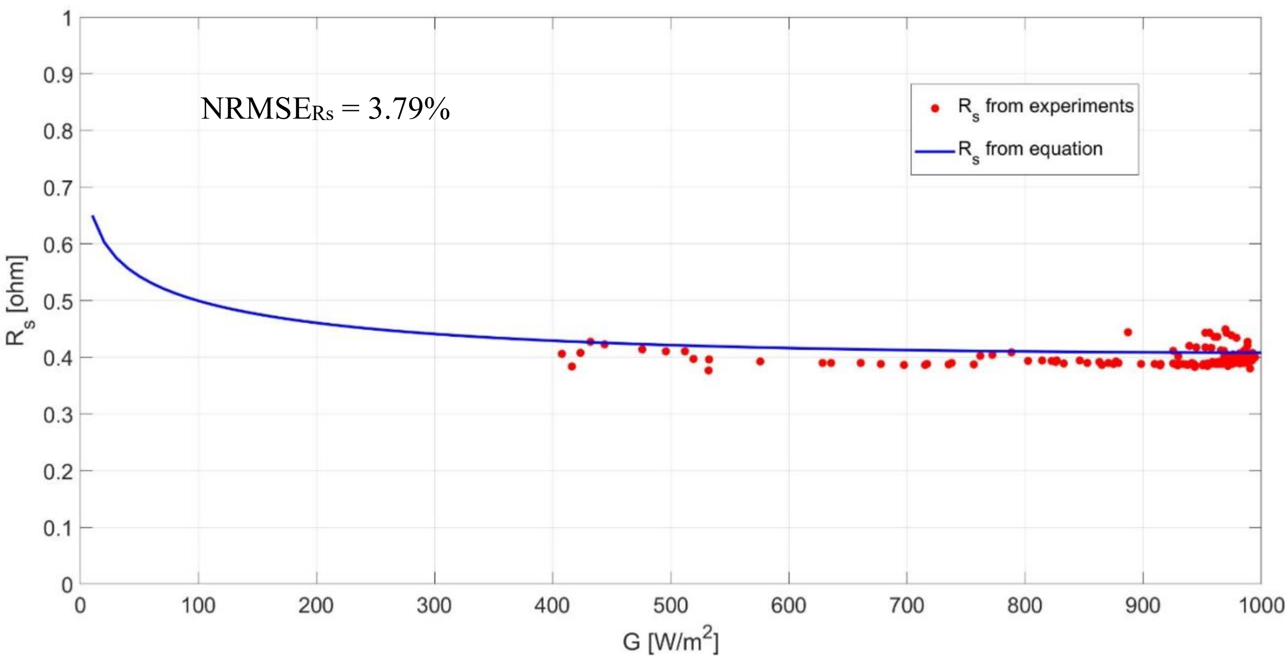

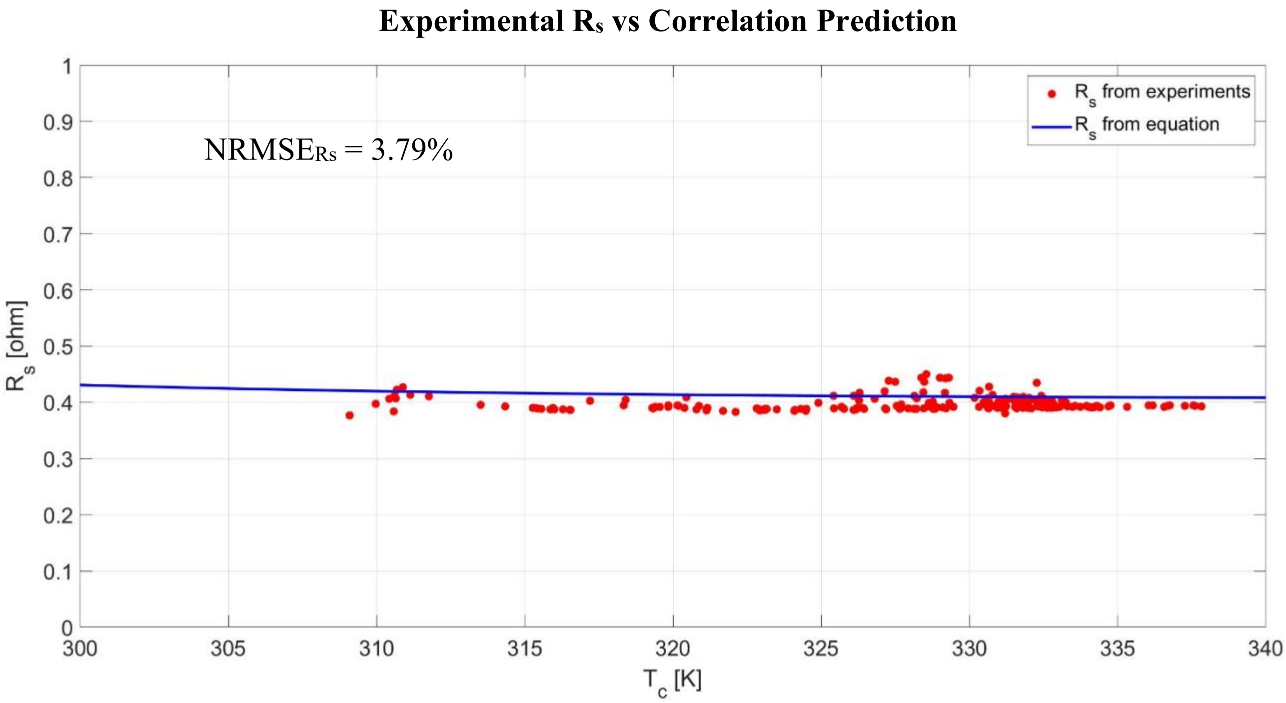

Figure 7-4: R_s tendency with irradiance and temperature.

$$R_s = 0.35 \cdot \frac{T_c}{T_{c,STC}} \cdot \left(1 - 0.115 \cdot \log\left(\frac{G}{G_{STC}}\right)\right)$$

The red dots show the R_s values from the LM optimization (i.e. experimental) while the blue line shows the trend of the correlation in the above equation. The goodness of the correlation is confirmed by the NRMSE value of 3.79%. This value is typical for the series resistance correlation. The series resistance shows an increased tendency with both irradiance and temperature.

Finally, the shunt resistance (R_{sh}) shows variation with irradiance and cell temperature. The shunt resistance presents a very disperse behaviour both with irradiance and temperature. Nonetheless, the non-linear regression has been applied anyway to find the correlations by optimizing a ($R_{sh,STC}$). The final result are computed but due to the high dispersion of the points it has been decided to not include the graphical representation since it has no clear tendency was observable while the NRMSE value of 182.11% is acceptable. The equations describing the behaviour of the shunt resistance is presented below.

$$R_{sh} = 5112 \cdot \frac{G_{STC}}{G}$$

The last analysis on the results of the correlation consists in redrawing the experimental I-V curve with the found correlations. Figure below shows the seven experimental I-V curves compared to the respective approximations found with the correlations.

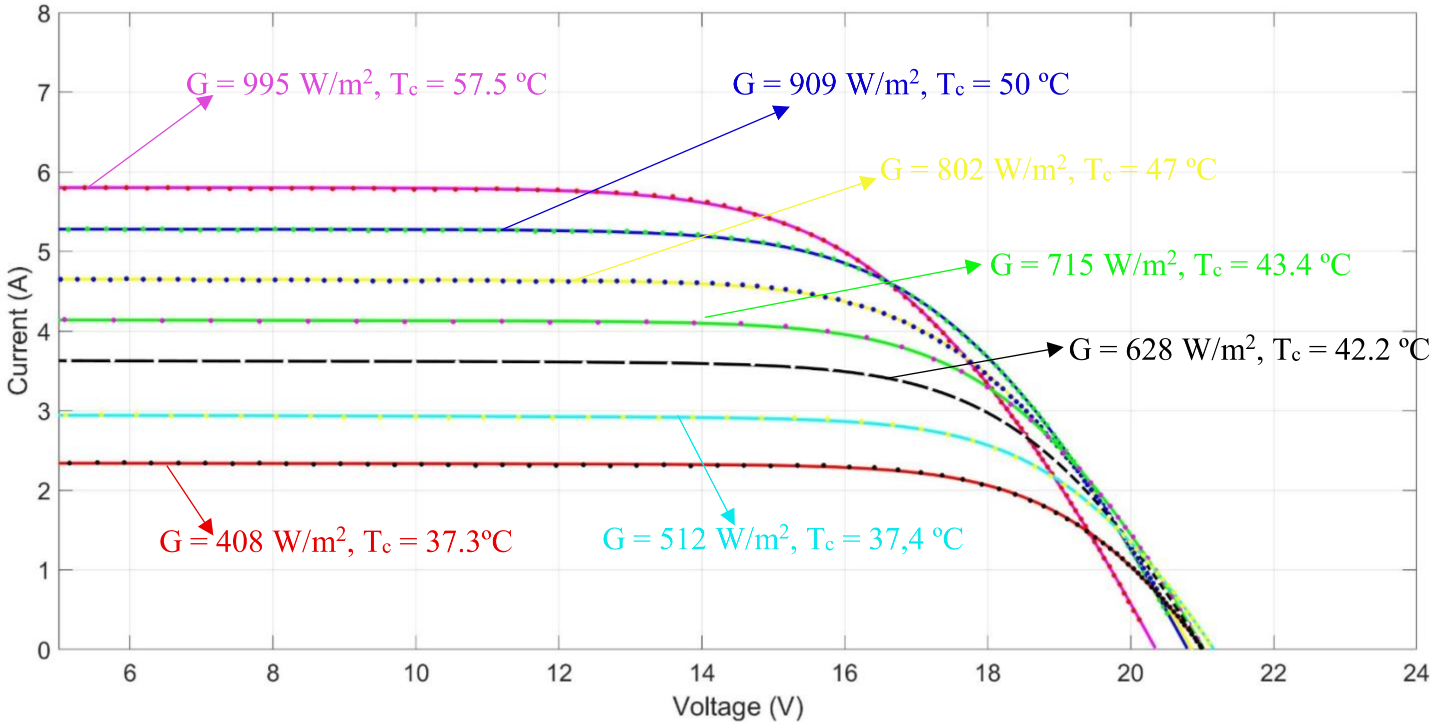

Figure 7-5: *I-V* curves experimentally measured (dots) and trend estimated with the correlation.

The model trends fit the experimental I-V curve with a good approximation for all the levels of irradiance.

7.3 Power Validation

The maximum power experimental data are compared to the estimated power from the two models (i.e. LM, and Osterwald). This comparison is performed in two ways, and the first analysis is performed on a single day. The figure below shows the shape of the power during a day. They overestimate the experimental power, especially during the central hour. In particular, the LM method presents an NRMSE of 3.36% for that day.

On the other hand, the Osterwald method overestimates, even more, the experimental data. In this case, the NRMSE value is 3.38%. In summary, using the proposed correlation method reduces the NRMSE compared to the Osterwald method.

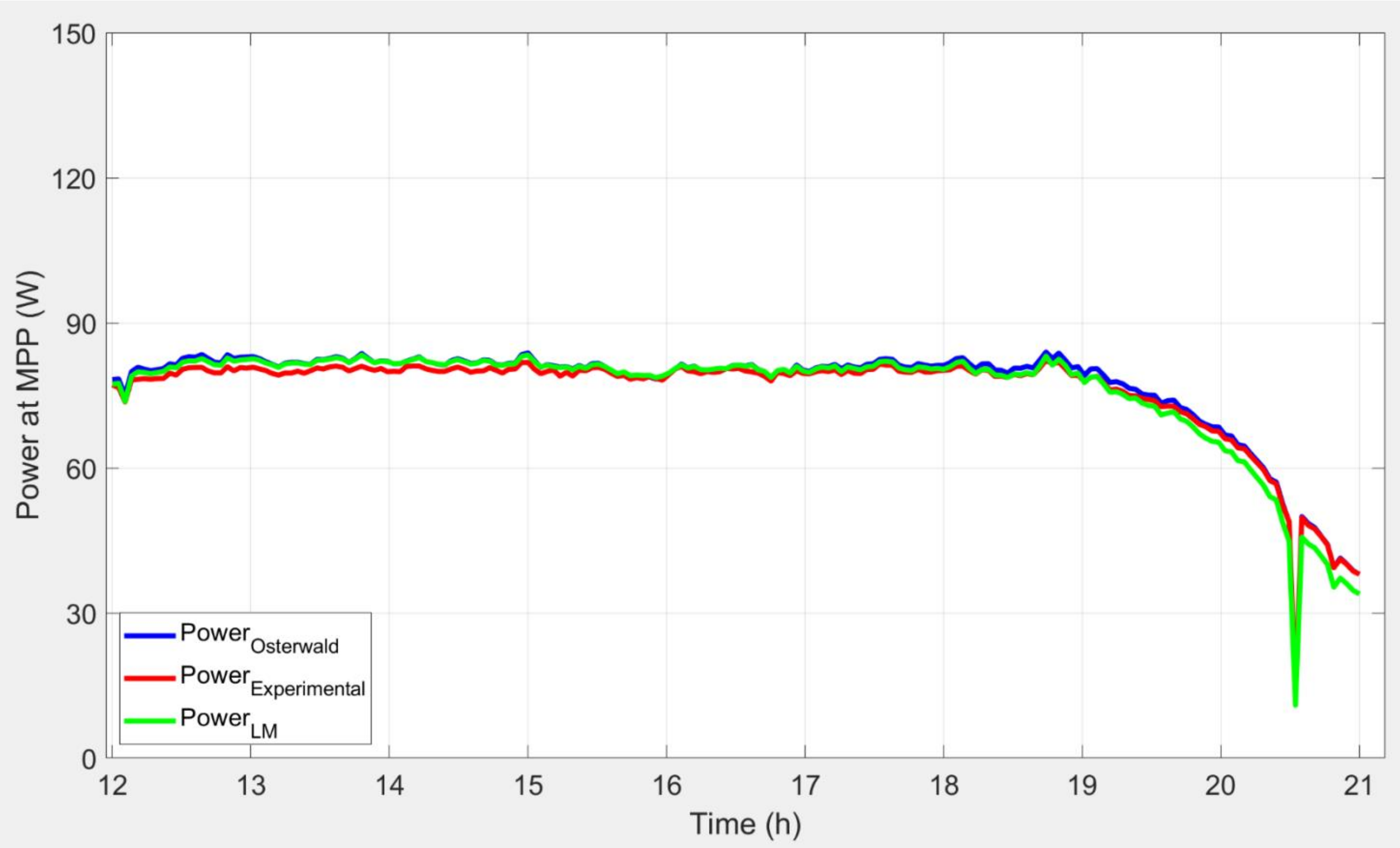

Figure 7-6: Comparison of power estimation for one day. LM and OM are overlapped.

In particular, a set of 126 curves is obtained with the LM algorithm, while the most significant error on the MPP with LM dataset coincide with the error on energy

Chapter 8

8 Conclusions

The operating function of photovoltaic generators can be illustrated using an equivalent circuit with variable parameters, which can be assumed to be constant. Moreover, the knowledge of their dependence concerning irradiance and cell temperature permits the prediction of the generated power of photovoltaic arrays in any environmental condition. This work is a part of a joint activity between Politecnico di Torino and the Universidad de Jaén (Spain): my main task of this thesis has been developed in Universidad de Jaén.

In the first part of the thesis, an ad hoc Graphical User interface (GUI) of MATLAB was used to analyse the PV module; the GUI tools allows to perform four operations: the pre-processing of the dataset; the extraction of the circuit parameters; the identification of equations, aiming at describing the dependence of each parameter concerning irradiance and cell temperature; and the comparison between experimental energy and the predicted value with several methods.

In the second part of this thesis, the GUI is applied to two monocrystalline silicon technology with high efficiencies photovoltaic modules such as Sharp NU series with a rated power of 245W and Luxor with a rated capacity of 100W. For the module of Luxor, 198 I-V curves are selected for the parameter's extraction. The remaining data are excluded due to different factors (measurement errors, mismatch conditions etc.). First, the performance of the photovoltaic module is described by the single diode model, which is an equivalent circuit consisting of five parameters. Then, the extraction procedure is performed using the optimisation method: the Levenberg-Marquardt (LM) algorithms.

Moreover, two additional filters are applied to the results of the parameters extraction to exclude the parameters sets leading to a high error in the Maximum Power Point (MPP). In particular, a group of 126 curves is obtained with the LM algorithm, while the most significant error on the MPP with LM dataset coincide with the error on energy. Starting from these two datasets, the equations describing the dependence of each parameter concerning irradiance and cell temperature are identified. The correlations show similar results to the analysed datasets. Regarding the most important parameters, the photogenerated current and the series resistance present, respectively, a Normalised Root Mean Square Error (NRMSE) of 0.07% and 3.79% for the LM datasets.

In comparison, the NRMSE of the reverse saturation current is 47.32%. In the last part of the analysis, the experimental energy and the predicted value with optimised equations are compared. Moreover, the proposed correlations are compared to the Osterwald Model (OM), the simplest and most common theoretical model used in literature to predict PV production. The results show that the LM equations predict PV energy with the lowest error, providing a deviation from experimental data of 3,36%, while the OM results exhibit an error of 3,38%.

Similarly, in the same way as above, 87 I-V curves are selected for the parameter's extraction in the Sharp module. Likewise, the remaining data are excluded due to errors or environmental conditions. Moreover, the Levenberg-Marquardt algorithm is used for optimisation at the parameter's extraction step. In addition, two additional filters are applied to the results of the parameters extraction to exclude the parameters sets leading to a high error in the Maximum Power Point (MPP). In particular, a group of 85 curves is obtained with the LM algorithm. The most significant error on the energy with the LM dataset is respective in power profile. The curve estimated with LM is closer to experimental data than the Osterwald one. The parameters correlations show results of this dataset the most essential parameters, the photogenerated current, and the series resistance present; respectively, a Normalised Root Mean Square Error (NRMSE) of 1.09% and 1.60% for the LM datasets.

In comparison, the NRMSE of the reverse saturation current is 23.13%. Moreover, the proposed correlations are compared to the Osterwald Model (OM), the simplest and most common theoretical model used in literature to predict PV production. The results show that the LM equations predict PV energy with the lowest error, providing a deviation from experimental data of 4.59%, while the OM results exhibit an error of 6.14%.

Chapter 9

9 References

[1] B. Anco S, Photovoltaics for Commercial and Utilities Power Generation, Lilburn (GA, USA): Fairmont Press, Inc., 2012.

[2] F. Spertino, Lezioni di "Solar Photovoltaic System', Torino: Politecnico di Torino, 2019/2020.

[3] M. Alonso Abella, Sistemas fotovoltaicos: introducción al diseño y dimensionado de instalaciones solares fotovoltaicas, Madrid: SAPT Publicaciones Técnicas S.L., 2005.

[4] D. Murgia, «Tecniche per l'identificazione dei difetti e per l'analisi delle performance nei moduli fotovoltaici,» Politecnico di Torino, Tesi di Laurea Magistrale, 2018.

[5] A. Scaiola, «Innovative technique to estimate the performance of a photovoltaic generator using the parameters of the single diode model equivalent circuit, » Politecnico di Torino, Tesi di Laurea Magistrale, 2019.

[6] [Online]. Available: https://www.futurasun.com/wp-content/uploads/2018/ 04/pannello-monocristallino_dettaglio.jpg.

[7] National Renewable Energy Laboratory (NREL), «Champion Photovoltaic Module Efficiency Chart,» NREL, 2019.

[8] [Online]. Available: http://www.fotovoltaicosulweb.it/immagini/upload/ guida/policristalline_panels1.jpg.

[9] SANYO Component Europe GmbH Solar Division, «HIT-240HDE4 HIT- 235HDE4 datasheet, » SANYO Component Europe GmbH, 2009.

[10] [Online]. Available: https://www.vpsolar.com/wp-content/uploads/2018/04/ tecnologia-perc-funzionamento.jpg.

[11] [Online]. Available: https://zeroemission.eu/wp-content/uploads/2020/02/ Thin-film-Solar-Cell-425x405.jpg.

[12] [Online]. Available: https://opentextbc.ca/chemistry/wp-content/uploads/sites/150/2016/05/CNX_Chem_08_04_Band.jpg.

[13] [Online]. Available: https://solarconsultant.ca/wp-content/uploads/ 2017/05/Silicon-Solar-Cell-Construction.png.

[14] U. Gangopadhyay, S. Das and S. Jana, "State of the Art of Photovoltaic Technology," in International Conference on Solar Energy Photovoltaics, Bhubaneswar, India, 2013.

[14] National Renewable Energy Laboratory (NREL), "Best Research-Cell Efficiency Chart," NREL, 2020.

[15] S. Mishra e D. Sharma, «Control of photovoltaic technology, » in *Electric Renewable Energy Systems*, Elsevier, 2016, pp. 457-486.

[16] A. Haque, «Solar energy, » in *Electric Renewable Energy Systems*, Elsevier, 2016, pp. 40-59.

[17] [Online]. Available: https://www.etechnog.com/2019/05/diode-used-solarpanel-relay.html.

[18] [Online]. Available: https://jerseyfirstis.com/wp-content/uploads/2018/ 06/solar-panel-inspection.jpg

[19] S. Gulkowski, J. V. Munoz Diez, J. Aguilera Tejero and G. Nofuentes, "Energy," Energy, vol. 172, pp. 380-390, 2019.

[20] D. W. Marquardt, «An Algorithm for Least-Squares Estimation of Nonlinear Parameters, » *Journal of the Society for Industrial and Applied Mathematics,* vol. 11, n. 2, pp. 431-441, 1963.

[21] J. A. Nelder e R. Mead, «A simple method for function minimization, » *The Computer Journal,* vol. 7, n. 4, pp. 308-313, 1965.

[22] G. Chicco, «Note sull'analisi e sull'ottimizzazione dei sistemi elettrici di distribuzione,» Politecnico di Torino, 2004.

[23] G. Blaesser and D. Munro, "Guidelines for the Assessment of Photovoltaic Plants, Document C, Initial and Periodic Tests on PV Plants," Office for Official Publications of the European Communities, Ispra, Italia, 1995.

[24] E. Durán, M. Piliougine, M. Sidrach-de-Cardona, J. Galán e J. Andújar, «Different methods to obtain the I–V curve of PV modules: A review,» in *2008 33rd IEEE Photovoltaic Specialists Conference*, San Diego, CA, USA, 2008.

[25] F. Spertino, J. Ahmad, A. Ciocia, P. Di Leo, A. F. Murtaza e M. Chiaberge, «Capacitor charging method for I–V curve tracer and MPPT in photovoltaic systems,» *Solar Energy,* vol. 119, pp. 461-473, 2015.

[26] R. Núñez, C. Domínguez, S. Askins, M. Victoria, R. Herrero, I. Antón e G. Sala, «Determination of spectral variations by means of component cells useful for CPV rating and design,» *Progress in Photovoltaics,* vol. 24, n. 5, pp. 663-679, May 2016.

[27] B. García Domingo, «Análisis, caracterización y modelado del comportamiento en exterior de módulos de concentración fotovoltaica,» Universidad de Jaén, Tesis Doctoral, 2014.

[28] Z. Stokes e A. Kaknevicius, «Reverse Current Protection in Load Switches, » TexasInstruments Inc., May 2016.

[29] S. Gulkowski, J. V. Muñoz Diez, J. Aguilera Tejero e G. Nofuentes, «Computational modeling and experimental analysis of heterojunction with intrinsic thin-layer photovoltaic module under different environmental conditions, » *Energy,* vol. 172, pp. 380-390, 2019.

[30] F. Spertino, A. Ciocia, P. Di Leo, S. Fichera, G. Malgaroli e . A. Ratclif, «Toward the Complete Self-Sufficiency of an nZEBs Microgrid by Photovoltaic Generators and Heat Pumps: Methods and Applications, » *IEEE Transactions On Industry Applications,* vol. 55, n. 6, pp. 7028-7040, Nov.-Dec. 2019..

[31] M. Norton, A. M. Gracia Amillo e R. Galleano, «Comparison of solar spectral irradiance 2015

[32] F. Ghani, M. Duke e J. Carson, «Numerical calculation of series and shunt resistance of a photovoltaic cell using the Lambert W-function: Experimental evaluation, » *Solar Energy,* vol. 87, pp. 246-253, January 2013.

[33] A. Molina-Garcia, M. Bueso, M. Kessler, J. Guerrero-Perez, J. Fuentes and E. Gomez-Lazaro, “CdTe thin-film solar module modeling using a non-linear regression approach,” in 17th Power system computation Conference, Stockholm (Sweden), 2011.

[34] R. Majdoul, E. Abdelmounim, M. Aboulfatah, A. w. Touati, A. Moutabir e A. Abouloifa, «Combined analytical and numerical approach to determine the four parameters of the photovoltaic cells models, » in *2015 International Conference on Electrical and Information Technologies (ICEIT)*, Marrakech, 2015.

[35] A. K. Tossa, Y. Soro, Y. Azoumah e D. Yamegueu, «A new approach to estimate the performance and energy productivity of photovoltaic modules in real operating conditions, » *Solar Energy,* vol. 110, pp. 543-560, 2014.

[36] M. Wolf e H. Rauschenbach, «Series resistance effects on solar cell measurements, » *Advanced Energy Conversion,* vol. 3, n. 2, pp. 455-479, 1963.

[37] C. R. Osterwald, «Translation of device performance measurements to reference conditions, » *Solar Cells,* vol. 18, n. 3-4, pp. 269-279, September–October 1985.

Chapter 10

10 Annexes

10.1 Annex A: Technical datasheet of measurement equipment

10.1.1 A.1 Technical datasheet Agilent 34411A Multimeters

Measurement Characteristics

DC Voltage

Measurement Method:
Continuously integrating multi-slope IV A/D converter

Linearity: (10 V range) 0.0002% of reading + 0.0001% of range

Input Resistance:
0.1 V, 1 V, 10 V Ranges: 10 MΩ or > 10 GΩ (Selectable)
100 V, 1000 V Ranges: 10 MΩ ± 1% (Fixed)

Input Bias Current: < 50 pA at 25 °C

Input Protection: 1000 V

DC CMRR: 140 dB[1]

True RMS AC Voltage

Measurement Method:
AC-coupled True RMS measurement. Digital sampling with anti-alias filter.

Crest Factor:
No additional error for crest factors < 10. Limited by peak input and 300 kHz bandwidth.

Peak Input:
300% of range or 1100 V

Overload Ranging:
Will select higher range if peak input overload is detected during auto range. Overload is reported in manual ranging.

AC CMR: 70 dB[2]

Maximum Input: 400 Vdc, 1100 Vpk

Input Impedance:
1 MΩ ± 2% in parallel with < 150 pF

Input Protection: 750 V_{rms} all ranges

Resistance

Measurement Method:
Selectable 2-wire or 4-wire. Current source referenced to LO input.

Offset Compensation:
Selectable on the 100 Ω, 1 kΩ, and 10 kΩ ranges

Max. Lead Resistance (4-wire):
10% of range per lead for 100 Ω, 1 kΩ. 1 kΩ per lead on all other ranges

Input Protection:
1000 V on all ranges

DC Current

Current Shunt:
200 Ω for 100 µA, 1 mA
2 Ω for 10 mA, 100 mA
0.1 Ω for 1 A, 3 A

Input Protection: 3 A, 250 V fuse

True RMS AC Current

Measurement Method:
AC-coupled True RMS measurement. Directly coupled to the fuse and shunt. Digital sampling with anti-alias filter.

Current Shunt:
200 Ω for 100 µA, 1 mA
2 Ω for 10 mA, 100 mA
0.1 Ω for 1 A, 3 A

Maximum Input:
The peak value of the DC + AC current must be < 300% of range. The RMS current must be < 3 A including the DC current content.

Input Protection: 3 A, 250 V fuse

Frequency and Period

Measurement Method:
Reciprocal-counting technique. AC-coupled input using the AC voltage measurement function.

Input Impedance:
1 MΩ ± 2% in parallel with < 150 pF

Input Protection: 750 V_{rms} all ranges

Capacitance

Measurement Method:
Current input with measurement of resulting ramp.

Connection Type: 2-wire

Temperature

Thermistor:
2.2 kΩ, 5 kΩ, and 10 kΩ

RTD: α = 0.00385
R_0 from 49 Ω to 2.1 kΩ

Continuity/Diode Test

Response Time:
300 samples/sec with audible tone

Continuity Threshold: Fixed at 10 Ω

Operating Characteristics
Maximum readings/second

	Digits		
Function[3]	4.5	5.5	6.5
DCV	50 k[4]	10 k	1 k
2-wire Ω	50 k[4]	10 k	1 k
DCI	50 k[4]	10 k	1 k
Frequency	500	90	10
Period	500	90	10
Filter setting	fast	med	slow
ACV	500	150	50
ACI	500	150	50

1. For 1 kΩ unbalanced in LO lead, ± 500 V peak maximum
2. For 1 kΩ unbalanced in LO lead and < 60 Hz, ± 500 V peak maximum
3. Maximum rate for DCV, DCI, and resistance functions (using zero settling delay, autozero off, manual range)
4. 34411A only

Additional 34411A Specifications

Resolution: See table on page 4

Overall Bandwidth, DCV & DCI:
15 kHz typical @ 20 µs aperture (-3 dB)

Triggering: Pre/Post, Int/Ext, Pos/Neg

Timebase Resolution: 19.9524 µs 0.01% accuracy

Trigger Jitter:
2 µs (p-p), 20 µs (p-p) when pre-triggered

Spurious-Free Dynamic Range & Signal to Noise Distortion Ratio

Function DCV	Range	Spur-Free	SNDR
	1 V	-75 dB	60 dB
	10 V[1]	-70 dB	60 dB
	100 V	-75 dB	60 dB

[1]10 V range: 2 V (p-p) < signal < 16 V (p-p)

Triggering and Memory

Reading Hold Sensitivity: 1% of reading

Samples per Trigger:
1 to 50,000 (34410A)
1 to 1,000,000(34411A)

Trigger Delay: 0 to 3600 s (20 µs step size)

External Trigger:
Programmable edge, Low-power TTL compatible
Delay: < 1 µs **Max rate:** 5,000/s
Jitter: < 1 µs **Min Pulsewidth:** 1 µs

Voltmeter Complete: 3 V Logic output, 2 µs pulse with programmable edge

Nonvolatile Memory: 50,000 readings

Volatile Memory:
50,000 readings (34410A)
1,000,000 readings (34411A)

Sample Timer:
Range: 0 to 3600 s (20 µs step sizes)
Jitter: < 100 ns

General Specifications

Power Supply:
100 V/120 V/220 V/240 V ± 10%

Power Line Frequency:
45 Hz to 66 Hz and 360 Hz to 440 Hz, Automatically sensed at power-on

Power Consumption: 25 VA peak (16 W average)

Operating Environment: Full accuracy for 0 °C to 55 °C, 80% R.H. at 40 °C non-condensing

Storage Temperature: -40 °C to 70 °C

Weight: 3.72 kg (8.2 lbs)

Safety: IEC 61010-1, EN 61010-1, UL 61010-1, CAN/CSA-C22.2 No. 61010-1, Refer to Declarations of Conformity for current revisions. Measurement CAT II 300 V, CAT I 1000 V. Pollution Degree 2

EMC: IEC 61326, EN 61326, CISPR 11, ICES-001, AS/NZS 2064.1, Refer to Declaration of Conformity for current revisions.

Vibration & Shock: MIL-T-28800E, Type III, Class 5 (Sine Only)

LXI Compliance: LXI Class C, ver. 1.0

Warranty: 3 year standard

A-to-D Converter Noise Performance

Integration Time (NPLC)	Resolution (ppm of range)[1]	Normal Mode Rejection (dB)[2]	Readings/Second[4]
0.001[5]	30	0	50,000
0.002[5]	15	0	25,000
0.006	6	0	10,000
0.02	3	0	3,000
0.06	1.5	0	1,000
0.2	0.7	0	300
1	0.3	55	60 (50)
2	0.2	110[3]	30 (25)
10	0.1	110[3]	6 (5)
100	0.03	110[3]	0.6 (0.5)

1. Resolution is defined as the typical DCV 10 V range RMS noise. Auto-zero on for NPLC ≥ 1. See manual for additional noise characteristics.
2. Normal mode rejection for power line frequency ± 0.1%.
3. For power-line frequency ± 1% 75 dB and for ± 3% 55 dB.
4. Maximum rate with auto-zero off for 60 Hz and (50 Hz) operation.
5. Only available for the 34411A.

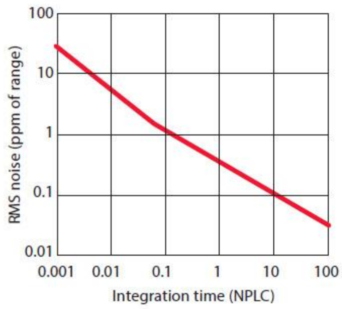

System Reading and Throughput Rates

DMM memory to PC (Maximum reading rate out of memory[6]
Drawing – Path B

Reading Format	GPIB Readings/s	USB 2.0 Readings/s	LAN (VXI-11) Readings/s	LAN (Sockets) Readings/s
ASCII	4,000	8,500	7,000	8,500
32-bit Binary	89,000	265,000	110,000	270,000
64-bit Binary	47,000	154,000	60,000	160,000

System Reading Architecture

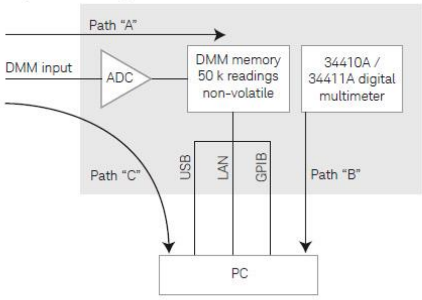

Direct I/O Measurements (Single reading – measure and I/O time)[6]

Drawing - Path C

Function	Resolution (NPLC)	GPIB ms	USB 2.0 ms	LAN (VXI-11) ms	LAN (sockets) ms	Maximum Reading Rate into Memory or to Direct I/O (Readings/s) Drawing - Path A or C
DCV/2-wire Resistance	0.006 (0.001)	2.6	2.9	4.6	3.2	10,000 (50,000)
ACV/ Frequency	Fast Filter 1 ms gate	10.0	10.0	10.0	10.0	500

6. 1/2 scale input signal, immediate trigger, trigger delay 0, auto-zero off, auto-range off, no math, null off, 60 Hz line frequency. Specifications are for 34410A or (34411A). See manual for performance on other functions.

System Performance

	Function Change (ms)[7]	Range Change (ms)[8] LAN/GPIB	Auto-range (ms)[9]	Maximum External Trigger Rate	Maximum Internal Trigger Rate[10]
DCV/2-wire Resistance	22	3.9/2.6	7.5	5,000/s	10,000/s (50,000/s)
ACV/ Frequency	37	6.5/6.4	19	500/s	500/s

7. Time to change from 2-wire Resistance to this specified function, or DCV to 2-wire Resistance using the SCPI "FUNC" command.
8. Time to change from one range to the next higher range, ≤ 10 V, ≤ 10 MΩ.
9. Time to automatically change one range and be ready for the new measurement, ≤ 10 V, ≤ 10 MΩ.
10. Specifications are for 34410A or (34411A).

Accuracy Specifications ± (% of reading + % of range)[1]

Function	Range[3]	Frequency, Test Current or Burden Voltage	24 Hour[2] Tcal ± 1 °C	90 Day Tcal ± 5 °C	1 Year Tcal ± 5 °C	Temperature Coefficient/°C 0 °C to (Tcal -5 °C) (Tcal +5 °C) to 55 °C
DC Voltage	100.0000 mV		0.0030 + 0.0030	0.0040 + 0.0035	0.0050 + 0.0035	0.0005 + 0.0005
	1.000000 V		0.0020 + 0.0006	0.0030 + 0.0007	0.0035 + 0.0007	0.0005 + 0.0001
	10.00000 V		**0.0015 + 0.0004**	**0.0020 + 0.0005**	**0.0030 + 0.0005**	**0.0005 + 0.0001**
	100.0000 V		0.0020 + 0.0006	0.0035 + 0.0006	0.0040 + 0.0006	0.0005 + 0.0001
	1000.000 V[4]		0.0020 + 0.0006	0.0035 + 0.0006	0.0040 + 0.0006	0.0005 + 0.0001
True RMS AC Voltage[5]	100.0000 mV to 750.000 V	3 Hz – 5 Hz	0.50 + 0.02	0.50 + 0.03	0.50 + 0.03	0.010 + 0.003
		5 Hz – 10 Hz	0.10 + 0.02	0.10 + 0.03	0.10 + 0.03	0.008 + 0.003
		10 Hz - 20 kHz	**0.02 + 0.02**	**0.05 + 0.03**	**0.06 + 0.03**	**0.005 + 0.003**
		20 kHz – 50 kHz	0.05 + 0.04	0.09 + 0.05	0.10 + 0.05	0.010 + 0.005
		50 kHz – 100 kHz	0.20 + 0.08	0.30 + 0.08	0.40 + 0.08	0.020 + 0.008
		100 kHz – 300 kHz	1.00 + 0.50	1.20 + 0.50	1.20 + 0.50	0.120 + 0.020
Resistance[6]	100.0000 Ω	1 mA	0.0030 + 0.0030	0.008 + 0.004	0.010 + 0.004	0.0006 + 0.0005
	1.000000 kΩ	1 mA	0.0020 + 0.0005	0.007 + 0.001	0.010 + 0.001	0.0006 + 0.0001
	10.00000 kΩ	**100 µA**	**0.0020 + 0.0005**	**0.007 + 0.001**	**0.010 + 0.001**	**0.0006 + 0.0001**
	100.0000 kΩ	10 µA	0.0020 + 0.0005	0.007 + 0.001	0.010 + 0.001	0.0006 + 0.0001
	1.000000 MΩ	5 µA	0.0020 + 0.0010	0.010 + 0.001	0.012 + 0.001	0.0010 + 0.0002
	10.00000 MΩ	500 nA	0.0100 + 0.0010	0.030 + 0.001	0.040 + 0.001	0.0030 + 0.0004
	100.0000 MΩ	500 nA ‖ 10 MΩ	0.200 + 0.001	0.600 + 0.001	0.800 + 0.001	0.1000 + 0.0001
	1.000000 GΩ	500 nA ‖ 10 MΩ	2.000 + 0.001	6.000 + 0.001	8.000 + 0.001	1.0000 + 0.0001
DC Current	100.0000 µA	< 0.03V	0.010 + 0.020	0.040 + 0.025	0.050 + 0.025	0.0020 + 0.0030
	1.000000 mA	**< 0.3 V**	**0.007 + 0.006**	**0.030 + 0.006**	**0.050 + 0.006**	**0.0020 + 0.0005**
	10.00000 mA	< 0.03V	0.007 + 0.020	0.030 + 0.020	0.050 + 0.020	0.0020 + 0.0020
	100.0000 mA	< 0.3 V	0.010 + 0.004	0.030 + 0.005	0.050 + 0.005	0.0020 + 0.0005
	1.000000 A	< 0.8 V	0.050 + 0.006	0.080 + 0.010	0.100 + 0.010	0.0050 + 0.0010
	3.000000 A	< 2.0 V	0.100 + 0.020	0.120 + 0.020	0.150 + 0.020	0.0050 + 0.0020
True RMS AC Current[7]	100.0000 µA to 3.00000 A	**3 Hz - 5 kHz**	**0.10 + 0.04**	**0.10 + 0.04**	**0.10 + 0.04**	**0.015 + 0.006**
		5 kHz – 10 kHz	0.20 + 0.04	0.20 + 0.04	0.20 + 0.04	0.030 + 0.006
Frequency or Period	100 mV to 750 V	3 Hz – 5 Hz	0.070 + 0.000	0.070 + 0.000	0.070 + 0.000	0.005 + 0.000
		5 Hz – 10 Hz	0.040 + 0.000	0.040 + 0.000	0.040 + 0.000	0.005 + 0.000
		10 Hz – 40 Hz	0.020 + 0.000	0.020 + 0.000	0.020 + 0.000	0.001 + 0.000
		40 Hz - 300 kHz	**0.005 + 0.000**	**0.006 + 0.000**	**0.007 + 0.000**	**0.001 + 0.000**
Capacitance[8]	1.0000 nF	500 nA	0.50 + 0.50	0.50 + 0.50	0.50 + 0.50	0.05 + 0.05
	10.000 nF	1 µA	0.40 + 0.10	0.40 + 0.10	0.40 + 0.10	0.05 + 0.01
	100.00 nF	10 µA	0.40 + 0.10	0.40 + 0.10	0.40 + 0.10	0.01 + 0.01
	1.0000 µF	10 µA	0.40 + 0.10	0.40 + 0.10	0.40 + 0.10	0.01 + 0.01
	10.000 µF	100 µA	0.40 + 0.10	0.40 + 0.10	0.40 + 0.10	0.01 + 0.01
Temperature[9]						
RTD	-200 °C to 600 °C		0.06 °C	0.06 °C	0.06 °C	0.003 °C
Thermistor	-80 °C to 150 °C		0.08 °C	0.08 °C	0.08 °C	0.002 °C
Continuity	1000.0 Ω	1 mA	0.002 + 0.010	0.008 + 0.020	0.010 + 0.020	0.0010 + 0.0020
Diode Test[10]	1.0000 V	1 mA	0.002 + 0.010	0.008 + 0.020	0.010 + 0.020	0.0010 + 0.0020

1. Specifications are for 90 minute warm-up and 100 PLC.
2. Relative to calibration standards.
3. 20% overrange on all ranges, except DCV 1000 V, ACV 750 V, DCI and ACI 3 A ranges.
4. For each additional volt over ± 500 V add 0.02 mV of error.
5. Specifications are for sinewave input > 0.3% of range and > 1 mVrms. Add 30 µV error for frequencies below 1 kHz. 750 VAC range limited to 8 x 107 Volts-Hz. For each additional volt over 300 Vrms add 0.7 mVrms of error.
6. Specifications are for 4-wire resistance measurements, or 2-wire using Math Null. Without Math Null, add 0.2 Ω additional error in 2-wire resistance measurements.
7. Specifications are for sinewave input > 1% of range and > 10 µArms. Frequencies > 5 kHz are typical for all ranges. For the 3 A range (all frequencies) add 0.05% of reading + 0.02% of range to listed specifications.
8. Specifications are for 1-hour warm-up using Math Null. Additional errors may occur for non-film capacitors.
9. For total measurement accuracy, add temperature probe error.
10. Accuracy specifications are for the voltage measured at the input terminals only. 1 mA test current is typical. Variation in the current source will create some variation in the voltage drop across a diode junction.

10.1.2 A.2 Technical datasheet Agilent 34970A Datalogger

34970A/34972A accuracy specifications ±(% of reading + % of range)[1]

Includes measurement error, switching error, and transducer conversion error

	Range [3]	Frequency, etc.	24 hour [2] 23 ±1°C	90 Day 23 ±5°C	1 Year 23 ±5°C	Temperature coefficient 0 – 18°C, 28 - 55°C
DC voltage						
	100.0000 mV		0.0030 + 0.0035	0.0040 + 0.0040	0.0050 + 0.0040	0.0005 + 0.0005
	1.000000 V		0.0020 + 0.0006	0.0030 + 0.0007	0.0040 + 0.0007	0.0005 + 0.0001
	10.00000 V		0.0015 + 0.0004	0.0020 + 0.0005	0.0035 + 0.0005	0.0005 + 0.0001
	100.0000 V		0.0020 + 0.0006	0.0035 + 0.0006	0.0045 + 0.0006	0.0005 + 0.0001
	300.000 V		0.0020 + 0.0020	0.0035 + 0.0030	0.0045 + 0.0030	0.0005 + 0.0003
True RMS AC voltage [4]						
	All ranges from 100.0000 mV to 100.0000 V	3 Hz–5 Hz	1.00 + 0.03	1.00 + 0.04	1.00 + 0.04	0.100 + 0.004
		5 Hz–10 Hz	0.35 + 0.03	0.35 + 0.04	0.35 + 0.04	0.035 + 0.004
		10 Hz–20 kHz	0.04 + 0.03	0.05 + 0.04	0.06 + 0.04	0.005 + 0.004
		20 kHz–50 kHz	0.10 + 0.05	0.11 + 0.05	0.12 + 0.05	0.011 + 0.005
		50 kHz–100 kHz	0.55 + 0.08	0.60 + 0.08	0.60 + 0.08	0.060 + 0.008
		100 kHz–300 kHz [5]	4.00 + 0.50	4.00 + 0.50	4.00 + 0.50	0.20 + 0.02
	300.0000 V	3 Hz–5 Hz	1.00 + 0.05	1.00 + 0.08	1.00 + 0.08	0.100 + 0.008
		5 Hz–10 Hz	0.35 + 0.05	0.35 + 0.08	0.35 + 0.08	0.035 + 0.008
		10 Hz–20 kHz	0.04 + 0.05	0.05 + 0.08	0.06 + 0.08	0.005 + 0.008
		20 kHz–50 kHz	0.10 + 0.10	0.11 + 0.12	0.12 + 0.12	0.011 + 0.012
		50 kHz–100 kHz	0.55 + 0.20	0.60 + 0.20	0.60 + 0.20	0.060 + 0.020
		100 kHz–300 kHz [5]	4.00 + 1.25	4.00 + 1.25	4.00 + 1.25	0.20 + 0.05
Resistance [6]						
	100.0000 Ω	1 mA current source	0.0030 + 0.0035	0.008 + 0.004	0.010 + 0.004	0.0006 + 0.0005
	1.000000 kΩ	1 mA	0.0020 + 0.0006	0.008 + 0.001	0.010 + 0.001	0.0006 + 0.0001
	10.00000 kΩ	100 µA	0.0020 + 0.0005	0.008 + 0.001	0.010 + 0.001	0.0006 + 0.0001
	100.0000 kΩ	10 µA	0.0020 + 0.0005	0.008 + 0.001	0.010 + 0.001	0.0006 + 0.0001
	1.000000 MΩ	5.0 µA	0.002 + 0.001	0.008 + 0.001	0.010 + 0.001	0.0010 + 0.0002
	10.00000 MΩ	500 nA	0.015 + 0.001	0.020 + 0.001	0.040 + 0.001	0.0030 + 0.0004
	100.0000 MΩ	500 nA || 10 MΩ	0.300 + 0.010	0.800 + 0.010	0.800 + 0.010	0.1500 + 0.0002
Frequency and period [7]						
	100 mV to 300V	3 Hz–5 Hz	0.10	0.10	0.10	0.005
		5 Hz–10 Hz	0.05	0.05	0.05	0.005
		10 Hz–40 Hz	0.03	0.03	0.03	0.001
		40 Hz–300 kHz	0.006	0.01	0.01	0.001
DC current (34901A only)						
	10.00000 mA	<0.1 V burden	0.005 + 0.010	0.030 + 0.020	0.050 + 0.020	0.002+ 0.0020
	100.0000 mA	<0.6 V	0.010 + 0.004	0.030 + 0.005	0.050 + 0.005	0.002 + 0.0005
	1.000000 A	<2 V	0.050 + 0.006	0.080 + 0.010	0.100 + 0.010	0.005 + 0.0010
True RMS AC current (34901A only)						
	10.00000 mA and [4] 1.000000 A	3 Hz–5 Hz	1.00 + 0.04	1.00 + 0.04	1.00 + 0.04	0.100 + 0.006
		5 Hz–10 Hz	0.30 + 0.04	0.30 + 0.04	0.30 + 0.04	0.035 + 0.006
		10 Hz–5 kHz	0.10 + 0.04	0.10 + 0.04	0.10 + 0.04	0.015 + 0.006
	100.0000 mA [8]	3 Hz–5 Hz	1.00 + 0.5	1.00 + 0.5	1.00 + 0.5	0.100 + 0.06
		5 Hz–10 Hz	0.30 + 0.5	0.30 + 0.5	0.30 + 0.5	0.035 + 0.06
		10 Hz–5 kHz	0.10 + 0.5	0.10 + 0.5	0.10 + 0.5	0.015 + 0.06

Temperature	Type	1-year accuracy [9]		Extended range 1-year accuracy [9]		Temp coefficient/°C
Thermocouple [10]	B	1100 to 1820°C	1.2°C	400 to 1100°C	1.8°C	0.03°C
	E	–150 to 1000°C	1.0°C	-200 to -150°C	1.5°C	
	J	–150 to 1200°C	1.0°C	–210 to -150°C	1.2°C	
	K	–100 to 1200°C	1.0°C	–200 to -100°C	1.5°C	
	N	–100 to 1300°C	1.0°C	–200 to -100°C	1.5°C	
	R	300 to 1760°C	1.2°C	–50 to 300°C	1.8°C	
	S	400 to 1760°C	1.2°C	–50 to 400°C	1.8°C	
	T	–100 to 400°C	1.0°C	–200 to -100°C	1.5°C	
RTD	R0 from 49 Ω to 2.1 kΩ	–200 to 600°C	0.06°C			0.003°C
Thermistor	2.2 k, 5 k, 10 k	–80 to 150°C	0.08°C			0.002°C

[1] Specifications are for 1 hr warm-up and 6½ digits, Slow ac filter
[2] Relative to calibration standards
[3] 20% over range on all ranges except 300 Vdc and ac ranges and 1 Adc and ac current ranges
[4] For sinewave input > 5% of range. For inputs from 1% to 5% of range and < 50 kHz, add 0.1% of range additional error
[5] Typically 30% of reading error at 1 MHz, limited to 1 x 108 V Hz
[6] Specifications are for 4- wire ohms function or 2-wire ohms using scaling to remove the offset. Without scaling, add 4 Ω additional error in 2-wire Ohms function
[7] Input > 100 mV. For 10 mV to 100 mV inputs multiply % of reading error x 10
[8] Specified only for inputs >10 mA
[9] For total measurement accuracy, add temperature probe error
[10] Thermocouple specifications not guaranteed when 34907A module is present. For < 1°C accuracy, a precision external reference is required.

Find us at www.keysight.com Page 16

Measurement characteristics[7]

DC voltage	
Measurement Method	Continuously Integrating Multi-slope III A-D converter
A/D linearity	0.0002% of reading + 0.0001 % of range
Input resistance	
100 mV, 1 V, 10 V ranges	Selectable 10 MΩ or > 10,000 MΩ
100 V, 300 V ranges	10 MΩ ±1%
Input bias current	< 30 pA at 25°C
Input protection	300 V all ranges
True RMS AC voltage	
Measurement method	AC coupled True RMS – measures the AC component of the input with up to 300 Vdc of bias on any range
Crest factor	Maximum of 5:1 at Full Scale
Additional crest factor errors (non-sinewave)	Crest Factor 1-2: 0.05 % of reading Crest Factor 2-3: 0.15 % of reading Crest Factor 3-4: 0.30 % of reading Crest Factor 4-5: 0.40 % of reading
Input impedance	1 MΩ ±2% in parallel with 150 pF
Input protection	300 Vrms all ranges
Resistance	
Measurement method	Selectable 4-wire or 2-wire Ohms Current source referenced to LO input
Offset compensation	Selectable on 100 Ω, 1 kΩ, 10 kΩ ranges
Maximum lead resistance	10% of range per lead for 100 Ω and 1 kΩ ranges. 1 kΩ on all other ranges
Input protection	300 V on all ranges
Frequency and period	
Measurement method	Reciprocal counting technique
Voltage ranges	Same as AC Voltage function
Gate time	1s, 100 ms, or 10 ms
Measurement timeout	Selectable 3 Hz, 20 Hz, 200 Hz LF limit
DC current	
Shunt resistance	5Ω for 10 mA, 100 mA; 0.1 Ω for 1 A
Input protection	1 A 250 V fuse on 34901A module
True RMS AC current	
Measurement method	Direct coupled to the fuse and shunt. AC coupled True RMS measurement (measures the ac component only)
Shunt resistance	5 Ω for 10 mA; 0.1 Ω for 100 mA, 1 A
Input protection	1 A 250 V fuse on 34901A module
Thermocouple	
Conversion	ITS-90 software compensation
Reference junction type	Internal, Fixed, or External
Open thermocouple check	Selectable per channel. Open > 5 kΩ
Thermistor	44004, 44007, 44006 series
RTD	α = 0.00385 (DIN) and α = 0.00391
Measurement noise rejection 60 (50) Hz [1]	
dc CMRR	140 dB
ac CMRR	70 dB
Integration time	**Normal mode rejection**[2]
200 plc/3.33s (4s)	110 dB [3]
100 plc/1.67s (2s)	105 dB [3]
20 plc/333 ms (400 ms)	100 dB [3]
10 plc/167 ms (200 ms)	95 dB [3]
2 plc/33.3 ms (40 ms)	90 dB
1 plc/16.7 ms (20 ms)	60 dB
< 1 plc	0 dB

Operating characteristics [4]

Single channel measurement rates [5]

Function	Resolution [8]	34970A/34972A readings/sec
dcV, 2-wire resistance	6½ digits (10 plc)	6 (5)
	5½ digits (1 plc)	54 (47)
	4½ digits (0.02 plc)	500
Thermocouple	0.1 °C (10 plc)	6 (5)
	0.1 °C (1 plc)	52 (47)
	(0.02 plc)	280
RTD, thermistor	0.01 °C (10 plc)	6 (5)
	0.1 °C (1 plc)	49 (47)
	1 °C (0.02 plc)	200
acV	6½ Slow (3 Hz)	0.14
	6½ Med (20 Hz)	1
	6½ Fast (200 Hz)	8
	6½ [6]	100
Frequency, period	6½ digits (1 s gate)	1
	5½ digits (100 ms)	9
	4½ digits (10 ms)	70

[1] For 1 KΩ unbalance in LO lead
[2] For power line frequency ±0.1%
[3] For power line frequency ±1% use 80 dB or ±3% use 60 dB
[4] Reading speeds for 60 Hz and (50 Hz) operation
[5] For fixed function and range, readings to memory, scaling and alarms off, AZERO OFF, USB datalogging OFF
[6] Maximum limit with de fault settling delays defeated
[7] Isolation voltage (ch-ch, ch-earth) 300 Vdc, ac rms
[8] 6½ digits = 22 bits, 5½ digits = 18 bits, 4½ digits = 15 bits

Find us at www.keysight.com Page 17

10.1.3 A.3 Technical datasheet Agilent 34901A 20-Channel General Purpose Multiplexer

Multiplexer selection guide

Choose between the broad functionality of the 34901A, the high speed scanning of the 34902A, or the single-ended density of the 34908A. These three modules are the only way to connect to the 34970A/34972A internal DMM. They can be used to scan with external instruments as well.

All multiplexer modules employ break-before-make scanning, ensuring only one closed channel (or channel pair) at a time. Multiple channel closures are allowed on the 34901A and 34902A modules when not configured for scanning.

The 34908A does not allow multiple channel closures at any time.

	34901A	34902A	34908A
Number of channels	20 + 2	16	40
Max scan speed	60 ch/s	250 ch/s	60 ch/s
Number of contacts	2 or 4	2 or 4	1
Temperature			
Thermocouple	•	•	•
2-wire RTD	•	•	•
4-wire RTD	•	•	
Thermistor	•	•	•
dc Volts	•	•	•
ac Volts	•	•	•
2-wire Ohms	•	•	•
4-wire Ohms	•	•	
Frequency	•	•	•
Period	•	•	•
dc current	•		
ac current	•		

34901A

20-Channel General Purpose Multiplexer

- 60 ch/s scanning
- Two- and four-wire scanning
- Built-in thermocouple reference junction
- 300 V switching

The Keysight 34901A is the most versatile multiplexer for general purpose scanning. It combines dense, multifunction switching with 60-channel/second scan rates to address a broad spectrum of data acquisition applications.

Two- and four-wire channels can be mixed on the same module. Two additional fused inputs (22 channels total) route up to 1 A of current to the internal DMM, allowing ac and dc current measurements without the need for external shunt resistors.

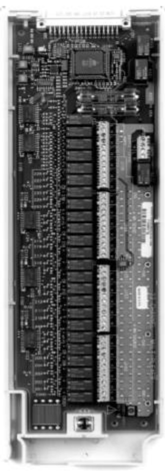

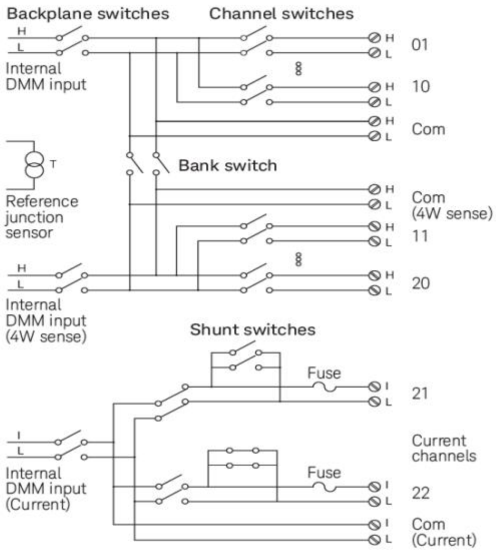

Find us at www.keysight.com Page 21

10.1.4 A.5 Technical datasheet Kipp and Zonnen CMP11 Pyranometer

Technical Specifications

	CMP10 | CMP11	SMP10 | SMP11
Classification to ISO 9060:2018	Spectrally Flat Class A	Spectrally Flat Class A
Sensitivity	7 to 14 μV/W/m²	-
Impedance	10 to 100 Ω	-
Expected output range (0 to 1500 W/m²)	0 to 20 mV	-
Maximum operational irradiance	4000 W/m²	-
Analog output • V-version	-	0 to 1 V
Analog output range*	-	-200 to 2000 W/m²
Analog output • A-version	-	4 to 20 mA
Analog output range*	-	0 to 1600 W/m²
Serial output	-	RS-485 Modbus®
Serial output range	-	-400 to 4000 W/m²
Response time (63 %)	< 1.7 s	< 0.7 s
Response time (95 %)	< 5 s	< 2 s
Spectral range (20 % points)	270 to 3000 nm	270 to 3000 nm
Spectral range (50 % points)	285 to 2800 nm	285 to 2800 nm
Zero offsets (unventilated) (a) thermal radiation (at 200 W/m²) (b) temperature change (5 K/h)	 < 7 W/m² < 2 W/m²	 < 7 W/m² < 2 W/m²
Non-stability (change/year)	< 0.5 %	< 0.5 %
Non-linearity (100 to 1000 W/m²)	< 0.2 %	< 0.2 %
Directional response (up to 80 ° with 1000 W/m² beam)	< 10 W/m²	< 10 W/m²
Spectral selectivity (350 to 1500 nm)	< 3 %	< 3 %
Tilt response (0 ° to 90 ° at 1000 W/m²)	< 0.2 %	< 0.2 %
Temperature response	< 1 % (-10 °C to +40 °C)	< 1 % (-20°C to +50 °C) < 2 % (-40 °C to +70 °C)
Field of view	180 °	180 °

Accuracy of bubble level	< 0.1 °	< 0.1 °
Power consumption (at 12 VDC)	-	V-version: 55 mW A-version: 100 mW
Supply voltage	-	5 to 30 VDC
Software, Windows™	-	SmartExplorer Software, for configuration, test and data logging
Detector type	Thermopile	Thermopile
Operating and storage temperature range	-40 °C to +80 °C	-40 °C to +80 °C
Humidity range	0 to 100 %	0 to 100 %
MTBF (Mean Time Between Failures)	> 10 years	> 10 years **
Ingress Protection (IP) rating	67	67
Recommended applications	Meteorological networks, PV panel and thermal collector testing, materials testing	High performance for PV panel and thermal collector testing, solar energy research, solar prospecting, materials testing, advanced meteorology and climate networks

Note: The performance specifications quoted are worst-case and/or maximum values.
* adjustable with SmartExplorer Software | ** extrapolated after introduction in January 2012

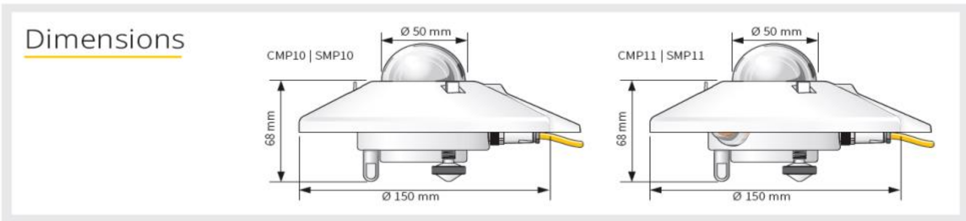

10.1.5 A.6 Technical datasheet Kipp and Zonnen CHP1 Pyrheliometer

Specifications	CHP 1	SHP1
ISO 9060:1990 CLASSIFICATION	First Class	First Class
Response time (63 %)	< 1.7 s	< 0.7 s
Response time (95 %)	< 5 s	< 2 s
Zero offsets due to temperature change (5 K/hr)	< 1 W/m²	< 1 W/m²
Non-stability (change/year)	< 0.5 %	< 0.5 %
Non-linearity (0 to 1000 W/m²)	< 0.2 %	< 0.2 %
Temperature dependence of sensitivity	< 0.5 % (-20 °C to +50 °C)	< 0.5 % (-30 °C to +60 °C)
Sensitivity	7 to 14 μV/W/m²	NA
Other specifications		
Analogue output	10 to 20 mV for 1400 W/m²	-V version: 0 to 1 V -A version: 4 to 20 mA
Analogue output range	0 to 4000 W/m²	-V version: -200 to 2000 W/m² (1) -A version: 0 to 1600 W/m²
Digital output	NA	2-wire RS-485, Modbus® protocol
Operating temperature	-40 °C to +80 °C	-40 °C to +80 °C
Full viewing angle	5° ±0.2°	5° ±0.2°
Maximum irradiance	4000 W/m²	4000 W/m²
Humidity	0 to 100% RH	0 to 100% RH
Spectral range (50 % points)	200 to 4000 nm	200 to 4000 nm
Required sun tracker accuracy	< 0.5° from ideal	< 0.5° from ideal
Weight (excluding cable)	0.9 kg	0.9 kg
Slope angle	1° ±0.2°	1° ±0.2°
Temperature sensor	Both Pt-100 and 10k thermistor as standard (2)	Internal (3)
Supply voltage	NA	5 to 30 VDC
Power consumption (at 12 VDC)	NA	-V version: 55 mW -A version: 100 mW
Expected daily uncertainty	< 1 %	< 1 %
Documentation	Calibration certificate traceable to WRR, multi-language instruction sheet, manual on CD-ROM	
Recommended applications	High performance direct radiation monitoring for meteorological stations or concentrated solar energy applications	

(1) The analogue output range of SHP1 can be rescaled by the user to a maximum of -200 to 4000 W/m²

(2) Supplied with individual temperature dependence test data

(3) Output data individually temperature corrected for each SHP1 over -40°C to +70°C

Pyheliometers have a standard cable length of 10 m. Optional cable lengths 25 m and 50 m

Note: The performance specifications quoted are worst-case and/or maximum values

KIPP & ZONEN
SINCE 1830

Go to www.kippzonen.com for your local distributor

10.1.6 A.7 Technical datasheet Eko MS-700 Spectroradiometer

EKO MS-700 Specifications *(Typical)*		
Sensor head	**MS-700**	**MS-700 DNI**
Wavelength range	350 to 1050 nm	
Wavelength interval	3.3 nm	
Spectral resolution FWHM	10 nm	
Wavelength accuracy	<0.3 nm	
Exposure time	10 ms to 5 s	
Temp. dependency (–20° to 50°C)	< ± 1 %	
Temperature control	25 ± 5ºC	
Cosine response (0º to 80º)	<7%	–
Aperture	180°	5°
Slope angle	–	1°
Stray light	0.15%	
Window material	Optical glass	Quartz glass
Communication	RS-422 (Between head and power supply)	
Cable length	10 m (Optional max. 30 m)	
Power requirements	12 Vdc, 50 VA (power supply)	
Operating temperature range (°C)	–20 to +50	
Dimensions (sensor)	200(φ)×175(H) mm (With sun screen: 240(φ)×175(H) mm)	200(φ)×300(H) mm
Weight (sensor)	4 kg	4.5 kg
Power supply		
AC supply voltage	AC100-240V, 50/60 Hz, 50 VA	
DC supply voltage	DC 12 V	
Operating environment	Temperature: 0º to 40ºC, Relative Humidity: 0 to 90%, non-condensing	
Dimensions	200 (W) x 140 (D) x 80 (H) mm	
Weight	1 kg	

10.1.7 A.8 Technical datasheet Tri-band Spectro-Heliometer IES-UPM ICU-3J24

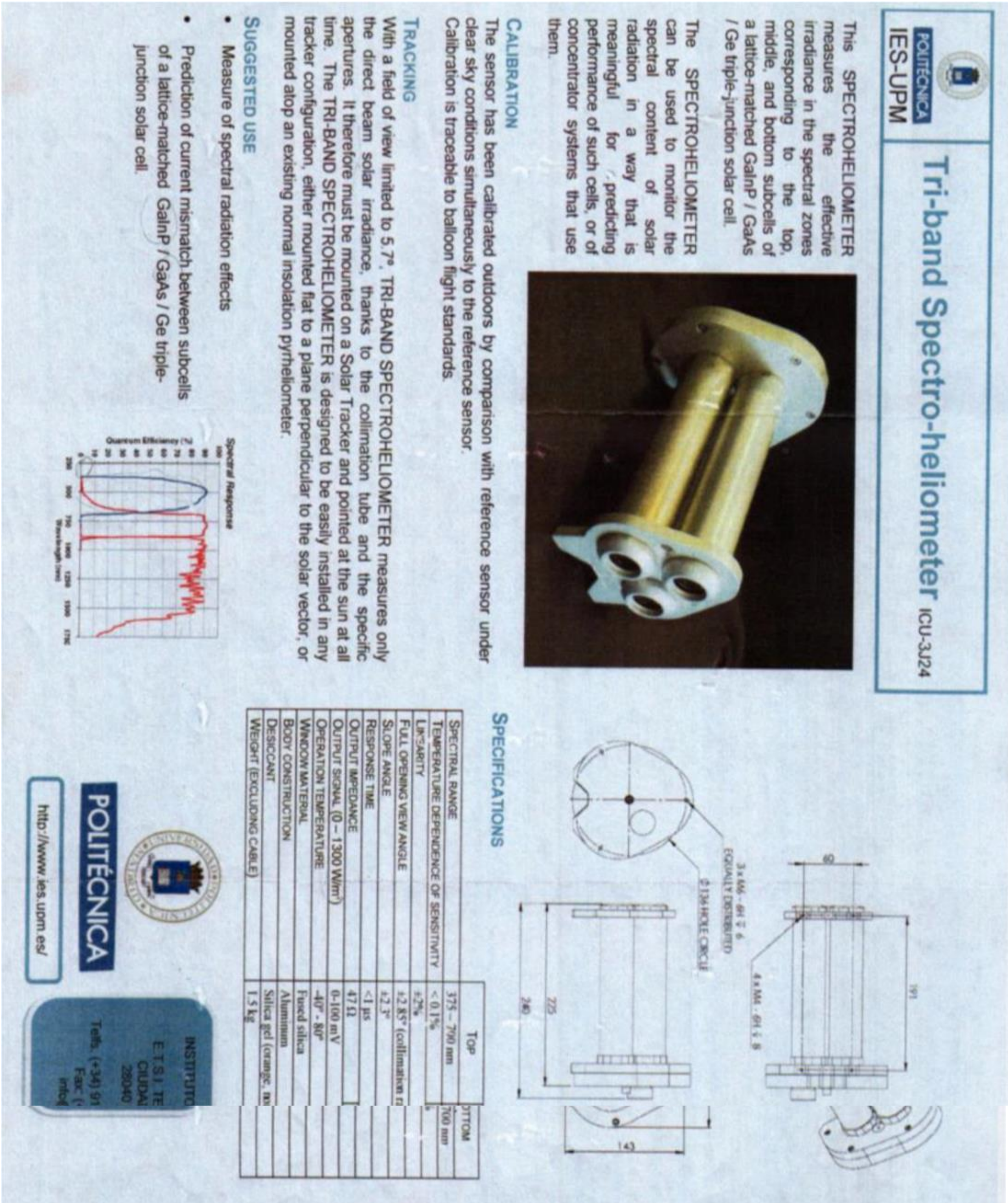

POLITÉCNICA IES-UPM

Tri-band Spectro-heliometer ICU-3J24

This SPECTROHELIOMETER measures the effective irradiance in the spectral zones corresponding to the top, middle, and bottom subcells of a lattice-matched GaInP / GaAs / Ge triple-junction solar cell.

The SPECTROHELIOMETER can be used to monitor the spectral content of solar radiation in a way that is meaningful for predicting performance of such cells, or of concentrator systems that use them.

CALIBRATION

The sensor has been calibrated outdoors by comparison with reference sensor under clear sky conditions simultaneously to the reference sensor. Calibration is traceable to balloon flight standards.

TRACKING

With a field of view limited to 5.7°, TRI-BAND SPECTROHELIOMETER measures only the direct beam solar irradiance, thanks to the collimation tube and the specific apertures. It therefore must be mounted on a Solar Tracker and pointed at the sun at all time. The TRI-BAND SPECTROHELIOMETER is designed to be easily installed in any tracker configuration, either mounted flat to a plane perpendicular to the solar vector, or mounted atop an existing normal insolation pyrheliometer.

SUGGESTED USE

- Measure of spectral radiation effects
- Prediction of current mismatch between subcells of a lattice-matched GaInP / GaAs / Ge triple-junction solar cell.

SPECIFICATIONS

	TOP	[B]OTTOM
SPECTRAL RANGE	375 – 700 nm	700 nm
TEMPERATURE DEPENDENCE OF SENSITIVITY	< 0.1%	
LINEARITY	±2%	
FULL OPENING VIEW ANGLE	±2.85° (collimation r[...]	
SLOPE ANGLE	±2.3°	
RESPONSE TIME	<1 µs	
OUTPUT IMPEDANCE	47 Ω	
OUTPUT SIGNAL (0 – 1300 W/m²)	0-100 mV	
OPERATION TEMPERATURE	-40° - 80°	
WINDOW MATERIAL	Fused silica	
BODY CONSTRUCTION	Aluminum	
DESICCANT	Silica gel (orange, m[...]	
WEIGHT (EXCLUDING CABLE)	1.5 kg	

POLITÉCNICA

http://www.ies.upm.es/

INSTITUTO [...]
E.T.S.I. TE[...]
CIUDA[...]
28040
Telf. (+34) 91 [...]
Fax: ([...]
info@[...]

10.1.8 A.9 Technical datasheet Young 05305VM anemometer

MODEL 05305V
WIND MONITOR-AQ
with VOLTAGE OUTPUTS

WIND SPEED SPECIFICATION SUMMARY

Range	0 to 40 m/s (90 mph), gust survival 100 m/s (220 mph)
Sensor	20 cm diameter 4-blade helicoid carbon fiber thermoplastic propeller, 30.7 cm air passage per revolution
Distance Constant	2.1 m (6.9 ft.) for 63% recovery
Threshold Sensitivity	0.4 m/s (0.9 mph)
Transducer	Centrally mounted stationary coil, 2K Ohm nominal DC resistance
Output Signal	0 to 1.00 VDC over specified range

Model No. Suffix	Range
M	0 to 50 M/S
P	0 to 100 MPH
N	0 to 100 KNOTS
K	0 to 200 KILOMETERS/HOUR

WIND DIRECTION (AZIMUTH) SPECIFICATION SUMMARY

Range	360° mechanical, 355° electrical (5° open)
Sensor	Balanced vane, 48.3 cm (19 in) turning radius.
Damping Ratio	0.45
Delay Distance	1.2 m (3.9 ft) for 50% recovery
Threshold Sensitivity	0.5 m/s (1.0 mph) at 10° displacement
Damped Natural Wavelength	4.9 m (16.1 ft)
Undamped Natural Wavelength	4.4 m (14.4 ft)
Transducer	Precision conductive plastic potentiometer, 10K ohm resistance (±20%), 0.25% linearity, life expectancy 50 million revolutions, rated 1 watt at 40°C, 0 watts AT 125°C
Output Signal	0 to 1.00 VDC for 0 to 360°

GENERAL

Power Requirement: 8 - 24 VDC (5mA @ 12 VDC)
Operating Temperature: -50 to 50°C (-58 to 122°F)

INTRODUCTION

The Wind Monitor measures horizontal wind speed and direction. Developed for air quality applications, it is accurate, sensitive, and corrosion resistant. The main housing, nose cone, propeller, and other internal parts are injection molded U.V. stabilized plastic. The tail section is lightweight expanded polystyrene. Both the propeller and vertical shafts use stainless steel precision grade ball bearings. Bearings have shields to help exclude contamination and moisture.

Propeller rotation produces an AC sine wave signal with frequency proportional to wind speed. Internal circuitry converts the raw signal to a linear voltage output.

Vane position is sensed by a 10K ohm precision conductive plastic potentiometer. This signal is also converted to voltage output.

The instrument mounts directly on standard one inch pipe, outside diameter 34 mm (1.34"). An orientation ring is provided so the instrument can be removed for maintenance and re-installed without loss of wind direction reference. Both the sensor and the orientation ring are secured to the mounting pipe by stainless steel band clamps. Electrical connections are made in a junction box at the base.

INITIAL CHECKOUT

When the Wind Monitor is unpacked it should be checked carefully for any signs of shipping damage.

Remove the plastic nut on the propeller shaft. Install the propeller on the shaft with the serial number of the propeller facing forward (into the wind). The instrument is aligned, balanced and fully calibrated before shipment; however, it should be checked both mechanically and electrically before installation. The vane and propeller should easily rotate 360° without friction. Check vane balance by holding the instrument base so the vane surface is horizontal. It should have near neutral torque without any particular tendency to rotate. A slight imbalance will not degrade performance.

INSTALLATION

Proper placement of the instrument is very important. Eddies from trees, buildings, or other structures can greatly influence wind speed and wind direction observations. To get meaningful data for most applications, locate the instrument well above or upwind from obstructions. As a general rule, the air flow around a structure is disturbed to twice the height of the structure upwind, six times the height downwind, and up to twice the height of the structure above ground. For some applications it may not be practical or necessary to meet these requirements.

FAILURE TO PROPERLY GROUND THE WIND MONITOR MAY RESULT IN ERRONEOUS SIGNALS OR TRANSDUCER DAMAGE.

Grounding the Wind Monitor is vitally important. Without proper grounding, static electrical charge can build up during certain atmospheric conditions and discharge through the transducers. This discharge may cause erroneous signals or transducer failure.

10.1.9 A.10 Technical datasheet Young 41382VC Relative Humidity and Temperature Probe

MODEL 41382VC

RELATIVE HUMIDITY / TEMPERATURE PROBE with VOLTAGE OUTPUT

INSTRUCTION SHEET 41382VC-90
REV E102613

INTRODUCTION

The Model 41382VC Relative Humidity/Temperature Probe combines high accuracy humidity and temperature sensors in a single probe. The output signal is 0-1 V (standard) or 0-5 V (user selected option) for both relative humidity and temperature. RH range is 0-100%. Temperature range is -50 to +50°C.

INSTALLATION

Install the probe in a naturally ventilated or fan aspirated radiation shield. Mount probe and shield in a location with good air circulation clear of large thermal masses (buildings, pavement, solar panels, etc.), exhaust vents, electrical machinery and motors, water fountains and sprinklers.

Set 0-1 V or 0-5 V output with jumpers as shown in diagram. These jumpers are located below the terminals in the junction box.

VOLTAGE OUTPUT SELECTION JUMPERS

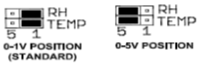

MAINTENANCE

The probe provides years of service with minimal maintenance. Humidity calibration, which may drift slightly with time, can be checked or restored at the factory.

Periodically clean the humidity sensor filter when used in areas of high dust or contamination (smokestacks, seawater, etc.) Soak in clean water or use a mild soap solution. DO NOT USE SOLVENTS.

CE COMPLIANCE

This product complies with the European CE directive on EMC compatibility. Shielded cable must be used.

WARRANTY

This product is warranted to be free of defects in materials and construction for a period of 12 months from date of initial purchase. Liability is limited to repair or replacement of defective item. A copy of the warranty policy may be obtained from R. M. Young Company.

SPECIFICATIONS

RELATIVE HUMIDITY:	
Measuring range:	0-100% RH
Accuracy at 23°C:	±1%
Stability:	Better than ±1%RH per year
Response Time:	10 seconds (Without Filter)
Sensor type:	Rotronic Hygromer
TEMPERATURE:	
Measuring Range:	-50 to +50°C
Accuracy at 23°C:	±0.3°C
Response Time:	10 seconds (Without Filter)
Sensor type:	Platinum RTD
Output signal:	0-1 or 0-5 VDC (jumper option)
Power Required:	8-30 VDC at 7 mA
Recommended Cable:	5 conductor shielded, Young 18446

Recommended Shields:
Young Model 43502 Aspirated Radiation Shield
Young Model 41003P Multi-Plate Radiation Shield

Declaration of Conformity

R. M. Young Company
2801 Aero Park Drive
Traverse City, MI 49686 USA

Model 41382VC RH/Temp Probe
The undersigned hereby declares on behalf of R. M. Young Company that the above-referenced product, to which this declaration relates, is in conformity with the provisions of:

Council Directive 2004/108/EC (December 15, 2004) on Electromagnetic Compatibility

David Poinsett
R&D Manager

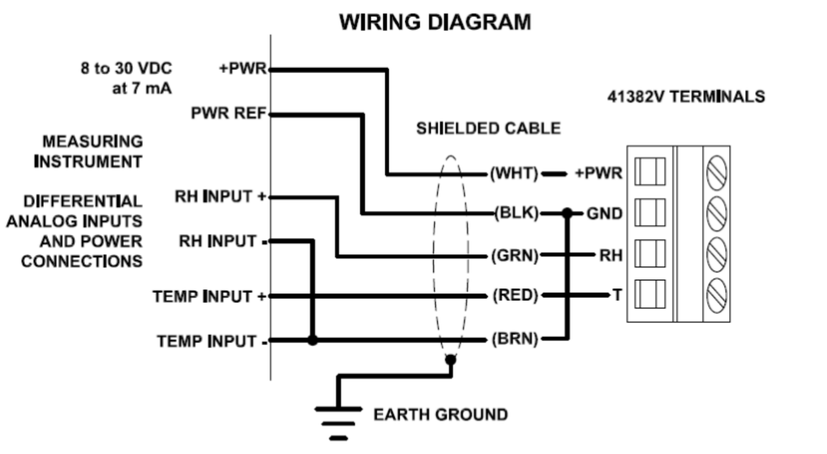

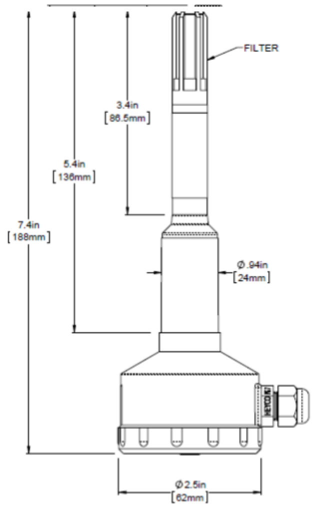

R. M. YOUNG COMPANY 2801 Aero Park Drive , Traverse City, Michigan 49686 USA
TEL (231) 946-3980 FAX (231) 946-4772

10.2 Annex B

B.1 Datasheet of Luxor LX-100M 125-36 module

SOLO LINE SOLO LINE 36/5 – 140 W

Mono-/Polycrystalline module family

Electrical data	LX-5M	LX-10M	LX-50P	LX-100M	LX-140P
Article description	LX-5M /62.5x15.625-36	LX-10M /62.5x31.25-36	LX-50P/156x52-36	LX-100M/125-36	LX-140P/156-36
Rated power Pmpp [Wp]	5	10	50	100	140
Rated voltage Vmpp [V]	17.39	17.39	17.44	18.70	17.97
Rated current Impp [A]	0.29	0.58	2.88	5.39	7.81
Power tolerance	0 / +5%	0 / +5%	0 / +5%	0 / +5%	0 / +5%
Max. system voltage [V]	150	150	400	1000	1000
Open-circuit voltage [V]	21.60	21.60	21.60	21.60	21.60
Short-circuit current Isc [A]	0.32	0.64	3.24	5.87	8.24

Temperature coefficient [%/°C]	LX-5M	LX-10M	LX-50P	LX-100M	LX-140P
Temperature coefficient [P]	-0.49%	-0.49%	-0.45%	-0.49%	-0.45%
Temperature coefficient [I]	0.05%	0.05%	0.05%	0.05%	0.05%
Temperature coefficient [V]	-0.35%	-0.35%	-0.32%	-0.35%	-0.32%

Specifications	LX-5M	LX-10M	LX-50P	LX-100M	LX-140P
Cell size	62.5 x 15.625 mm	62.5 x 31.25 mm	52 x 156 mm	125 x 125 mm	156 x 156 mm
Number of cells | cell type	4 x 9 | mono	4 x 9 | mono	4 x 9 | poly	4 x 9 | mono	4 x 9 | poly
Weight	1.2 kg	1.5 kg	5.5 kg	7.8 kg	11.5 kg
Cable length	-	-	850 mm	850 mm	850 mm
Cable diameter	-	-	4 mm²	4 mm²	4 mm²
Diode	-	-	-	2 x 12 A	2 x 12 A
Socket	IP 54	IP 54	IP 54	IP 65	IP 65

Front view / Back view / Side view

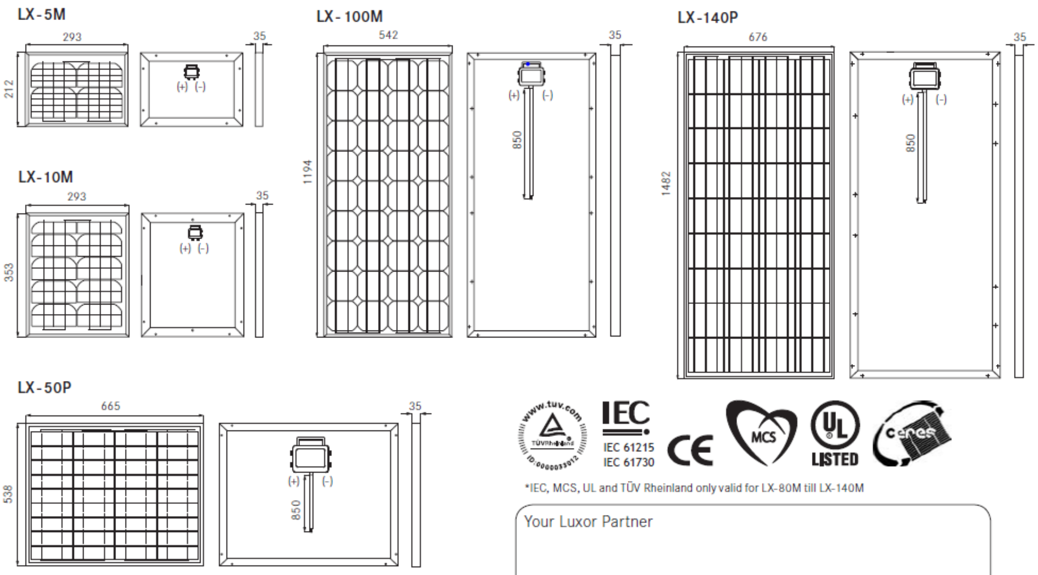

IEC 61215
IEC 61730

*IEC, MCS, UL and TÜV Rheinland only valid for LX-80M till LX-140M

Your Luxor Partner

Printed on Recystar Polar, recycling paper with FSC certificate and the "Blue Angel" eco-label.

FSC RECYCLED Paper FSC® C089401

ClimatePartner
klimaneutral gedruckt
Zertifikatsnummer: 778-53212-0511-1068
www.climatepartner.com

Solo Line 36/5-140W_052013

B.2 Datasheet of Sharp NU-E245J5 module

Datasheet Sharp solarmodule
NU-E245 (J5) 245 Wp

SOLAR ACCES

SHARP

NU Series (60 cells)
245 W | 240 W | 235 W

Monocrystalline silicon photovoltaic modules

Say yes to solar power!
Because it protects the climate.

Innovations from a photovoltaic pioneer

As a solar specialist with 50 years' experience in photovoltaics (PV), Sharp makes significant contributions to ground-breaking progress in solar technology.

Sharp photovoltaic modules in the NU series are designed for applications with high power requirements. These quality monocrystalline modules produce a continuous, reliable yield, even under demanding operational conditions.

All Sharp NU series modules offer system integration which is optimal both technically and economically, and are suitable for installations in on and off-grid PV systems.

Brief details for the installer

- 156.5 mm × 156.5 mm dark blue monocrystalline solar cells
- 60 cells in series
- 2,400 N/m² mechanical load-bearing capacity (245 kg/m²)
- 1,000 V DC maximum system voltage
- IEC/EN 61215, IEC/EN 61730, Application class A
- Class II (VDE: 40021391)

Product features

- High-performance photovoltaic modules made of dark blue monocrystalline (156.5 mm)² silicon solar cells with module efficiencies of up to 14.9 %.
- Anti-reflex coating to increase light absorption (for NU-E245J5 and NU-E240J5).
- Bypass diodes which minimise the loss in output when shading occurs.
- Textured cell surface for particularly high electricity yields.
- BSF structure (Back Surface Field) to optimise cell efficiency.
- Use of tempered white glass, EVA plastic, and weather protection film, as well as a silver anodised aluminium frame with drainage holes for long-term use.
- Output: connection cable with waterproof plug connector.

Quality from Sharp

Benchmarks are set by the quality standards of Sharp Solar. Continual checks guarantee a consistently high level of quality. Every module undergoes visual, mechanical, and electrical inspection. This is recognisable by means of the original Sharp label, the serial number, and the Sharp guarantee:

- 5 year product guarantee
- 10 year performance guarantee for a power output of 90%
- 25 year performance guarantee for a power output of 80%

The detailed guarantee conditions and additional information can be found at **www.sharp.eu.**

As at: December 2010

SolarAccess UK Ltd.
5 Silverdown Office Park, Fair Oak Close, Clyst Honiton • EX5 2UX Exeter
Tel: +44 (0) 1392 916 000 • Fax: +44 (0) 1392 366 654
www.SolarAccess.co.uk • info@SolarAccess.co.uk

Datasheet Sharp solarmodule NU-E245 (J5) 245 Wp

SOLAR ACCESS

Mechanical data

Cell	Monocrystalline (156.5 mm)² silicon solar cell
Quantity and wiring of cells	60 in series
Dimensions	1,652 × 994 × 46 mm (1.64 m²)
Weight	19 kg
Connection type	Cable with plug connector (MC-3)

Limit values

Operating temperature (cell) Storage temperature	– 40 to + 90	°C
Storage air humidity (relative)	up to 90	%
Maximum system voltage	1,000	V DC
Maximum mechanical load	2,400	N/m²
Over-current protection	15	A

Electrical data

		NU-E245 (J5)	NU-E240 (J5)	NU-E235 (E2)	
Maximum power	P_{max}	245 W_p	240 W_p	235 W_p	
Open-circuit voltage	V_{OC}	37.5	37.3	37.0	V
Short-circuit current	I_{SC}	8.73	8.63	8.60	A
Voltage at point of maximum power	V_{mpp}	30.5	30.2	30.0	V
Current at point of maximum power	I_{mpp}	8.04	7.95	7.84	A
Module efficiency	η_m	14.9	14.6	14.3	%
NOCT		47.5	47.5	47.5	°C
Temperature coefficient – open-circuit voltage	αV_{OC}	– 130	– 130	– 130	mV / °C
Temperature coefficient – short-circuit current	αI_{SC}	+0.053	+0.053	+0.053	% / °C
Temperature coefficient – power	αP_{max}	– 0.485	– 0.485	– 0.485	% / °C

The electrical data applies under standard test conditions (STCs): irradiation 1,000 W/m² with light spectrum AM 1.5 and a cell temperature of 25 °C. The rated electrical characteristics are subject to a manufacturing tolerance of – 5% / + 10%. NOCT conditions: irradiation of 800 W/m², ambient temperature of 20 °C and wind speed of 1 m/sec.

Characteristic curves NU-E245 (J5)

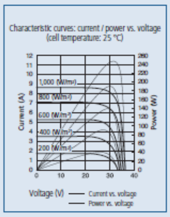

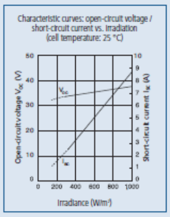

Applications

- On-grid PV systems
- On-roof PV systems
- Off-grid PV systems
- Ground-mounted PV systems

Please read our detailed installation manual carefully before installing the photovoltaic modules.

Registration

Sharp Solar guarantees safety, product quality and value stability for many years – the only thing we ask is: that you register your modules with the serial numbers so we can send you the warranty certificate. It is quick and easy to register your modules at **www.brandaddedvalue.net**

Exterior dimensions

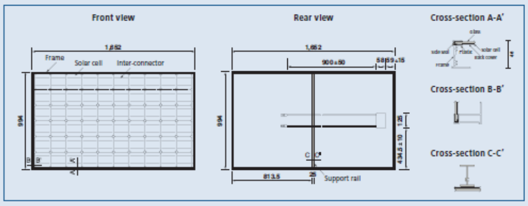

Note

Technical data is subject to change without prior notice. Before using Sharp products, please request the latest data sheets from Sharp. Sharp accepts no responsibility for damage to devices which have been equipped with Sharp products on the basis of unverified information.

The specifications may deviate slightly and are not guaranteed. Installation and operating instructions are to be found in the corresponding handbooks, or can be downloaded from **www.sharp.eu.**

This module should not be directly connected to a load.

Sharp Energy Solution Europe
a division of Sharp Electronics (Europe) GmbH
Sonninstrasse 3, 20097 Hamburg, Germany
Tel: +49(0)40/2376-0 • Fax: +49(0)40/2376-2193
www.sharp.eu

Local responsibility:

Austria SolarInfo.at@sharp.eu
Benelux SolarInfo.seb@sharp.eu
Central & Eastern Europe SolarInfo.scee@sharp.eu
Denmark SolarInfo.dk@sharp.eu
France SolarInfo.fr@sharp.eu
Germany SolarInfo.de@sharp.eu
Scandinavia SolarInfo.sen@sharp.eu
Spain & Portugal SolarInfo.es@sharp.eu
Switzerland SolarInfo.ch@sharp.eu
United Kingdom SolarInfo.uk@sharp.eu

SHARP

SolarNU_60NF_E1210

SolarAccess UK Ltd.
5 Silverdown Office Park, Fair Oak Close, Clyst Honiton • EX5 2UX Exeter
Tel: +44 (0) 1392 916 000 • Fax: +44 (0) 1392 366 654
www.SolarAccess.co.uk • info@SolarAccess.co.uk